

For Reference

NOT TO BE TAKEN FROM THIS ROOM

Ex LIBRIS
UNIVERSITATIS
ALBERTAEASIS



THE UNIVERSITY OF ALBERTA

RELEASE FORM

NAME OF AUTHOR

Chin Ark Lee

TITLE OF THESIS

An Experimental Study Of Refrigerant Charged
Two-Phase Solar Collector Systems

DEGREE FOR WHICH THESIS WAS PRESENTED Master of Science

YEAR THIS DEGREE GRANTED Fall 1983

Permission is hereby granted to THE UNIVERSITY OF
ALBERTA LIBRARY to reproduce single copies of this
thesis and to lend or sell such copies for private,
scholarly or scientific research purposes only.

The author reserves other publication rights, and
neither the thesis nor extensive extracts from it may
be printed or otherwise reproduced without the author's
written permission.



THE UNIVERSITY OF ALBERTA

An Experimental Study Of Refrigerant Charged Two-Phase Solar
Collector Systems

by



Chin Ark Lee

A THESIS

SUBMITTED TO THE FACULTY OF GRADUATE STUDIES AND RESEARCH
IN PARTIAL FULFILMENT OF THE REQUIREMENTS FOR THE DEGREE
OF Master of Science

Department of Mechanical Engineering

EDMONTON, ALBERTA

Fall 1983

A faint, grayscale watermark-style image of a classical building with four prominent columns and a triangular pediment occupies the background of the page.

Digitized by the Internet Archive
in 2019 with funding from
University of Alberta Libraries

https://archive.org/details/Lee1983_0

THE UNIVERSITY OF ALBERTA
FACULTY OF GRADUATE STUDIES AND RESEARCH

The undersigned certify that they have read, and recommend to the Faculty of Graduate Studies and Research, for acceptance, a thesis entitled An Experimental Study Of Refrigerant Charged Two-Phase Solar Collector Systems submitted by Chin Ark Lee in partial fulfillment of the requirements for the degree of Master of Science.

To My Parents

Abstract

A two-phase thermosyphon flat plate solar collector system charged with Freon R-11 was tested outdoors and results obtained are comparable with those of a conventional hydronic system that was tested simultaneously. The utilization of latent heat to transfer energy keeps the collector temperature low and close to the temperature of water in the hot water storage tank.

An indoor unit of the thermosyphon system was tested by electrically heating the absorber plate to study the effects of the liquid charge level, input heat flux to the absorber plate, expansion tank, accumulator for separating the liquid and vapour, and cooling water flow rate on the thermal performance. The vapour quality generated and the Freon mass flow rate through the collector appear to be the governing parameters in evaluating the performance of these systems. The pressure drops across the collector panel and the heat exchanger are well correlated with the Lockhart-Martinelli parameter. The average heat transfer coefficients of the collector tubes calculated are well correlated with the Lockhart-Martinelli parameter and the Convection number.

A preliminary study on flow visualization of the two-phase flow patterns in a single inclined test tube shows that a high liquid charge level delays the transition to annular flow regime, and a low liquid charge level causes slug flow regime. Forced circulation of the Freon in the test tube tends to prolong the bubbly flow regime.

Acknowledgement

The author wishes to express his sincere gratitude to Dr. K.C. Cheng, thesis supervisor, for his excellent guidance and assistance in the course of this study, and Professors G.W. Sadler and K. Fukuda (Kyushu University, Japan) for their useful advice and encouragement.

Special thanks go to Victor Sanchez for his excellent work in constructing the experimental apparatus, and Terry Nord, for his assistance in setting up the electronic instrumentation. Useful discussions with fellow graduate students of the Mechanical Engineering Department, especially M. Zeheeruddin and A. Buhdiman, have helped greatly in this study.

Financial aid from the Department of Mechanical Engineering in the form of teaching assistantship, Alberta/Canada Energy Resources Research Fund (ERRF) under Contract U-79-9, and the Natural Sciences and Engineering Research Council (NSERC) of Canada under Strategic Grant #G-0822 is greatly appreciated.

Table of Contents

Chapter		Page
1.	Introduction	1
	1.1 Background Information	1
	1.2 Scope Of The Study	5
	1.3 Format Of Presentation	7
2.	Simultaneous Thermal Performance Tests On Hydronic And Refrigerant Charged Flat Plate Collector Systems	8
	2.1 Introduction	9
	2.2 Experimental Apparatus And Testing Procedures ...	11
	2.2.1 The Collector Systems	11
	2.2.2 Instrumentation	17
	2.2.3 Experimental Procedures	19
	2.3 Systems Analyses	21
	2.3.1 The Two-Phase Thermosyphon System	21
	2.3.2 The Hydronic System	24
	2.4 Results And Discussion	24
	2.5 Concluding Remarks	49
3.	Some Operating Characteristics Of A Two-Phase Thermosyphon Solar Collector System Using Freon R-11 By Indoor Test	51
	3.1 Introduction	52
	3.2 The Thermosyphon Indoor Test Facility	53
	3.3 System Characteristics And Efficiency	62
	3.4 Results And Discussion	65
	3.5 Concluding Remarks	90
4.	Pressure Drop And Heat Transfer Characteristics Of Freon R-11 In Solar Collector Under Thermosyphon And Forced Flow Conditions	93
	4.1 Introduction	94

4.2 Governing Equations	95
4.2.1 Pressure Drop Analysis	95
4.2.2 Heat Transfer Analysis	99
4.3 Results And Discussion	102
4.3.1 Pressure Drops Results	102
4.3.2 Heat Transfer Results	112
4.4 Concluding Remarks	120
5. Two-Phase Flow Patterns In A Heated Inclined Tube -- A Preliminary Study	123
5.1 Introduction	124
5.2 Experimental Apparatus	125
5.3 Results And Discussion	127
5.4 Concluding Remarks	139
6. Conclusions	141
6.1 Scope Of Results	141
6.2 Future Studies	142
References	144
Appendix A : Flow Chart For Experimental Instrumentation	148

List Of Tables

Table		Page
2.1	Specifications of the thermosyphon and hydronic systems.	16
2.2	Test dates, operating conditions and weather condition during tests.	25
2.3	Characteristics of the thermosyphon (R-11) system.	26
2.4	Comparison between operating conditions and temperature rise in water of the thermosyphon and hydronic systems.	28
2.5	Comparison between the thermosyphon and hydronic systems.	29
2.6	Absolute errors in the instantaneous and system efficiencies calculated.	32
5.1	Operating conditions of the flow patterns depicted in Figures 5.1 to 5.6.	137

List Of Figures

Figure		Page
2.1	Schematic diagram of the experimental hydronic (P-G) system.	12
2.2	Schematic diagram of the experimental thermosyphon (R-11) system.	14
2.3	Schematic diagram showing the relative distance between the collector and heat exchanger, and the liquid refrigerant charge levels.	20
2.4	Efficiency curves for both the thermosyphon and hydronic systems.	30
2.5	Operating characteristics of the thermosyphon system.	33
2.6	Temperature of the water and Freon lines of the thermosyphon system.	34
2.7	Temperature of the Freon line of the thermosyphon system.	35
2.8	Temperature of the water and propylene glycol of the hydronic system.	37
2.9	Comparison of the temperature characteristics between the thermosyphon and hydronic systems.	38
2.10a	The effect of liquid charge level on the instantaneous efficiency of the thermosyphon system (accumulator downcomer open).	40
2.10b	The effect of liquid charge level on the instantaneous efficiency of the thermosyphon system (accumulator downcomer closed).	41
2.11a	Collector tube wall axial temperature distribution at different time of the day (charge level 4 with accumulator downcomer open).	42
2.11b	Collector tube wall axial temperature distribution at different time of the day (charge level 4 with accumulator downcomer closed).	43

Figure		Page
2.11c	Collector tube wall axial temperature distribution at different time of the day (charge level 1 with accumulator downcomer closed).	44
2.12a	Comparison between measured and idealized values of Freon flow rate and vapour quality (accumulator downcomer open).	46
2.12b	Comparison between measured and idealized values of Freon flow rate and vapour quality (accumulator downcomer closed).	46
2.13	Schematic diagram of experimental apparatus for heat loss test of the thermosyphon system.	48
3.1	Schematic diagram of two-phase thermosyphon flat plate solar collector indoor testing facility.	54
3.2	Cross section of collector and heater arrangement, and plan view of a heating element depicting the dimensions.	57
3.3	Effect of heat input and charge level upon the collector tube wall axial temperature distribution (cooling water flow rate at 40 cc/s).	68
3.4	Effect of charge level on the system efficiency at different heat input (cooling water flow rate at 40 cc/s).	70
3.5	Effect of expansion tank on system efficiency and pressure at 100 percent charge (cooling water at 34 cc/s).	71
3.6	Effect of liquid separation at collector exit, with an accumulator, upon the collector tube wall axial temperature distribution (cooling water flow rate at 40 cc/s).	73
3.7	Effect of liquid separation at collector exit, with an accumulator, upon the system performance (cooling water flow rate at 40 cc/s).	75

Figure		Page
3.8	Dependence of overall heat transfer coefficient on the cooling water flow rate at 71 percent charge.	77
3.9	Effect of water flow rate and input heat flux upon the overall heat transfer coefficient at 71 percent charge.	78
3.10	Effect of charge level upon the overall heat transfer coefficient showing the transition at 71 percent charge.	80
3.11	Effect of cooling water and Freon flow rates upon the vapour quality at two representative input heat fluxes.	81
3.12	Effect of liquid Freon flow rate on collector tube wall axial temperature distribution.	82
3.13	Overall heat transfer coefficient at different Freon flow rates, along with the effects of input heat flux and cooling water flow rate.	83
3.14	Effect of cooling water and Freon flow rates upon the average tube wall heat flux at different input heat flux.	84
3.15	Effect of Freon flow rate on collector tubes average heat transfer coefficient at various input heat flux.	85
3.16	Plot of all data according to the Hottel-Whillier equation showing the scattering of results with changing parameters.	89
4.1	Total collector pressure drop as a function of the collector exit vapour mass quality showing the effects of Freon flow rate and input heat flux.	103
4.2	Total collector pressure drop as a function of the Lockhart-Martinelli parameter showing the effects of Freon flow rate and input heat flux.	105

Figure		Page
4.3	Correlation of the ratio of two-phase to single-phase pressure drops (assuming total flow as liquid phase) across the collectors in terms of the Lockhart-Martinelli parameter.	106
4.4	Correlation of the ratio of two-phase to single-phase pressure drops (assuming liquid phase flowing alone) across the collectors in terms of the Lockhart-Martinelli parameter.	107
4.5	Pressure drop across the heat exchanger as a function of the vapour mass quality at the heat exchanger inlet.	110
4.6	Ratio of two-phase to single-phase pressure drops across the heat exchanger as a function of the Lockhart-Martinelli parameter.	111
4.7	Heat flux to flowing Freon in the collector tubes as a function of the Lockhart-Martinelli parameter.	113
4.8	Heat flux to flowing Freon in the collector tubes as a function of Boiling number.	114
4.9	Ratio of experimental two-phase to single-phase Nusselt numbers as a function of Boiling number.	115
4.10	Ratio of experimental two-phase to single-phase Nusselt numbers as a function of the Lockhart-Martinelli parameter.	116
4.11a	Comparison of correlation by Schrock and Grossman with experimental results.	119
4.11b	Comparison of correlation by Shah with experimental results.	119
5.1	Schematic diagram of the thermosyphon loop for flow visualization study.	126
5.2	Flow patterns along tube at high heat flux and high charge level.	129
5.3	Transition from churn flow to annular flow at high heat flux.	131

Figure		Page
5.4	Slug flow with bursting of the vapour bubble at low charge level and low heat flux.	133
5.5	Fluctuating system pressure and test tube pressure drop during slug flow regime.	134
5.6	Prolonged bubbly flow under forced flow condition.	136
A.1	Flow chart of data acquisition system used in experiments.	149

Nomenclature

A_c	absorber plate area, m^2
A_t	total collector tubes inside surface area, m^2
A_w	coil inside surface area, m^2
C	constant used in Eq.(4.23)
C_p	specific heat at constant pressure, $\text{kJ/kg-}^\circ\text{C}$
dp/dz	pressure drop per unit length, Pa/m
D	collector tube inside diameter, m
f_t	two-phase friction factor
g	gravitational constant, m/s^2
G	Freon mass flux through collector tube cross sectional area, kg/s-m^2
h	average heat transfer coefficient defined by Eq.(3.7), $\text{kW/m}^2-{}^\circ\text{C}$
h_{fg}	latent heat of vapourization, kJ/kg
I	solar insolation, kJ/s-m^2
l_s	single-phase tube length in the collector tubes, m
L	collector tube total length, m
L'	fraction of Freon liquid height in the collector
\bar{m}_ℓ	total liquid flow rate, kg/s
$\bar{m}_{\ell 1}$	Freon flow rate through heat exchanger, kg/s
$\bar{m}_{\ell 2}$	Freon flow rate via downcomer of accumulator, kg/s
\bar{m}_w	water flow rate through heat exchanger, kg/s
M_w	water mass in the hot water storage tanks, kg
n	exponent used in Eq.(4.12)
ΔP_c	pressure drop across the collector, Pa
ΔP_e	pressure drop across the heat exchanger, Pa
Q_b	latent heat gain by Freon in collector tubes, kW

Q_c	total heat gain by Freon in collector tubes, kW
Q_i	input heat flux at absorber plate surface, kW/m^2
Q_w	heat gain by water in heat exchanger, kW
T	temperature, $^\circ\text{C}$
T_a	ambient temperature, $^\circ\text{C}$
T_s	saturation temperature, $^\circ\text{C}$
\bar{T}_t	average collector tube outer wall temperature, $^\circ\text{C}$
ΔT	temperature difference, $^\circ\text{C}$
U	overall heat transfer coefficient defined by Eq.(3.8), $\text{kW}/\text{m}^2 \cdot ^\circ\text{C}$
x	local vapour mass quality
x_o	collector exit vapour mass quality
x_i	heat exchanger inlet vapour mass quality
z	axial length along collector tube, m
τ	time, s
η_τ	instantaneous efficiency defined by Eq.(2.9)
η_s	system efficiency defined by Eqs.(2.10) and (3.3)
ρ	density, kg/m^3
$\bar{\rho}$	homogeneous density, kg/m^3
μ	viscosity, $\text{kg}/\text{s}\cdot\text{m}$
$\bar{\mu}$	homogeneous viscosity, $\text{kg}/\text{s}\cdot\text{m}$
v	specific volume, m^3/kg
v_{fg}	vapour-liquid specific volume difference, m^3/kg
\bar{v}	homogeneous specific volume, m^3/kg
θ	collector inclination angle
Φ^2	two-phase frictional pressure drop multiplier defined by Eqs.(4.7) and (4.8)
ψ	ratio of two-phase to single-phase Nusselt number

Dimensionless Numbers

Bo	Boiling number defined by Eq.(4.16)
Co	Convection number defined by Eq.(4.17)
Nu	Nusselt number
Pr	Prantdl number
Re	Reynolds number
X _{t,t}	Lockhart-Martinelli parameter defined in Eq.(4.9), given as the ratio of liquid phase pressure drop to vapour phase pressure drop

Subscripts

ci	collector inlet
co	collector outlet
hi	heat exchanger inlet, Freon line
ho	heat exchanger outlet, Freon line
l	liquid phase of Freon
s	single-phase Freon liquid
t	two-phase
v	vapour phase of Freon
w	water line
wi	heat exchanger inlet, water line
wo	heat exchanger outlet, water line
a	accelerational component
f	frictional component
g	gravitational component

1. Introduction

1.1 Background Information

The concept of a naturally circulating fluid transferring heat from a heat source to a heat sink with the fluid returning by gravity is not new: the thermosyphon reboiler of a chemical distillation column and solar water heaters employing thermosyphonic flow are two examples of processes utilizing this idea. Serious interests in two-phase thermosyphon first arose when this process was used to cool gas-turbine rotor blades. More recently, this process was studied for use in the preservation of permafrost because it acts as a thermal rectifier, capable of transferring heat only in one direction. Two-phase thermosyphon is presently finding application in solar collector systems since it is capable of transferring heat from one place to another with small temperature differences.

In non-freezing climatic regions, thermosyphon flat plate solar water heaters¹ rely on the buoyancy force, instead of a pump, to transport heated water flowing in the collector tubes to the top of an elevated storage tank. Colder liquid at the bottom of the tank then returns to the collector. This method fails in cold regions unless draindown freeze protection is maintained when the

¹ a solar collector system in this thesis shall refer to only flat plate solar collector system unless specified otherwise

temperature drops below freezing point [1]². Employment of a primary loop using a low freezing temperature fluid, e.g., silicon liquid and propylene glycol, as the heat transfer medium solves the problem but not without drawbacks; the higher viscosity of such fluid, especially at low temperature, results in a very low flow rate and hence low thermal efficiency. An alternate approach is to use a fluid that will undergo phase change upon heating, thus transporting energy in the form of latent heat instead of sensible heat to the water. Doron[2] suggested a testing procedure in 1965 for passive phase change systems but attracted little attention then. More recently, the feasibility of this idea was verified [3-8], along with some field testing using refrigerants [9-11] and hydrocarbons [12-13], as well as finding application in solar water pump [14].

A closed loop refrigerant charged solar collector system is essentially a system with an evaporator and a condenser coupled together: the refrigerant in the collector tubes, the evaporator, flows upwards due to the buoyancy force caused by density change upon heating by incoming solar irradiance, with boiling occurring axially because of the low saturation temperature; the vapour gives up its latent energy in the heat exchanger, the condenser, and the condensed liquid then returns to the evaporator via gravity, thus completing the loop. The utilization of boiling and

² numbers in square brackets denote reference numbers at the end of the thesis

condensation heat transfer in the evaporator and condenser, respectively, lowers the collector plate and fluid temperatures due to the enhanced heat transfer characteristics. The phase change characteristics result in a fairly isothermal absorber surface and hence a reduction in heat loss.

Analyses by Downing and Waldin[4], and by Schreyer[8] show that certain fluorocarbon refrigerants, notably Freon R-11, R-113 and R-114, with their low heat capacitance, low saturation pressure within the operating temperature range of solar water heaters, low freezing and boiling point appear to suit this role well . Advantages of such systems include low operating cost since no pump and controls are required, elimination of fouling, scaling and freezing problems, low toxicity and a theoretically higher thermal performance. Compatibility and stability of Freon R-11 and R-114 with steel and copper have been addressed by Downing[15], indicating favourable results within the operating conditions of solar water heaters, although his results also show that Freon R-11 decomposes rapidly in the presence of copper at high temperature which would be undesirable during stagnation.

DeAngelis and Nordham[7] provided an account on the other variables inherent in designing and installing these collectors, e.g., pipe size, materials and sealings compatible with refrigerants as well as leakage prevention, along with criteria for choosing the working fluid. A system

using Freon R-11 with no liquid separator and a heat exchanger located inside the storage tank above the collector was later tested by DeAngelis et al.[11]. A stated efficiency of 35 percent, including tank losses, was achieved. Schreyer[8] used the same fluid, but with a liquid separator and secondary loop for water, and obtained an energy recovery of 66 percent based on total daily solar flux from 6:00 a.m. to 6:00 p.m. during the test month of August 1977. Kissner[6] reported the advantages that are possible with phase change collectors in cold regions and tested with Freon R-114 [10].

A working fluid other than refrigerant was tested by Davic and Bol[13] using n-butane. It was stated, however, that the use of n-butane is only to prove the feasibility of such collectors and is not recommended for domestic use. Soin et al.[12] worked with acetone and petroleum ether 40-60°C and managed to reduce the scattering of their results by an intuitively modified Hottel-Whillier equation.

A theoretical model for a flat plate collector with fluid undergoing phase change was introduced recently by Kaushika et al.[16]. This model takes into account the effects of mass flux, latent heat of vapourization and liquid phase length in the collector tubes. Complete vapourization was assumed and maximum efficiency was obtained when the saturated vapour state was attained at the collector exit. The suggested collector efficiency equation reduces to the Hottel-Whillier-Bliss equation when liquid

fills the whole tube. Chaturvedi et al.[17] proposed an analytical model, valid only for horizontal tubes because the gravitational pressure drop was neglected, applicable to two-phase exit condition. The latter model was developed primarily for collectors coupled to a heat pump where exit superheating is desirable. Both models require an iterative procedure to reach a solution since the flow rate, pressure drop and exit quality are unknown quantities.

1.2 Scope Of The Study

The performance of thermosyphon solar water heaters with water as the heat removal medium has been in use for many years and extensive research studies, both analytical and experimental, are available in the literature. In contrast, thermosyphon systems using a medium that undergoes phase change have received relatively little attention although several commercial units are available [18-19].

The present study involves investigation whether a thermosyphon solar water heater system charged with Freon R-11 can be operated efficiently in cold regions, finding the design parameters of such a system and how each parameter affects the overall thermal performance.

The first objective was achieved by simultaneously testing, under clear sky and no-draw conditions, a conventional hydronic unit using propylene glycol and the thermosyphon unit. Simultaneous testing allows direct comparisons between the thermosyphon unit and the much

proven hydronic unit (Chapter 2). The second objective was achieved with an indoor test unit heated electrically from the back of the absorber plate, thus allowing the control of heat flux onto the collector. The amount of wall heat flux affects the vapour quality and pressure of the system as the subcooled liquid entering the collector panel gains sensible heat and begins to boil when the saturation temperature is exceeded. Liquid carried over to the heat exchanger will affect the condensation heat transfer mechanism. The effects of refrigerant charge, expansion tank, liquid separation at the collector exit with an accumulator and cooling water flow rate at the heat exchanger on thermal performance were examined (Chapter 3).

Since boiling heat transfer is the predominant heat transfer mechanism in this process, a study of the two-phase pressure drop and heat transfer is in order. Results obtained were compared with some existing correlations (Chapter 4).

Unlike single phase flow, two-phase flow is further sub-divided into different flow regimes depending on parameters such as tube size, inclination angle, vapour quality, void fraction, mass flux etc. These flow regimes differ in heat transfer and flow characteristics. A preliminary visual study of this phenomenon was done by way of a heated inclined Pyrex tube, filled with Freon-11, under different system pressure, refrigerant charge level and wall heat flux (Chapter 5).

1.3 Format Of Presentation

In view of the different aspects of the investigation undertaken, it was decided that each chapter would be written so as to be self-explanatory. References in a chapter to those in other chapters of the thesis will be avoided unless unnecessarily long repetitions render this inappropriate. Each chapter will consist of an introduction, its results and conclusions. A final chapter will then link the separate findings together, providing an overall result of the study.

The data acquisition system and the associated instrumentation used in different parts of this study are outlined in Appendix A for reference.

2. Simultaneous Thermal Performance Tests On Hydronic And Refrigerant Charged Flat Plate Collector Systems

Summary

Simultaneous testings under similar test conditions of a conventional hydronic system and a two-phase thermosyphon system charged with Freon R-11 show the latter to be a viable alternative to the commonly used single-phase systems. Thermal efficiency based on the usable energy gained by the water in the hot water storage tank were compared. Operating characteristics of the thermosyphon system are plotted and major results tabulated for comparisons. Operating parameters of the thermosyphon system changed during the test period were the liquid charge level and the closing of the downcomer from the accumulator. Low liquid charge with the downcomer closed resulted in superheating of the vapour at collector exit. The absorber plate temperature of the thermosyphon system is generally lower than that of the hydronic system because energy is transferred in the form of latent heat. Higher efficiency is achieved with the thermosyphon system at the beginning of the day when the water temperature in the hot water storage is low, thus keeping the Freon temperature low.

2.1 Introduction

The applications of flat plate solar collector systems for domestic hot water heating in cold regions encounter additional problems relating to freezing and large heat losses due to low ambient temperature. The use of conventional solar collector technology applicable to mild climatic regions is supplemented with such provisions as utilizing low freezing fluids and draindown freeze protection. Thus, the availability of phase change collector systems offers an attractive alternative to the conventional liquid systems. The refrigerant charged phase change collector systems utilize boiling in the collector tubes upon heating (evaporators) and condensation in the heat exchanger to transfer heat to the water. Higher heat transfer coefficients in the tubes can be attained with phase change thermal process than single-phase flow. A completely passive system is possible if the insulated hot water storage tank with a heat exchanger located inside can be accommodated above the collectors. Otherwise a secondary water loop with a pump is required to circulate the cooling water from the storage tank to the heat exchanger.

In order to study and compare the thermal performance of the conventional hydronic system and the two-phase thermosyphon system, a series of simultaneous experiments were performed under identical conditions. The use of vapourizing/condensing fluids in solar applications is relatively new and at present only limited published data on

field testing is available. Of these, there are only two where comparative testing between the two cases mentioned here were performed simultaneously. The first is by Bottum[20] using Freon R-11 as the working fluid. Identical collector systems were used for both cases. The results show that the thermosyphon system has a consistently lower absorber plate temperature and higher thermal efficiency under both clear and cloudy sky conditions. These results represent testing over a period of five years. The other work is by Cheng[19,Chapter 3] where Revere™ collectors were used for both systems. Freon R-113 was used in this case and the tests lasted from March 9 to May 13, 1981. It was reported that the system efficiency of the hydronic system was at least ten percent higher than that of the thermosyphon system. The large discrepancy may be due to the collectors not designed for two-phase operation and the heat exchanger being located outdoors.

The present study represents an extension of the earlier work [19]. A Refrigeration Research™ two-phase thermosyphon collector was installed with Freon R-11 as the working fluid and Revere™ collectors filled with propylene glycol solution were used for the hydronic system. Simultaneous testings allowed direct comparison between the two systems.

2.2 Experimental Apparatus And Testing Procedures

2.2.1 The Collector Systems

Two different commercial collector systems were used since each involved a different thermal process in transferring heat. This leads to different absorber plate sizes and cover plate materials, but also eliminated the possibility of a particular design favourable to one system being used for the other.

The schematic diagram of the hydronic system is shown in Fig. 2.1. The working fluid used was sixty percent propylene glycol/water solution with a freezing point below -46°C. Each of the two solar collectors measured 90 x 197 x 11.5 cm³ and the copper Tube-In-Strip™ absorber plate has black chrome selective surface treatment. The cover plate consisted of double low iron glass. The water storage tank has a capacity of 248 litres with a coiled, integrally finned copper tube heat exchanger built inside the bottom section of the tank. Two collector panels were connected in parallel with a total absorber plate area of 3.24 m². A 31 watt centrifugal pump was used to circulate the working fluid between the collectors and the heat exchanger. A differential temperature controller was used to activate the pump when the temperature difference between the fluid at the collector outlet and the temperature in the tank reached 8.3°C.

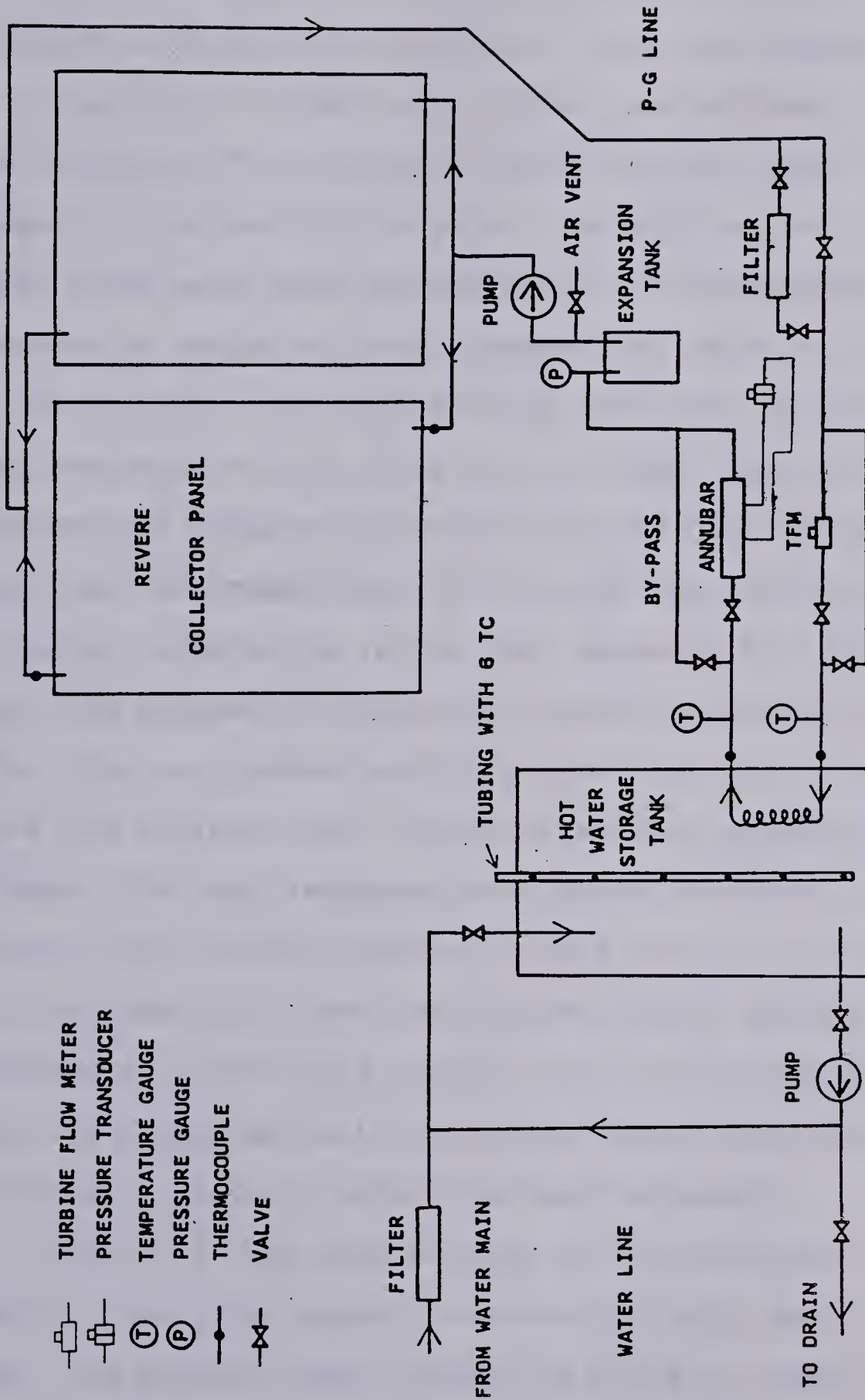


Fig. 2.1 Schematic diagram of the experimental hydronic (P-G) system.

The Refrigeration Research™ phase change solar collector system used consisted of two loops. The primary loop for the naturally circulating Freon between the collector and the heat exchanger. The heat exchanger, with an integral low finned coil inside, was located 0.63 m above the collector. The collector has thirty-two steel tubes brazed to the steel plate with a surface area of 3.39 m². Steel tubes were used because Freon R-11 decomposes in the presence of copper at high temperature. Water was circulated in the secondary loop between the 248 litre tank and the heat exchanger with a 66 watt centrifugal pump. A differential temperature controller was used to start the pump when the temperature of Freon at the collector exit and the water temperature in the tank exceeded 6°C. Fig. 2.2 shows the schematic diagram of the thermosyphon system. The water loop was pressurized to prevent air gap in the pipes above the storage tank, and the flow rate adjusted using a by-pass. The heat exchanger was located outdoors and the storage tank located indoors. Liquid Freon at the collector exit was separated from the flowing vapour using an accumulator. The liquid return line from the accumulator could be closed off with the globe valve installed, allowing two-phase mixture to enter the heat exchanger.

Freon R-11 was used because of its combination of low specific heat, low vapour pressure and high specific latent heat. Low specific heat allows the fluid to reach saturation temperature quickly, and high latent heat is desirable to

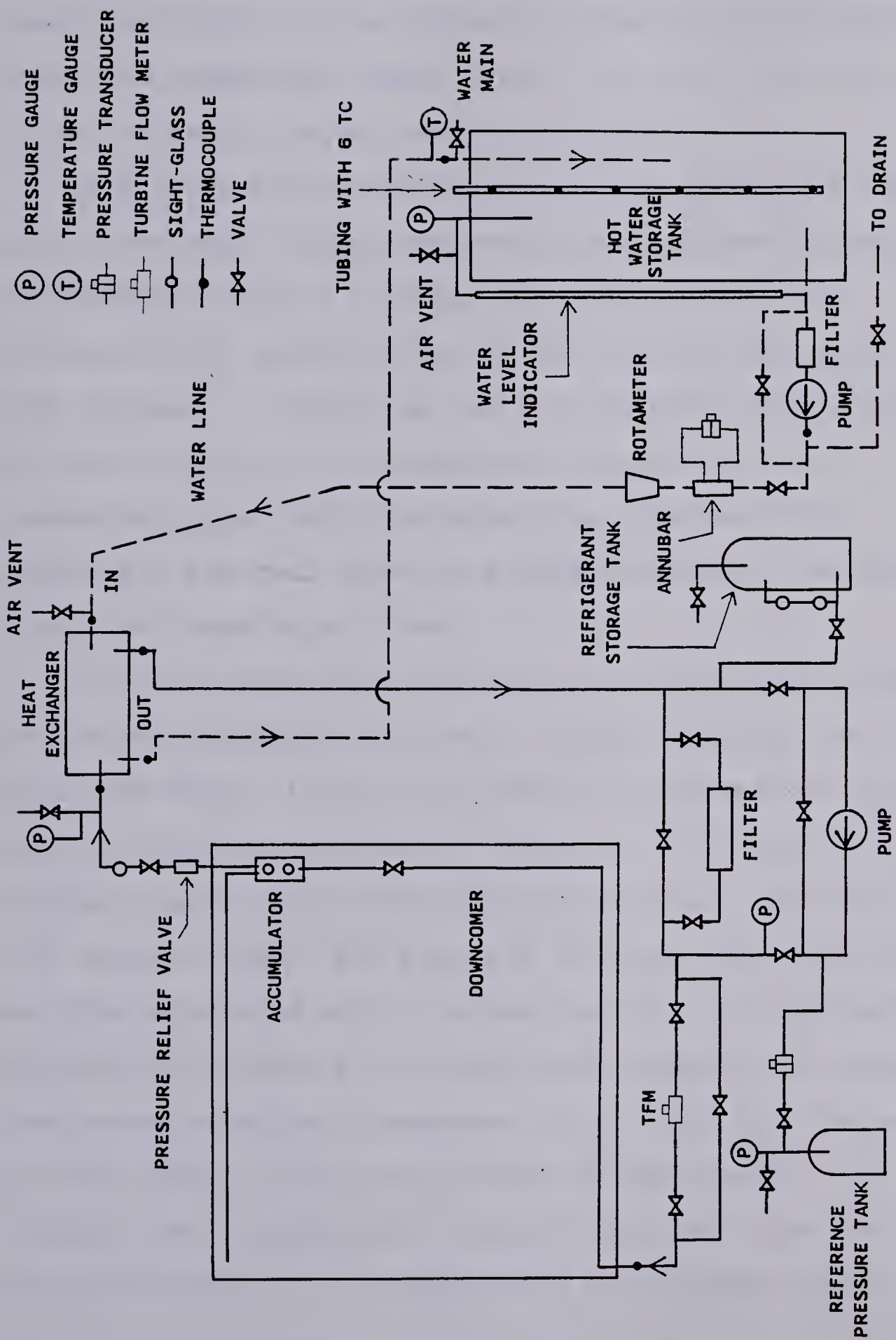


Fig. 2.2 Schematic diagram of the experimental thermosyphon (R-11) system.

prevent complete vapourization of the fluid in the collector tubes. Consideration of vapour pressure is for the safe operating limits of the collectors. Downing and Waldin[4] presented comparisons among Freon R-11, R-12, R-113 and R-114 for use in phase change collectors.

The solar collectors were installed facing due South on top of the east wing of the Mechanical Engineering Building at the University of Alberta (latitude $53^{\circ}34'$). The collector tilt angle was set at 68° from the horizontal for both systems. A summary of the main physical characteristics for both collectors is presented in Table 2.1. All connecting pipes were insulated with Armaflex pipe insulation and heat tapes were used to protect the water line from freezing at night.

All the connecting joints of the thermosyphon system were silver soldered to prevent leakage. Leakage testing was done with Snoop (liquid leak detector) and halogen leak detector by pressurizing the collector with Freon R-12. Pressure testing was first achieved with air (420 kPa) and then with nitrogen (870 kPa) for 24 hours. The whole system was then evacuated with a vacuum pump for 12 hours before charging with Freon R-11. The system pressure was always kept above atmospheric pressure, but it did fall below that on cold nights. During the course of experiments, the collector was occasionally charged fully and some Freon was purged from the top to release any air trapped inside.

Table 2.1 Specifications of the thermosyphon and hydronic systems.

DESCRIPTION	2-PHASE THERMOSYPHON (R-11) SYSTEM	HYDRONIC (P-G) SYSTEM
MAKE	Refrigeration Research	Revere Sun-aid
NO. OF COLLECTOR PANELS	One	Two in parallel
ABSORBER PLATE	Steel tubes hydrogen/copper brazed to steel plate with copper fused. Average surface thickness = .76 mm with microsorb coating. Area: 3.39 sq.m	.8 mm copper with black chrome coating, absorptivity 0.95, emissivity 0.08 Heat removal efficiency 97.5% Area: 3.23 sq.m
COLLECTOR TUBES	32 tubes/panel Length 1.75 m 9.5 mm o.d. steel tubes brazed to 19 mm o.d. headers	Revere tube-in-strip Length 1.9 m, 6 tubes/panel Type RM 12.7 mm o.d. copper connected to 15.9 mm headers
COVER PLATE	0.1 mm (4 mil) duPont Tedlar PVF (double glazing) Transmittance= 0.9	No: 2; thickness: 3.2mm low iron glass, 85.5% transmittance/cover
BACK INSULATION	50.8 mm fiberglass insulation	76.2 mm fiberglass insulation density 0.008 Kg/cu.m
FRAME	Aluminum case	Aluminum case
CONNECTING TUBES	12.7 mm male pipe thread, 19 mm Type L copper tubes	Type L 19 mm copper tubes
WORKING FLUID	R-11, boiling point at 1 atm. pressure = 23.8 C, freezing point = -111 C	60% propylene glycol/water solution, freezing point -46 C
STORAGE TANK	248 liters	248 litres
HEAT EXCHANGER	Finned 15.9 mm o.d. copper coil Linear length: 7.31 m Outer surface area: 0.9 sq.m (water) Water velocity: 0.85 m/sec	Finned copper coil, heating surface area of 0.929 sq.m

2.2.2 Instrumentation

Sheathed iron-constantan (0.7 mm o.d.) thermocouples were used to measure fluid bulk temperatures with mesh screens inserted to disturb the flow just before the thermocouples. The water temperature in the tank, collector tube wall and absorber plate temperatures were measured using 0.225 mm o.d. iron-constantan thermocouples. A sheathed thermocouple located behind a collector panel was used to monitor the ambient temperature. Wind barriers installed beside this thermocouple eliminated wind effect. All thermocouples were calibrated using a quartz thermometer connected to a HP2801A device. A total of five thermocouples were attached to the absorber plate surface of the hydronic system and forty-nine thermocouples on the thermosyphon system to measure temperature distribution over the absorber plate as well as the collector tubes. The reference junction used was an Omega Ice-Point cell. The error in temperature measurements using a least square fit is $\pm 0.3^{\circ}\text{C}$.

Flow rates of the working fluids were measured with turbine flow meters. A rotameter was used for the water loop of the thermosyphon system. The calibration of the turbine flow meters was achieved using Freon R-113 and water since Freon R-11 has a low boiling point (23.8°C) at atmospheric pressure and room temperature. The errors in flow rate measurements are estimated to be ± 0.5 percent for the turbine flow meters and ± 3 percent for the rotameter.

The system pressure and pressure drop across the collector panels for the thermosyphon system were measured using Validyne pressure transducers with diaphragms of 12.5 psi (87.3 kPa) and 5.0 psi (35 kPa), respectively. The pressure transducers were calibrated using a hand operated pump and mercury manometer. A reference pressure tank filled with compressed air provided the differential pressure required to operate within the range of the 12.5 psi diaphragm, as shown in Fig. 2.2. The pressure in the reference tank was adjusted accordingly during experiment. The atmospheric pressure was read from a barometer.

The pressure drop readings were discarded because the density of Freon in the long connecting tubings between the pressure tap and pressure transducers varies with respect to the surrounding temperature. Long connecting tubings were used because the instrumentation has to be located indoors. Furthermore, it was not known if the tubing was completely filled with liquid Freon.

An Eppley pyranometer installed parallel to the collector panels was used to measure the instantaneous solar radiation intensity, I . The cumulative solar energy, Q_{1-2} , between the time interval t_1 and t_2 is calculated from

$$Q_{1-2} = A_C (t_2 - t_1) (I_{t_1} + I_{t_2})/2 \quad (2.1)$$

The time interval used was five seconds. The integrated value at the end of each testing was found to be less than 0.2 percent off from the value obtained from an Eppley

precision integrator.

All measuring devices were connecting to a HP3497A data acquisition unit. Monitoring was achieved via a HP85 micro-computer, with data stored on magnetic tapes as well as printed out on hard copies.

2.2.3 Experimental Procedures

The thermosyphon experimental set-up allowed changing of the Freon charge level and closing of the downcomer from the accumulator. The liquid charge level was set at one of the six levels noted in Fig. 2.3 during the night to avoid vapourization in the collector. Only levels 2, 3 and 6 shown were located with sight glasses, the rest were estimated between the sight glasses since no liquid level indicator was installed.

Both hot water storage tanks were filled with equal amounts of cold tap water and all measuring devices along with associated equipment were switched on the night before each experiment. The data acquisition system was controlled with a timer which was set to start the experiments at 7.00 a.m. each morning and terminate at 6.30 p.m., or when the differential temperature controllers turned off the pumps. The computer program triggered the scanner (HP3497A) every 6 to 7 minutes to take all measurements twice consecutively and the averages were used for computations. The instantaneous solar insolation was taken every five seconds.

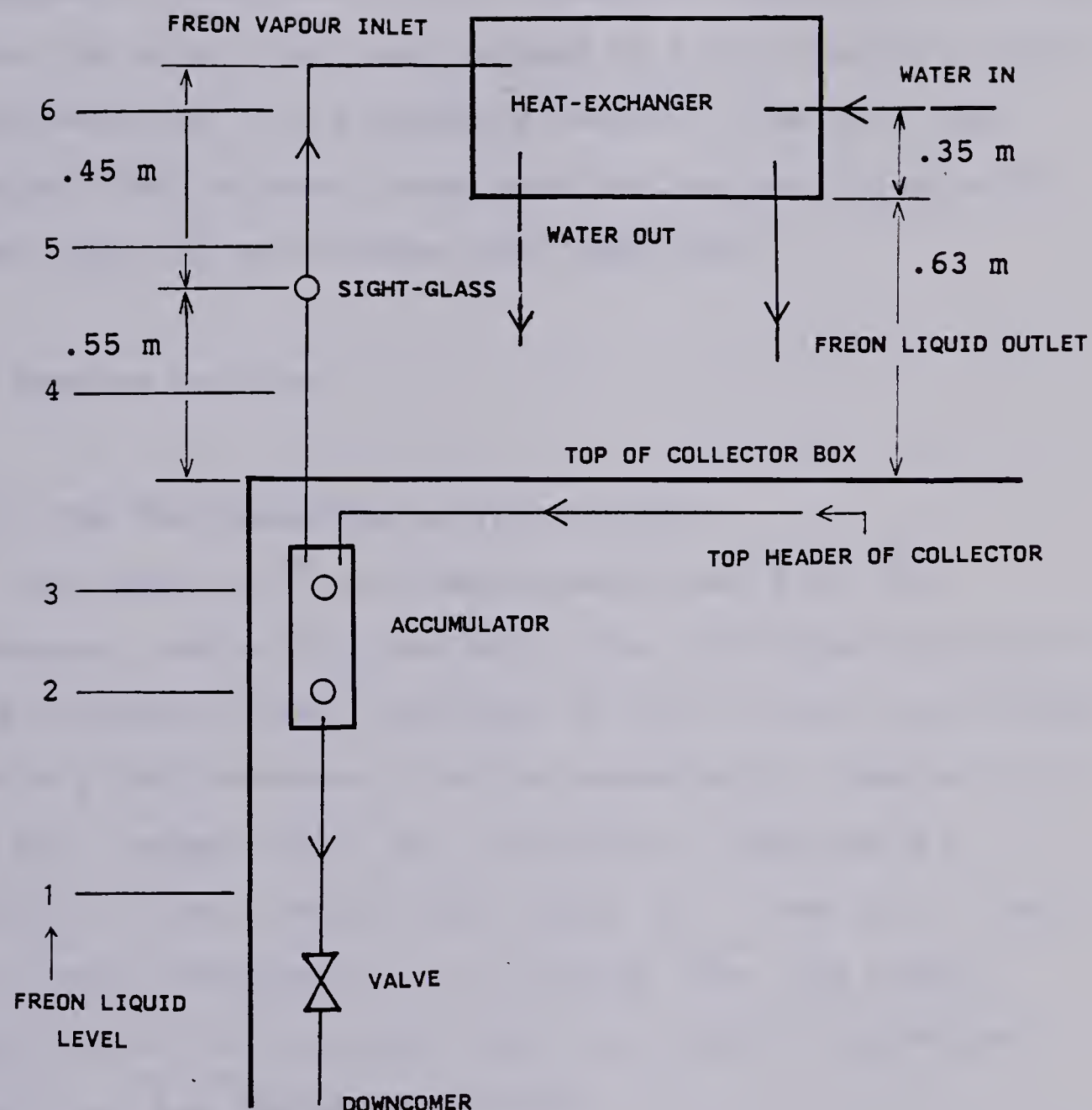


Fig. 2.3 Schematic diagram showing the relative distance between the collector and heat exchanger, and the liquid refrigerant charge levels.

Readings not monitored with the scanner were recorded manually. These readings include the reference pressure tank reading, value from the Eppley precision integrator, atmospheric pressure and the rotameter reading for the water loop. The water flow rate changed by 3 ml/s during a day's experiment due to the pressure change in the tank upon heating. Both storage tanks were drained and filled with fresh cold tap water after each experiment.

2.3 Systems Analyses

2.3.1 The Two-Phase Thermosyphon System

Two cases, for the opening and closing of the downcomer, are to be considered. The first case involves the flow through the heat exchanger as well as the recirculated flow via the downcomer from the accumulator, denoted by \bar{m}_{ℓ_1} and \bar{m}_{ℓ_2} , respectively. \bar{m}_{ℓ_2} is totally liquid but \bar{m}_{ℓ_1} consists of both vapour and liquid, $\bar{m}_{\ell_1,v}$ and $\bar{m}_{\ell_1,l}$, due to the liquid entrainment in the vapour flow. The vapour qualities at the collector exit, x_o , and heat exchanger inlet, x_1 , are therefore given as

$$x_o = \bar{m}_{\ell_1,v} / (\bar{m}_{\ell_2} + \bar{m}_{\ell_1}) \quad (2.2)$$

$$x_1 = \bar{m}_{\ell_1,v} / \bar{m}_{\ell_1} \quad (2.3)$$

When the downcomer is closed, $\bar{m}_{\ell_2}=0.0$ and $x_o=x_1$, if the heat loss along the connecting lines is neglected.

Heat gained by the vapourizing Freon in the collectors is thus given as

$$Q_C = \bar{m}_f [C_{p_f}(T_s - T_{ci}) + x_0 \cdot h_{fg} + C_{p_v}(T_{co} - T_s)] \quad (2.4)$$

The three terms on the right hand side represent liquid sensible heat gain, latent heat gain and vapour sensible heat gain, respectively. The last term drops out when there is no superheating of the vapour at the collector exit since $T_{co} = T_s$. Heat released by the Freon in the heat exchanger is

$$Q_h = \bar{m}_f [C_{p_f}(T_s - T_{ho}) + x_1 \cdot h_{fg} + C_{p_v}(T_{hi} - T_s)] \quad (2.5)$$

and heat gain by the cooling water is

$$Q_w = \bar{m}_w \cdot C_{p_w}(T_{wo} - T_{wi}) \quad (2.6)$$

Difficulties arise in calculating the collector heat gain because the recirculated flow \bar{m}_f via the downcomer was not measured. A flow measuring device was not installed because it might have impeded the flow and affected the thermal efficiency of the system. This was further complicated by the unknown liquid entrainment in the vapour flow. In an ideal case where there is no vapour superheating and heat loss from the heat exchanger is neglected, i.e., by assuming $Q_h = Q_w$, an idealized vapour quality at the heat exchanger inlet, x_1' , can be obtained using Eqs.(2.5) and (2.6), giving

$$x'_1 = [(\bar{m}_w/\bar{m}_{\ell 1}) \cdot C_p_w(T_{wo} - T_{wi}) - C_p_{\ell}(T_{hi} - T_{ho})]/h_{fg} \quad (2.7)$$

For the case with a closed downcomer, Q_c of Eq.(2.4) can be approximated by using x'_1 and assuming no collector heat losses. This latter assumption is erroneous but does offer a way to approximate an idealized collector heat gain. If the heat loss characteristic of the system is known, then correction can be made to improve Eqs.(2.7) and (2.4).

In a fictitious situation where all solar insolation incident upon the absorber plate is transferred to the Freon and the collector exit quality $x_o = 1.0$, then an ideal flow rate \bar{m}'_{ℓ} can be expressed as

$$\bar{m}'_{\ell} = I \cdot A_c / [C_p_{\ell}(T_{co} - T_{ci}) + h_{fg}] \quad (2.8)$$

This value would serve as a check for the measured value $\bar{m}_{\ell 1}$.

Since determination of Q_c was not possible in these experiments, the instantaneous system efficiency will be defined using the heat gained by water flowing through the heat exchanger

$$\eta_r = Q_w / (I \cdot A_c) \quad (2.9)$$

The cumulative system efficiency is defined using the usable energy gained by the water in the hot water storage tank

$$\eta_s = \bar{m}_w (C_p_t \cdot \bar{T}_t - C_p_i \cdot \bar{T}_i) / (A_c \cdot \int_i^t I d\tau) \quad (2.10)$$

where the subscripts t and i refer to value at time t and the value at the beginning of experiment.

2.3.2 The Hydronic System

Analyses of hydronic systems are well documented and can be found in standard text such as Duffie and Beckman[21]. In order for the comparisons with the thermosyphon system to be compatible, the instantaneous efficiency here is defined as the ratio of heat loss by the propylene glycol solution flowing through the heat exchanger and the instantaneous solar insolation

$$\eta_t = \bar{m}_{PG} \cdot C_{PG} \cdot \Delta T_{PG} / (I \cdot A_c) \quad (2.11)$$

and the cumulative system efficiency is similar to that of Eq.(2.10) except that heat gain is calculated from the storage tank of the hydronic system.

2.4 Results And Discussion

A total of 22 tests lasting from August 14 to September 17, 1981 were obtained. Table 2.2³ gives the test conditions as well as the weather conditions. Two operating variables are noted, the Freon charge level and closing of the downcomer, besides comparison of thermal efficiencies with those of the hydronic system. Major results of each test of the thermosyphon system are given in Table 2.3 with the

³The thermosyphon and hydronic systems will be denoted by R-11 and P-G, respectively, in the tables and figures

Table 2.2 test dates, operating conditions and weather condition during tests.

TEST DATE (1981)	CHARGE LEVEL (see Fig. 2.3)	VALVE POSITION	WEATHER CONDITION
AUGS14	2	OPEN	SUNNY & CLEAR ALL DAY
AUGS15	2	OPEN	SUNNY, CLOUDY IN THE EVENING
AUGS17	2	CLOSED	CLOUDY WITH INTERMITTENT SUN-SHINE ALL DAY
AUGS18	2	CLOSED	SUNNY, OVER-CAST IN THE AFTERNOON
AUGS19	3	OPEN	SUNNY, WITH INTERMITTENT CLOUDINESS
AUGS20	3	CLOSED	CLOUDY(MORNING), SUNNY(NOON), OVER-CAST(EVENING)
AUGS21	3	CLOSED	CLOUDY TILL 1500hr, SUNNY AFTER THAT
AUGS22	3	CLOSED	SUNNY ALL DAY
AUGS25	6	OPEN	SUNNY & SLIGHTLY HAZY
AUGS26	6	OPEN	SUNNY & SLIGHTLY HAZY
AUGS27	6	CLOSED	CLOUDY TILL 1100hr, SUNNY AFTER THAT
AUGS28	6	CLOSED	CLOUDY TILL 1200hr, SUNNY AFTER THAT
SEPT01	5	OPEN	SUNNY & CLEAR TILL 1430hr, OVER-CAST AFTER THAT
SEPT05	5	OPEN	SUNNY TILL NOON, INTERMITTENT CLOUDINESS AFTER NOON
SEPT06	5	CLOSED	CLOUDY TILL 1030hr, SUNNY & CLEAR AFTER THAT
SEPT07	5	CLOSED	SUNNY & CLEAR ALL DAY
SEPT08	4	OPEN	SUNNY & CLEAR ALL DAY
SEPT09	4	CLOSED	SUNNY & CLEAR ALL DAY
SEPT14	1	OPEN	SUNNY & SLIGHTLY HAZY ALL DAY
SEPT15	1	CLOSED	SUNNY & SLIGHTLY HAZY ALL DAY
SEPT16	1	OPEN	SUNNY & CLEAR ALL DAY
SEPT17	1	CLOSED	SUNNY & CLEAR WITH FEW CLOUDY PERIODS

Table 2.3 Characteristics of the thermosyphon (R-11) system.

TEST DATE (1981)	AVE. WATER TEMPERATURE INITIAL / FINAL (°C)	TANK MAXIMUM AMBIENT TEMPERATURE (°C)	AVERAGE R-11 FLOW-RATE (m/sec)	AVERAGE WATER FLOW-RATE (m/sec)	SOLAR ENERGY COLLECTED / AVAILABLE (kw-hr)	CUMULATIVE SYSTEM EFFICIENCY (%)
AUGS14	23.8 / 49.2	28.2	3.1	111	6.17 / 21.77	28.3
AUGS15	22.5 / 49.9	30.2	3.9	111	6.80 / 18.51	36.8
AUGS17	24.5 / 39.0	27.0	2.2	117	3.59 / 11.19	32.1
AUGS18	23.3 / 49.8	27.9	3.9	117	6.60 / 19.87	33.2
AUGS19	24.6 / 50.4	30.9	11.4	114	6.42 / 18.90	34.0
AUGS20	24.0 / 43.8	25.4	14.4	116	4.90 / 14.30	34.3
AUGS21	24.2 / 38.8	25.8	13.3	117	3.51 / 11.41	30.8
AUGS22	22.7 / 51.2	28.0	15.4	116	7.07 / 20.89	33.9
AUGS25	24.5 / 47.4	28.1	12.0	116	5.65 / 19.27	29.3
AUGS26	23.8 / 50.7	29.9	12.3	116	6.70 / 20.71	32.3
AUGS27	24.9 / 52.2	27.7	15.5	116	6.79 / 20.35	33.4
AUGS28	23.8 / 48.6	24.8	15.1	116	6.15 / 18.82	32.7
SEPT01	20.9 / 44.4	21.3	12.0	116	5.84 / 17.34	33.7
SEPT05	20.8 / 43.1	20.5	11.9	114	5.55 / 17.40	31.9
SEPT06	20.2 / 45.4	22.9	15.9	116	6.28 / 16.93	37.1
SEPT07	20.3 / 51.1	27.0	15.8	116	7.67 / 22.05	34.8
SEPT08	21.9 / 53.0	29.3	11.5	115	7.74 / 21.09	36.7
SEPT09	21.4 / 54.1	30.4	15.7	115	8.14 / 22.47	36.2
SEPT14	21.1 / 46.9	20.0	4.3	112	6.42 / 19.42	33.1
SEPT15	19.7 / 45.9	22.7	3.9	113	6.51 / 21.91	29.7
SEPT16	19.7 / 50.7	28.2	4.5	112	7.71 / 22.03	35.0
SEPT17	20.8 / 49.9	28.8	4.3	113	7.19 / 21.62	33.2

corresponding comparisons with the conventional system presented in Tables 2.4 and 2.5.

Tabulated results in Table 2.3 show the much lower flow rate at charge levels 1 and 2 (see Fig. 2.3) did not affect the cumulative efficiency significantly. The reason being that energy is transferred predominantly in the form of latent heat. The increase in flow rate through the heat exchanger with respect to charge level is expected since for levels above the accumulator, the liquid carried over by the flowing vapour increases. Closing of the downcomer of the accumulator decreases the vapour quality by forcing the liquid flow through the heat exchanger.

Table 2.4 shows that the thermosyphon system compares well with the hydronic system. The former has a higher thermal capacitance evidenced by the slower starting time, despite the lower temperature difference required to activate the pump (6.0°C to 8.3°C). It should be noted that the absorber plate area of the hydronic system is slightly smaller, therefore a direct comparison of the water tank temperature rise is not valid. The cumulative system efficiency of the thermosyphon system is slightly lower than that of the hydronic system in most cases as listed.

However, it is interesting to note that the average water temperature in the tank of the thermosyphon system is higher at 1330hr in most cases, even though it started operating later. Fig. 2.4 depicts the varying instantaneous efficiency and cumulative efficiency for test run on SEPT09;

Table 2.4 Comparison between operating conditions and temperature rise in water of the thermosyphon and hydronic systems.

TEST DATE (1981)	AVE. TEMP. (R11) (°C)	WATER TANK TEMP. (P-G) (°C)	AVE. WATER TANK TEMP. AT 1330hr (°C)	AVE. WATER TANK TEMP. AT 1330hr (°C)	OPERATING TIME R11 SYSTEM (hr:min)	OPERATING TIME P-G SYSTEM (hr:min)	CUMULATIVE SYSTEM EFFICIENCY (%)
	INITIAL / FINAL	INITIAL / FINAL	R11 / P-G	R11 / P-G	START / END	START / END	R11 / P-G
AUGS14	23.8 / 49.2	24.1 / 49.5	37.0 / 36.3	7:55 / 18:00	9:26 / 18:30	28.3 / 31.2	
AUGS15	22.5 / 49.9	22.7 / 48.9	37.3 / 35.9	9:41 / 18:00	9:41 / 17:31	36.8 / 37.9	
AUGS17	24.5 / 39.0	23.8 / 39.5	30.2 / 30.1	9:44 / 17:12	9:31 / 18:00	32.1 / 33.0	
AUGS18	23.3 / 49.8	22.8 / 48.5	38.7 / 36.9	9:24 / 18:00	9:17 / 18:00	33.2 / 33.7	
AUGS19	24.6 / 50.4	24.4 / 49.6	38.8 / 37.8	10:10 / 17:05	9:16 / 17:14	34.0 / 34.5	
AUGS20	24.0 / 43.8	24.4 / 44.0	36.3 / 35.6	9:10 / 16:23	9:10 / 17:32	34.3 / 32.9	
AUGS21	24.2 / 38.8	24.5 / 39.4	27.2 / 28.0	10:54 / 17:40	10:40 / 18:00	30.8 / 32.9	
AUGS22	22.7 / 51.2	22.9 / 50.4	38.4 / 37.0	9:28 / 17:50	9:17 / 18:00	33.9 / 34.1	
AUGS25	24.5 / 47.4	24.2 / 48.1	36.8 / 36.5	9:37 / 17:52	9:16 / 18:00	29.3 / 32.2	
AUGS26	23.8 / 50.7	23.8 / 51.3	37.9 / 37.6	9:25 / 17:58	9:11 / 18:11	32.4 / 33.9	
AUGS27	24.9 / 52.2	24.5 / 52.1	39.9 / 39.1	9:10 / 17:29	9:16 / 17:29	33.4 / 35.2	
AUGS28	23.8 / 48.6	24.0 / 49.2	35.6 / 35.5	9:52 / 17:54	9:16 / 17:54	32.7 / 34.8	
SEPT01	20.9 / 44.4	20.1 / 44.2	37.1 / 35.9	9:40 / 16:22	9:16 / 16:40	33.7 / 35.5	
SEPT05	20.8 / 43.1	21.3 / 44.1	36.2 / 36.5	9:32 / 16:39	9:17 / 16:53	31.9 / 33.8	
SEPT06	20.2 / 45.4	20.4 / 45.1	34.4 / 33.5	10:40 / 16:37	9:58 / 16:50	37.1 / 37.3	
SEPT07	20.3 / 51.1	20.4 / 50.7	37.9 / 36.5	9:29 / 17:44	9:11 / 18:10	34.8 / 35.3	
SEPT08	21.9 / 53.0	21.4 / 51.7	39.8 / 37.8	9:22 / 17:15	9:16 / 17:56	36.8 / 36.0	
SEPT09	21.4 / 54.1	21.0 / 52.6	40.4 / 38.1	9:25 / 17:49	9:11 / 18:00	36.2 / 35.9	
SEPT14	21.1 / 46.9	21.4 / 46.7	34.4 / 33.9	9:37 / 17:34	9:22 / 17:55	33.1 / 33.5	
SEPT15	19.7 / 45.9	20.0 / 48.3	34.2 / 35.1	9:32 / 17:55	9:11 / 18:00	29.7 / 33.6	
SEPT16	19.7 / 50.7	20.2 / 50.0	37.2 / 36.2	9:31 / 18:00	9:10 / 18:00	35.0 / 35.1	
SEPT17	20.8 / 49.9	21.0 / 51.9	37.3 / 37.5	9:42 / 18:00	9:05 / 18:00	33.2 / 37.2	

Table 2.5 Comparison between the thermosyphon and hydronic systems.

TEST DATE (1981)	MAX. PLATE (mid-pt.) TEMP. (°C)	MAX. FLUID EXIT TEMP. (°C)	COLLECTOR R-11 / P-G	AVE. FLOW RATE (ml/sec)	FLUID R-11 / P-G	COLLECTED ENERGY (kW - hr) R-11 / P-G
AUGS14	55.2 / 70.1	51.6 / 68.2		3.1 / 28.5		6.17 / 6.30
AUGS15	57.1 / 70.8	53.4 / 69.7		3.9 / 28.7		6.80 / 6.51
AUGS17	47.2 / 63.0	41.7 / 61.0		2.2 / 27.8		3.59 / 3.91
AUGS18	55.4 / 71.9	51.8 / 70.3		3.9 / 28.4		6.60 / 6.37
AUGS19	57.6 / 74.6	53.5 / 70.2		11.3 / 28.4		6.42 / 6.28
AUGS20	54.3 / 69.9	48.6 / 68.1		14.4 / 28.1		4.90 / 4.87
AUGS21	46.4 / 64.4	42.5 / 62.9		13.3 / 27.5		3.51 / 3.64
AUGS22	58.4 / 70.4	55.6 / 69.7		15.4 / 28.5		7.07 / 6.87
AUGS25	55.1 / 68.7	51.2 / 66.8		12.0 / 28.5		5.65 / 5.92
AUGS26	57.5 / 72.5	53.7 / 71.2		12.3 / 28.6		6.70 / 6.82
AUGS27	59.9 / 74.2	56.4 / 72.4		15.5 / 28.6		6.79 / 6.85
AUGS28	56.3 / 71.0	52.8 / 68.9		15.1 / 28.2		6.15 / 6.26
SEPT01	54.6 / 70.8	48.6 / 68.7		12.0 / 28.3		5.84 / 5.99
SEPT05	51.7 / 70.1	47.0 / 66.8		11.9 / 28.2		5.55 / 5.67
SEPT06	55.5 / 70.7	49.7 / 68.4		15.9 / 28.2		6.28 / 6.13
SEPT07	57.4 / 72.7	55.6 / 70.6		15.8 / 28.4		7.67 / 7.55
SEPT08	60.1 / 74.6	56.3 / 72.4		11.5 / 28.6		7.74 / 7.55
SEPT09	59.0 / 74.5	56.6 / 72.6		15.7 / 28.5		8.14 / 7.88
SEPT14	51.7 / 68.3	49.3 / 65.2		4.3 / 28.3		6.42 / 6.32
SEPT15	64.0 / 69.7	53.6 / 66.6		3.9 / 28.4		6.51 / 7.06
SEPT16	55.7 / 70.8	53.7 / 68.2		4.5 / 28.4		7.71 / 7.42
SEPT17	70.9 / 72.6	60.2 / 70.5		4.3 / 28.5		7.19 / 7.66

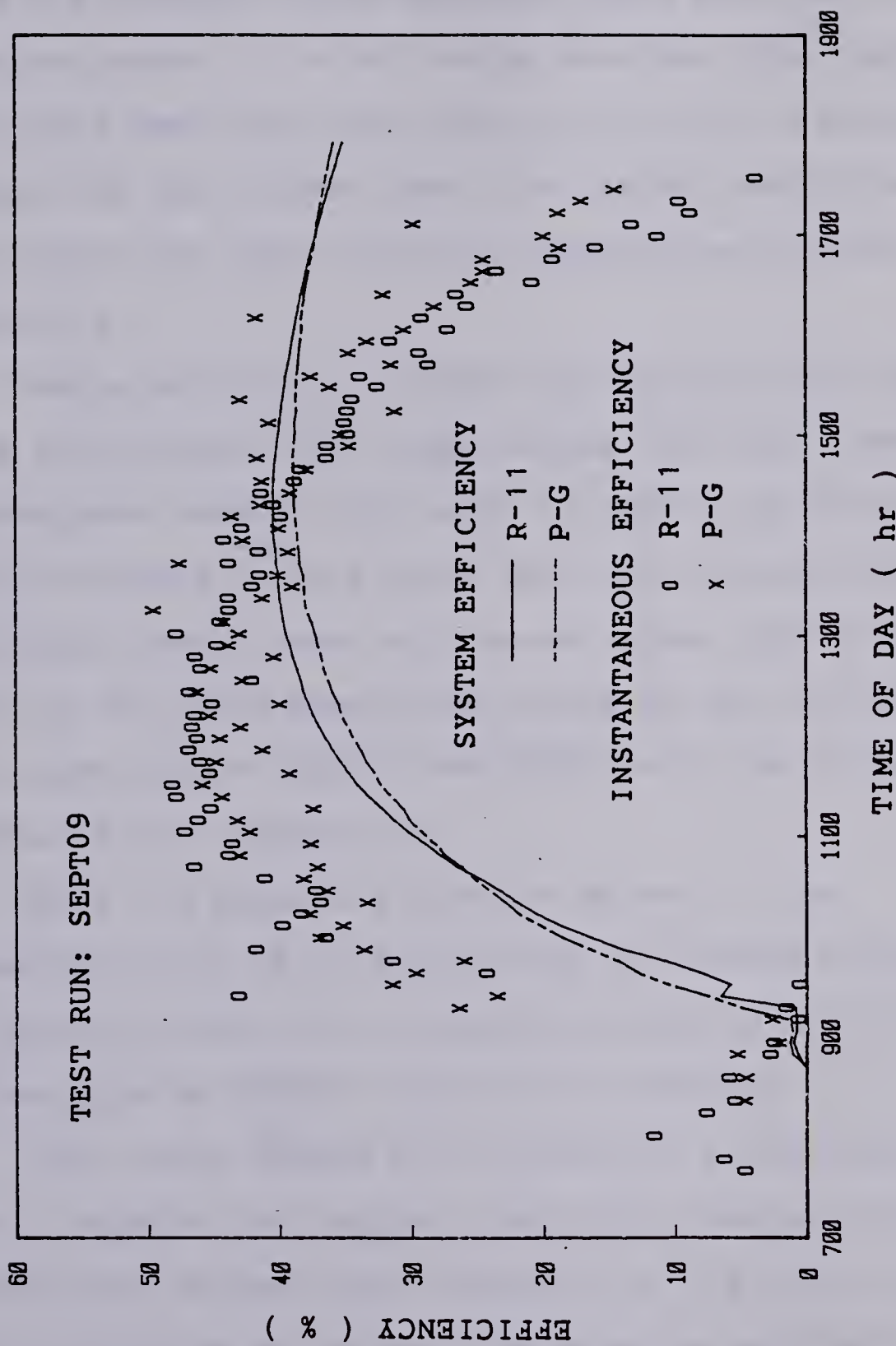


Fig. 2.4 Efficiency curves for both the thermosyphon and hydronic systems.

the thermosyphon system is seen to operate more efficiently at the beginning. It appears that heat losses are higher in this system as temperature increases or the different cover plate and absorber plate materials used may have resulted in different amount of solar energy absorbed. The cumulative efficiency used here then offers a value for comparison between the two systems under the tested conditions but does not reflect the upper limit of operating efficiency of these collectors.

Tabulated results in Table 2.5 show that the absorber plate and working fluid temperatures were much lower in the thermosyphon system. This ought to reduce the heat losses if both collectors share similar heat loss characteristics. A low liquid charge level will cause vapour superheating when there is no liquid separation device at the collector exit, as in test runs on SEPT15 and SEPT16 with the higher absorber plate temperature.

Table 2.6 shows the absolute errors in the determination of the instantaneous and system efficiencies. The absolute error of the system efficiency calculated in the test run on SEPT09 would be ± 4.3 percent.

Test run on SEPT09 will be used as a representative case in showing the typical operating characteristics of the thermosyphon system. Time variation of the system pressure, solar insolation and Freon flow rate are depicted in Fig. 2.5. The fluid bulk temperatures at various locations are plotted in Figs. 2.6 and 2.7. The initial fluctuations shown

Table 2.6 Absolute errors in the instantaneous and system efficiencies calculated.

Instantaneous Efficiency

$$\eta_{\tau} = \bar{m} C_p \Delta T / A_C \int I d\tau$$

$^{\circ}\text{C}$	ΔT	10	15	20	25	30
$\frac{\delta \eta_{\tau}}{\eta_{\tau}} \times 100\%$	R11	± 9.5	± 7.5	± 6.5	± 5.9	± 5.5
	PG	± 8.7	± 6.7	± 5.7	± 5.1	± 4.7

System Efficiency

$$\eta_s = \dot{M}_w C_p \Delta T / A_C \int I d\tau$$

$^{\circ}\text{C}$	ΔT	5	10	15	20	25	30	35
$\frac{\delta \eta_s}{\eta_s} \times 100\%$		± 14.5	± 8.4	± 6.4	± 4.8	± 4.4	± 4.1	± 3.9

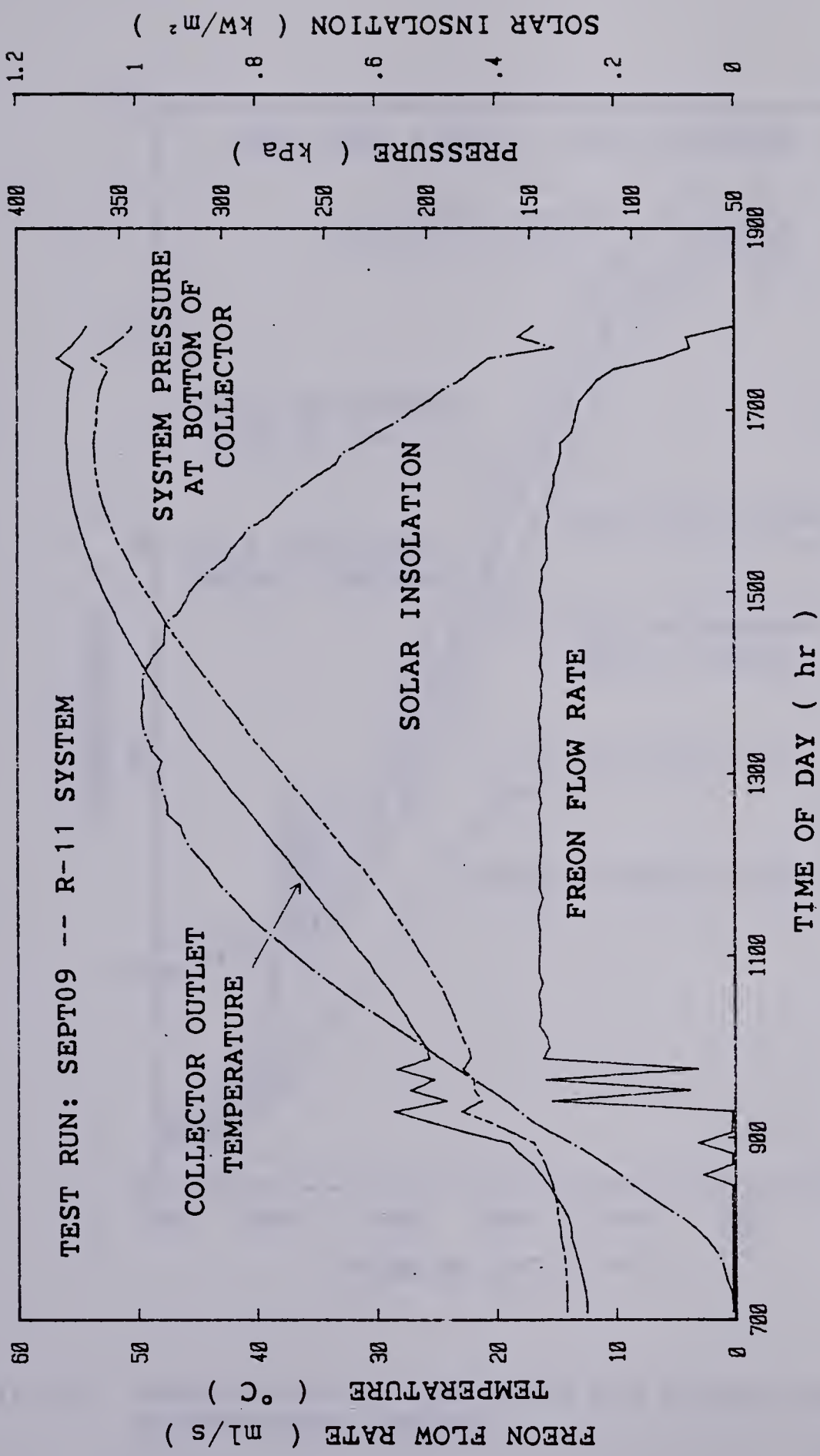


Fig. 2.5 Operating characteristics of the thermosyphon system.

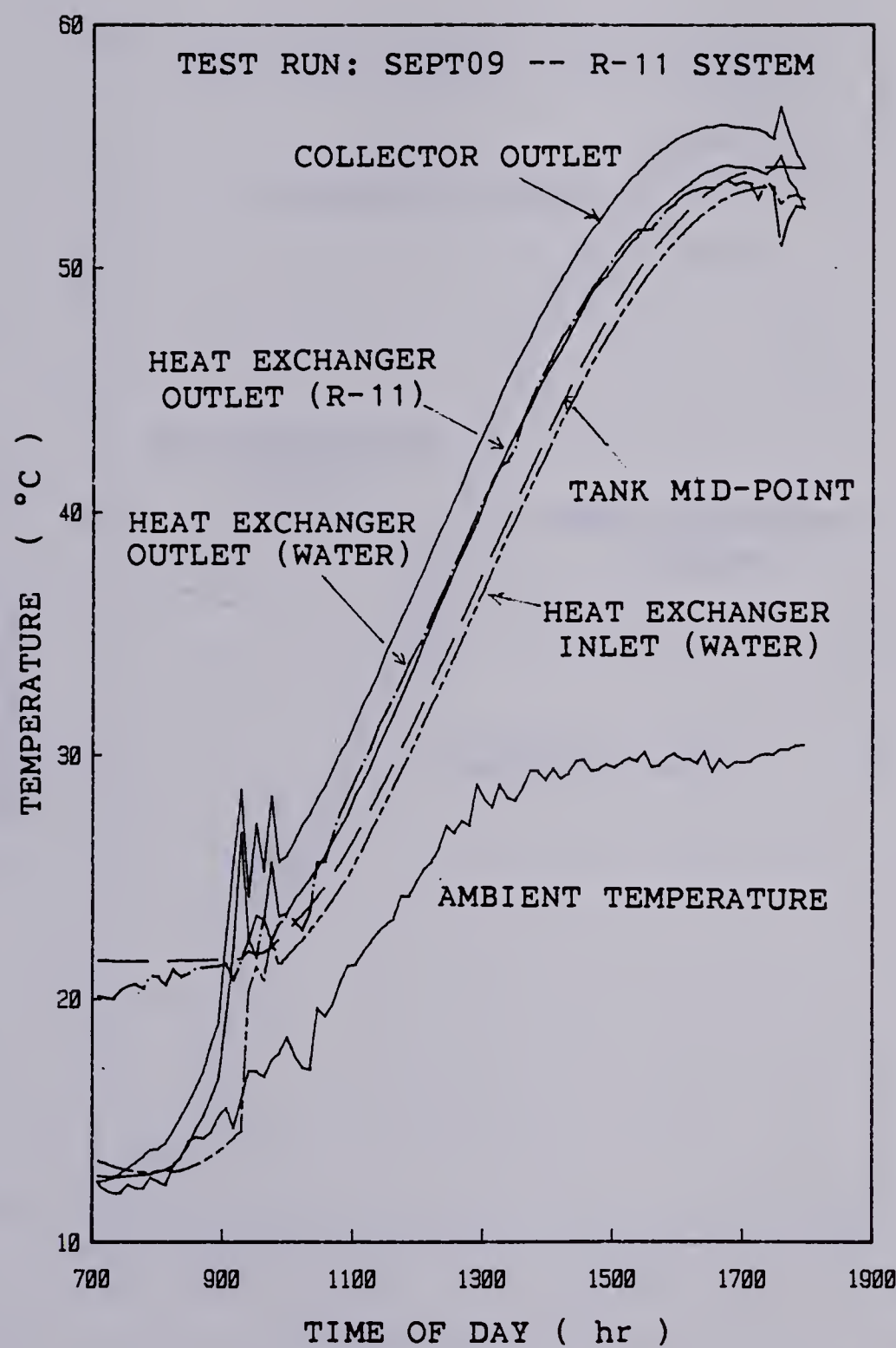


Fig. 2.6 Temperature of the water and Freon lines of the thermosyphon system.

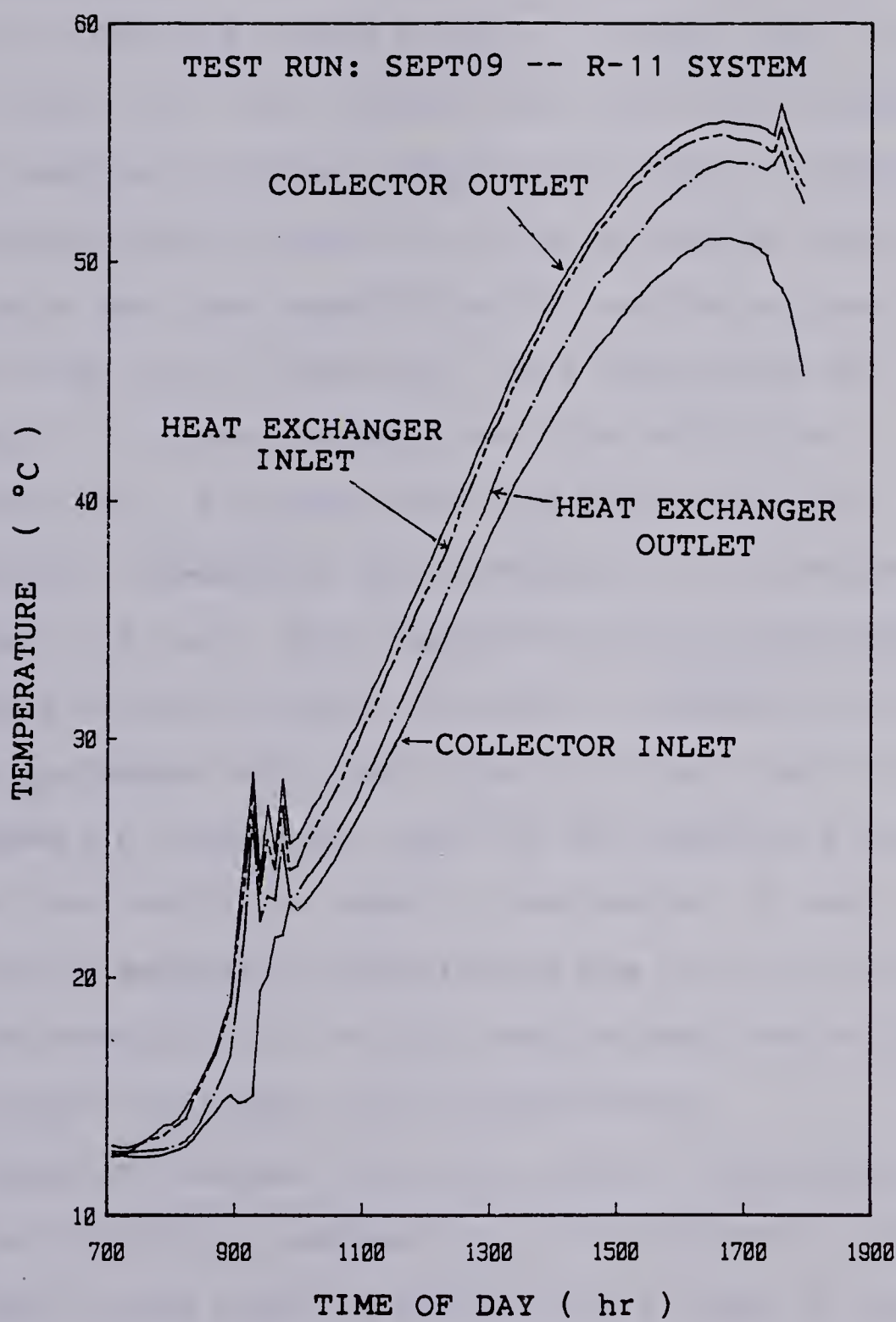


Fig. 2.7 Temperature of the Freon line of the thermosyphon system.

in all three graphs were caused by the activation of the cooling water pump upon reaching the pre-set temperature difference. This cooled the Freon and reduced the pressure in the collector, which in turn initiated boiling in the collector tubes and caused a surge in Freon flow rate as shown on Fig. 2.5. The cooling water flow then stopped due to the reduction in Freon temperature. This is associated with bursting type of boiling in the collector tubes. The whole cycle was then repeated until reaching a quasi-steady state at high solar insolation. This phenomenon was repeated, to a lesser extent, near the end of the experiment. Fig. 2.6 shows that the Freon and water temperatures remained at approximately 5°C difference throughout the test. This characteristic is favourable since it reduces the heat losses. The drop in temperature between the heat exchanger exit and collector inlet shown on Fig. 2.7 suggests a large heat loss via the connecting pipes in spite of the insulation used. A combination of heat loss and reduction in saturation temperature due to the higher elevation resulted in a slight drop between the collector exit and heat exchanger inlet temperatures.

Comparison between Figs. 2.6 and 2.8 shows the much higher working fluid temperature of the hydronic system. Heat loss in this case was significant as seen by the temperature drop from the collector exit to the heat exchanger inlet shown in Fig. 2.8. Fig. 2.9 shows the significantly higher absorber plate temperature of the

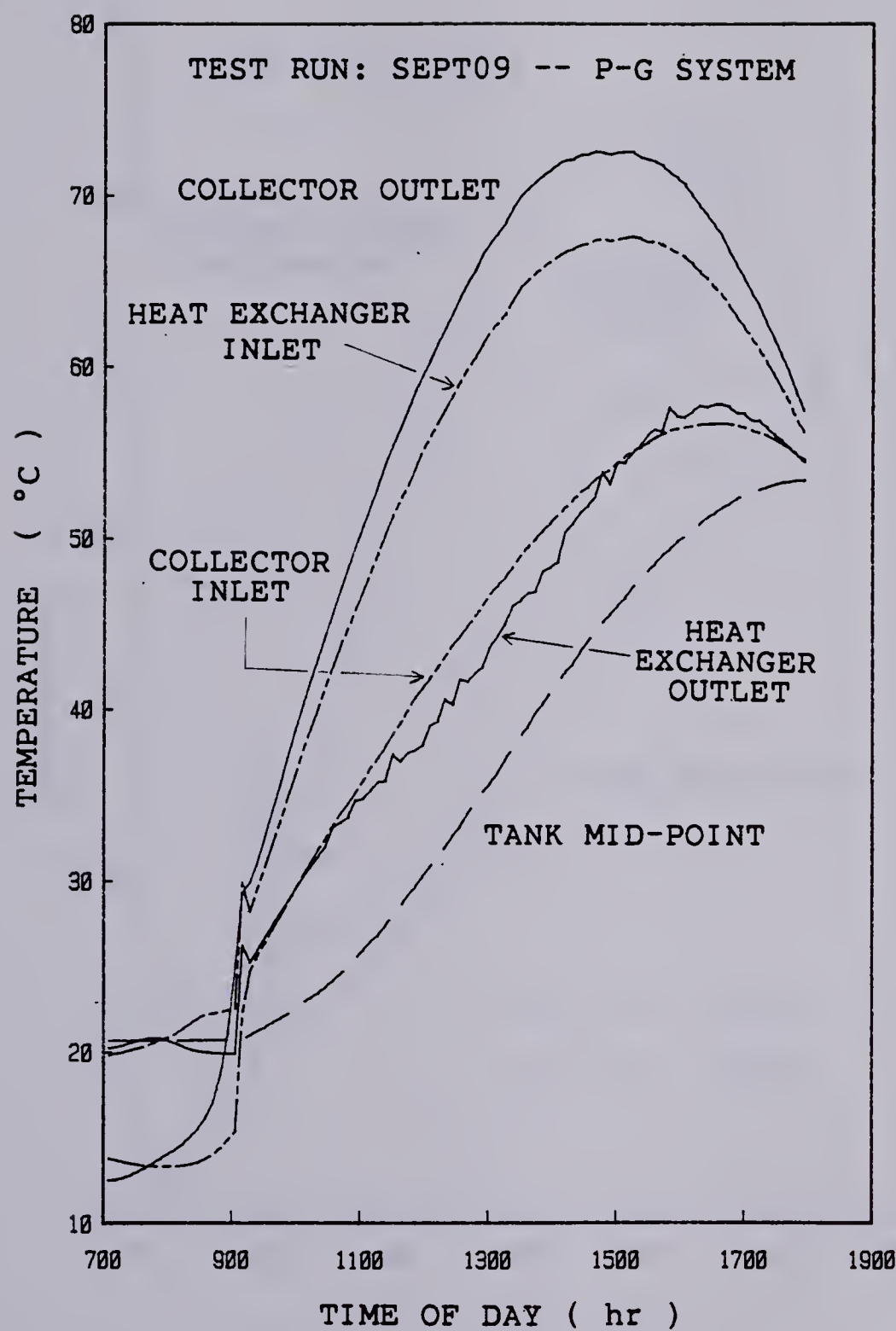


Fig. 2.8 Temperature of the water and propylene glycol of the hydronic system.

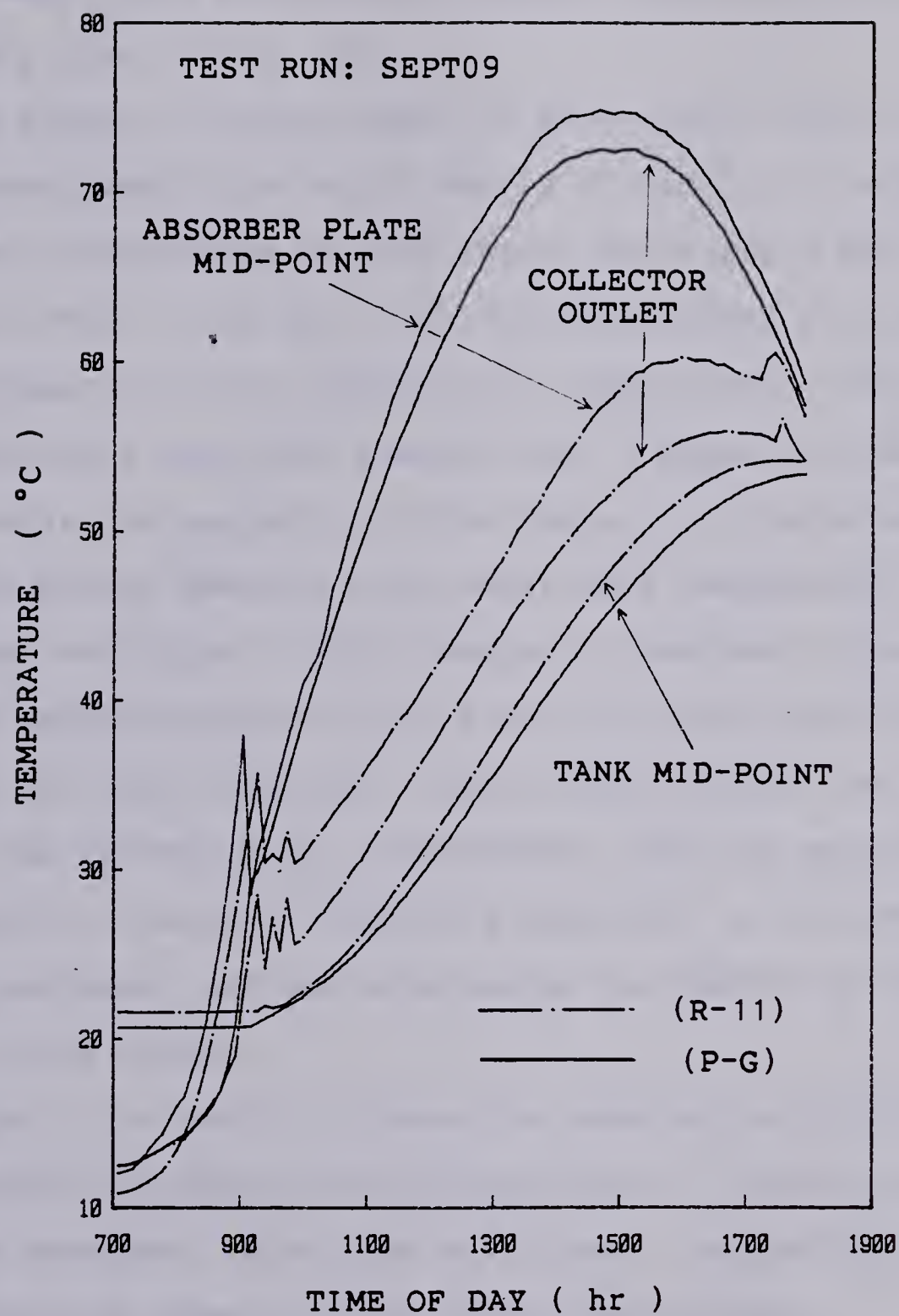


Fig. 2.9 Comparison of the temperature characteristics between the thermosyphon and hydronic systems.

hydronic system. It is interesting to note that the water tank temperature of the thermosyphon system reached a maximum value earlier, while the hydronic system was still gaining heat. This observation is also depicted in the efficiency plot in Fig. 2.4.

The effect of charge level is best shown with the instantaneous efficiencies of Eqs.(2.9) and (2.11) since the collector efficiencies are not known. The results are plotted in Fig. 2.10a and 2.10b for opening and closing of the downcomer from the accumulator, respectively. For the test conditions specified charge level 4 appears to be most effective at the beginning of the tests, but trails behind the other charge levels as the water tank temperature increases. Sufficient liquid charge is required to prevent complete vapourization but too much will cause more liquid to enter the heat exchanger. Lower liquid charge also reduces the thermal mass. Furthermore, the flow pattern and heat transfer characteristics are dependent on the amount of vapour generated, and are affected by the amount of liquid charge in the system.

Figs. 2.11a and 2.11b show the temperature profiles of a collector tube outer wall during tests at charge level 4 with the downcomer valve open and closed, respectively. Fig. 2.11c shows the case of lower charge level where superheating occurred. Boiling started first at the top section of the tube because of lower pressure. This is shown by the lower temperature at the top before 0900hr on Fig.

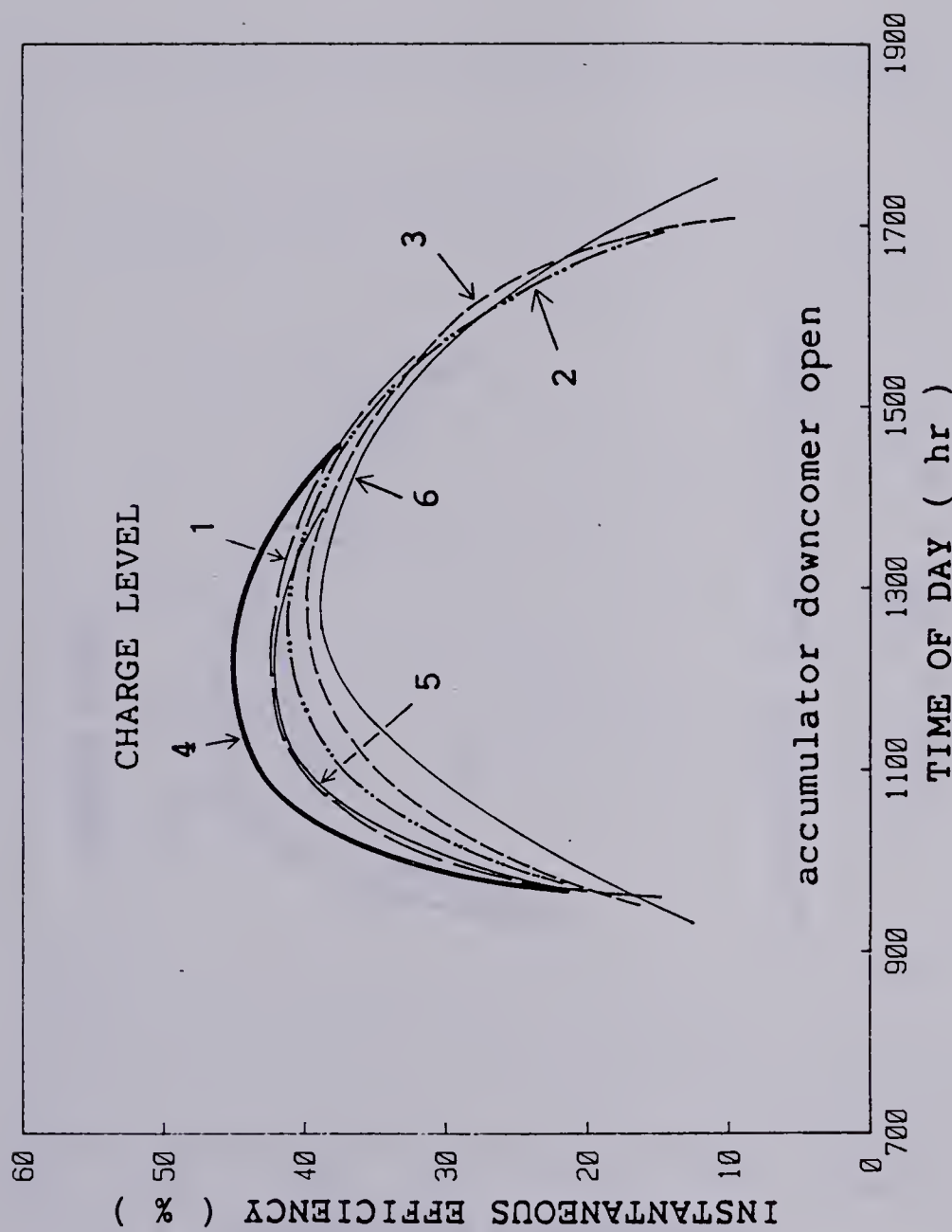


Fig. 2.10a The effect of liquid charge level on the instantaneous efficiency of the thermosyphon system.

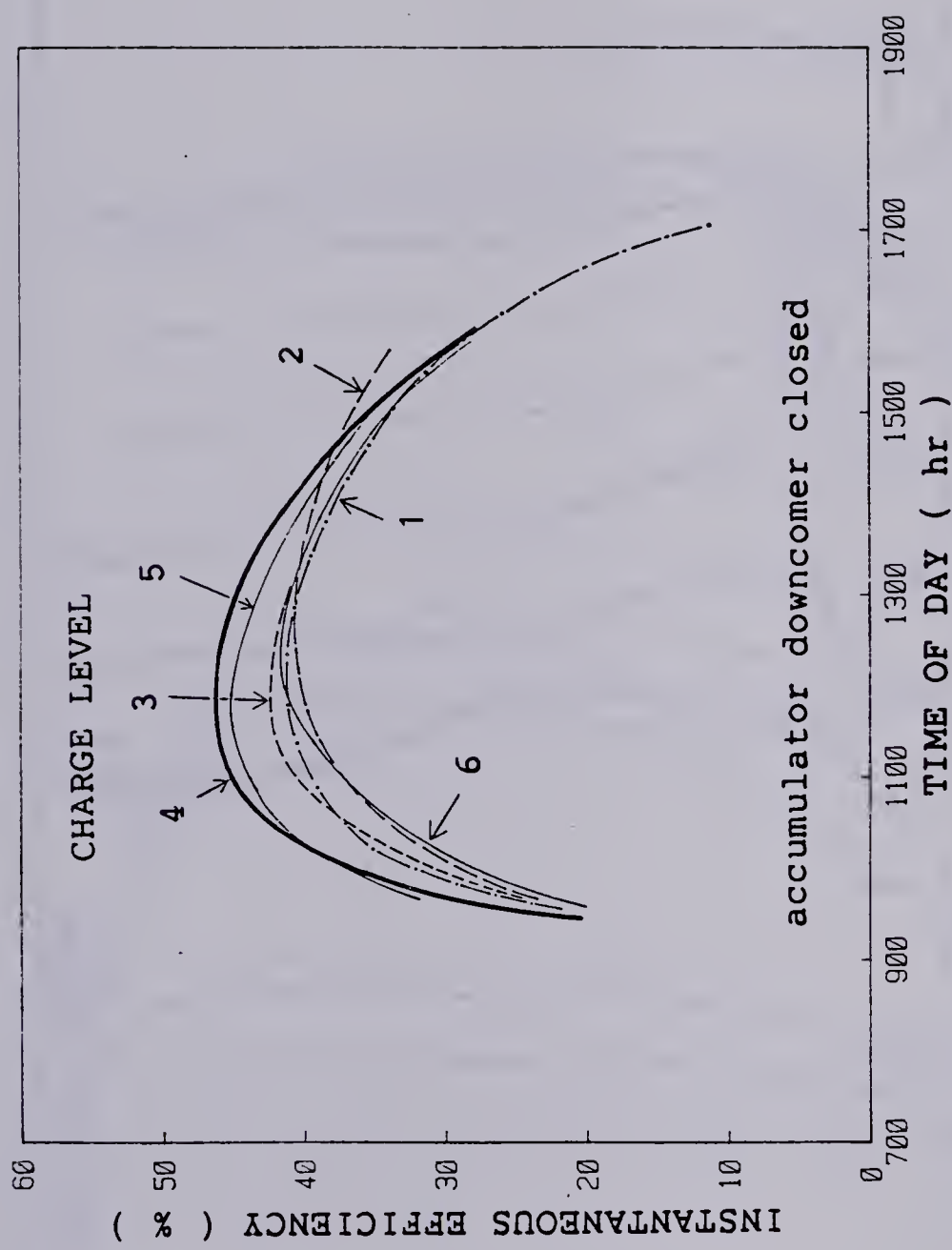


Fig. 2.10b The effect of liquid charge level on the instantaneous efficiency of the thermosyphon system.

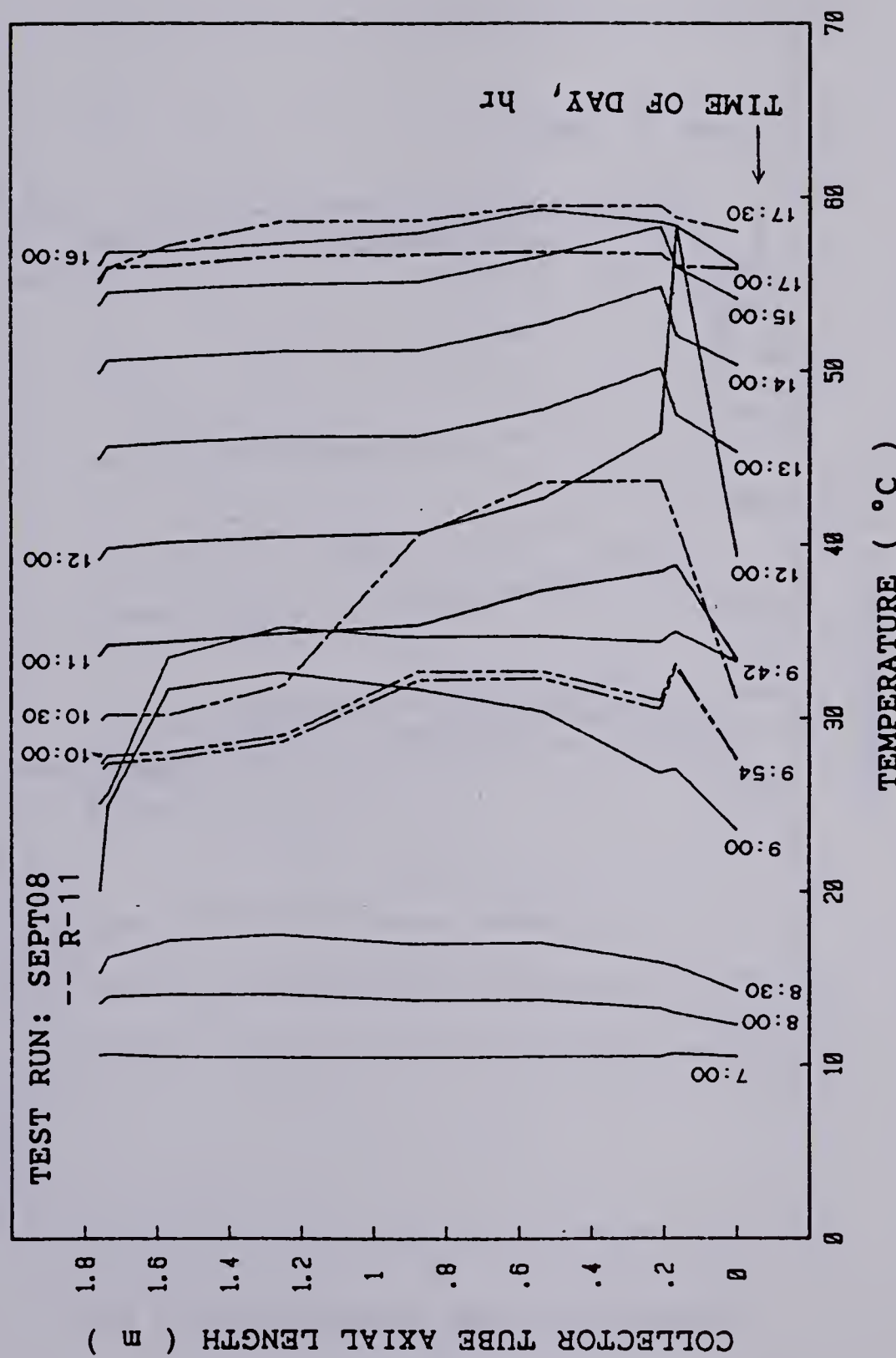


Fig. 2.11a Collector tube wall temperature distribution at different time of the day (charge level 4 with accumulator downcomer open).

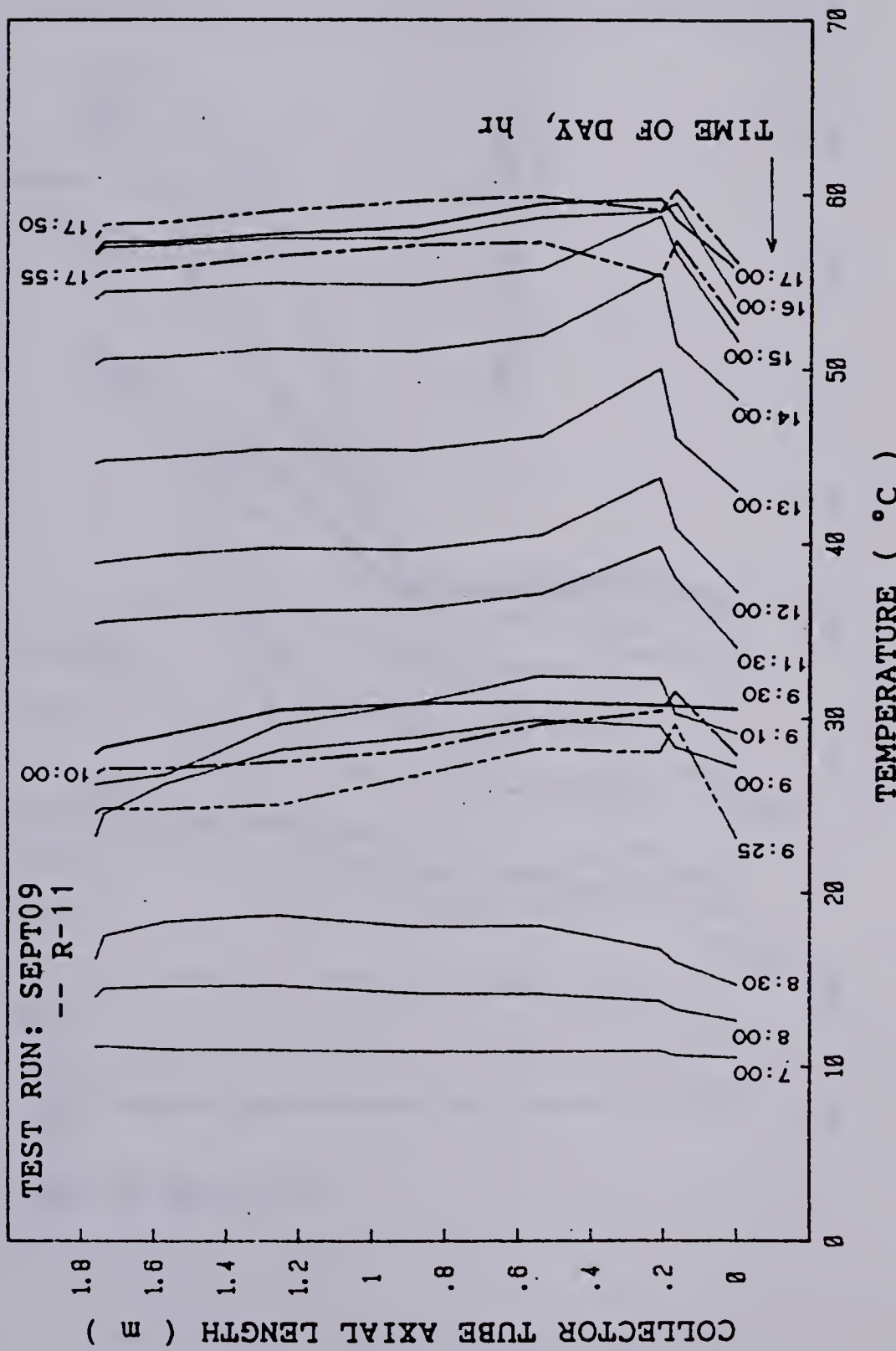


Fig. 2.11b Collector tube wall axial temperature distribution at different time of the day (charge level 4 with accumulator downcomer closed).

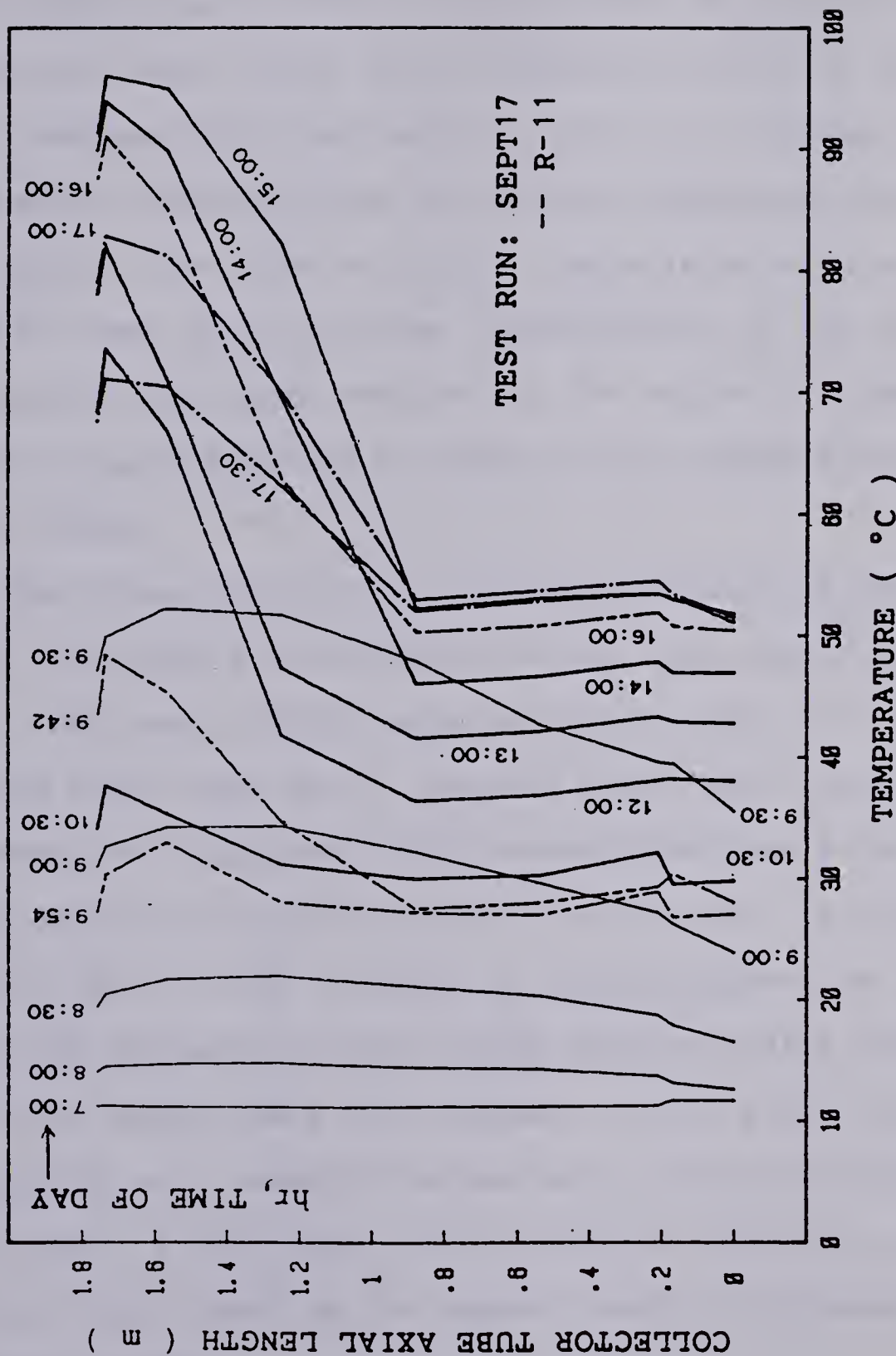
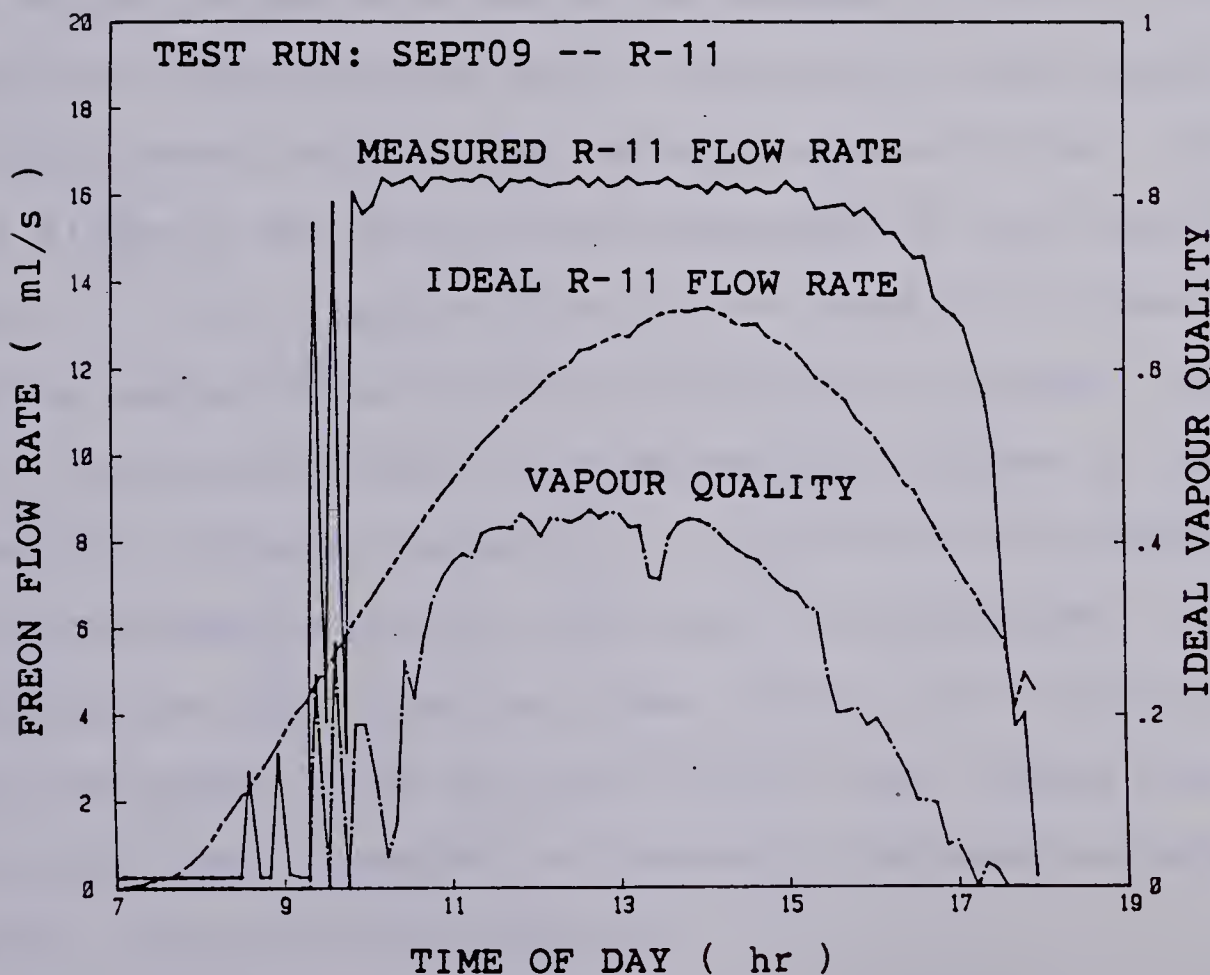
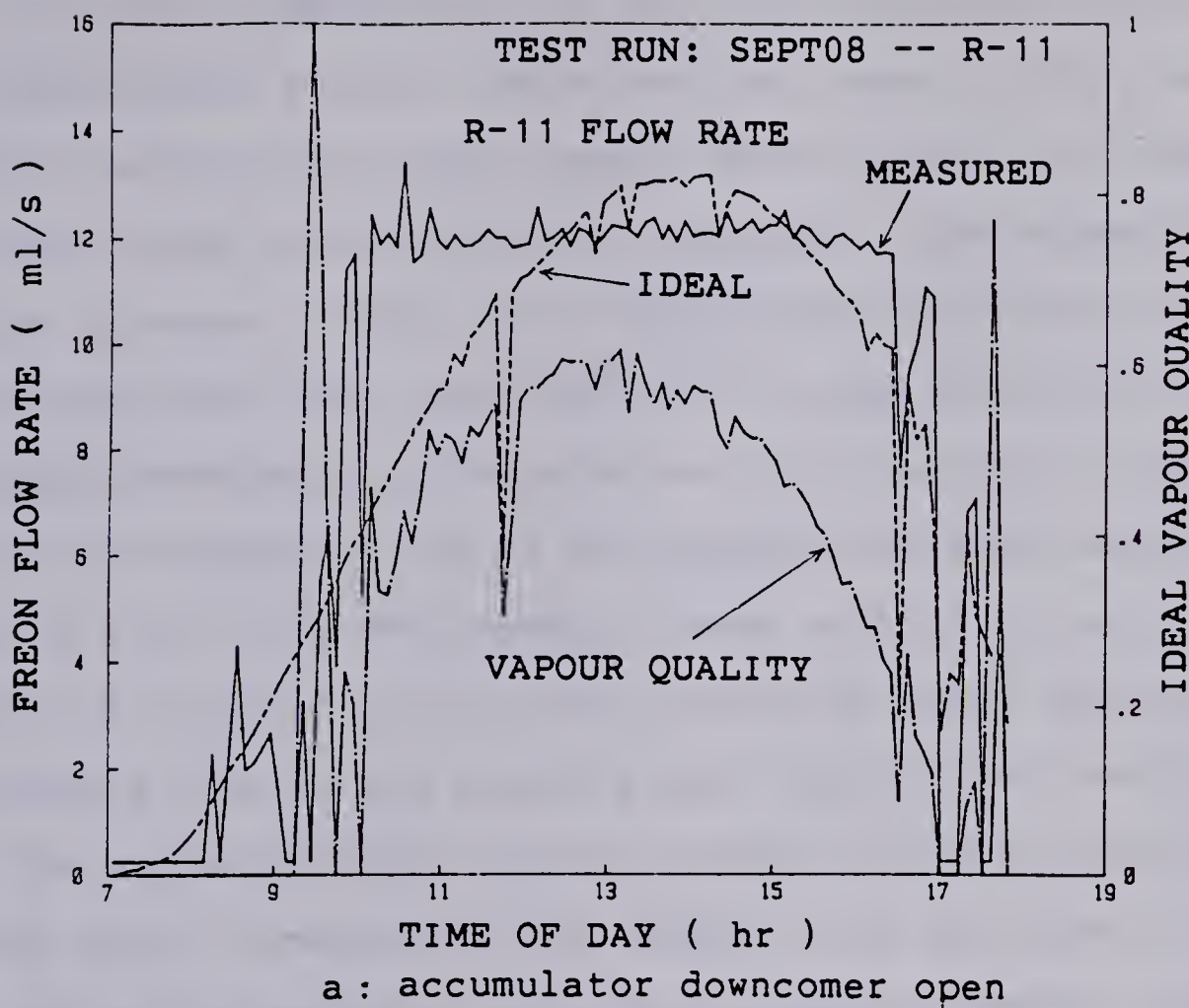


Fig. 2.11c Collector tube wall axial temperature distribution at different time of the day (charge level 1 with accumulator downcomer closed).

2.11a. The relatively isothermal surface when boiling was initiated is shown by the sudden drop in temperature from 0900hr to 0925hr on Fig. 2.11b, with higher temperature at the bottom section of the tube because of the lower single-phase heat transfer coefficient. Fluctuation in temperature was caused by the turning on and off of the water pump as explained earlier. Fig. 2.11c shows the increase in sensible heat and slight boiling at the top up till 0930hr, and then a drop in temperature with boiling started lower down the tube. Superheating of the vapour occurred in the upper section of the collector tubes at higher solar insolation as shown by the temperature profiles after 1200hr.

The Freon flow rate is inherently small as shown in Figs. 2.12a and 2.12b because of the high specific latent heat. The ideal quality calculated using Eq.(2.7) is seen to be much lower than unity, meaning heat loss from the heat exchanger was high and liquid entrainment was significant. Lower quality is expected when the downcomer is closed, as shown in Fig. 2.12b, because no liquid separation took place after the collector. Even though theoretically the Freon flow rate should vary with respect to the solar insolation during the day, measured values were relatively constant. The reason is not clear but it could be related to the rising liquid level as the vapour quality increases in the collector tubes.



b : accumulator downcomer closed

Fig. 2.12 Comparison between measured and idealized values of Freon flow rate and vapour quality.

In order to determine the heat loss characteristic of the thermosyphon system, tests were performed during the night by using electrically heated water to heat the Freon that was forced through the heat exchanger. The schematic diagram is shown in Fig. 2.13. Temperature distributions across the panel show that the Freon flowed upwards only in the tubes immediate to the inlet section, leaving a large portion of stagnant fluid in the middle and right section as shown in Fig. 2.13. The probable cause of this is the higher density of the cold fluid in the collector tubes resisting the upwards flow of the heated Freon with lighter density from the bottom manifold. This top-heavy situation resulted in flow only in portion of the tubes. It is not known if flow recirculation occurred in the stagnation region. Panel temperature distributions show a decreasing trend upwards in the tubes where Freon flowed through because of heat loss, and a slightly decreasing trend downwards in the stagnation region. A likely cause of this is heat conduction downwards from the heated Freon flowing through the top header. The heat loss characteristic is indeterminate because of the stagnation region encountered. It is believed this problem can be overcome by forcing the Freon flow downwards, i.e., reversing the flow direction shown on Fig. 2.13. This will allow the heated Freon to flow from the top, loses heat along the tubes downwards and return to the heat exchanger from the bottom of the collector.

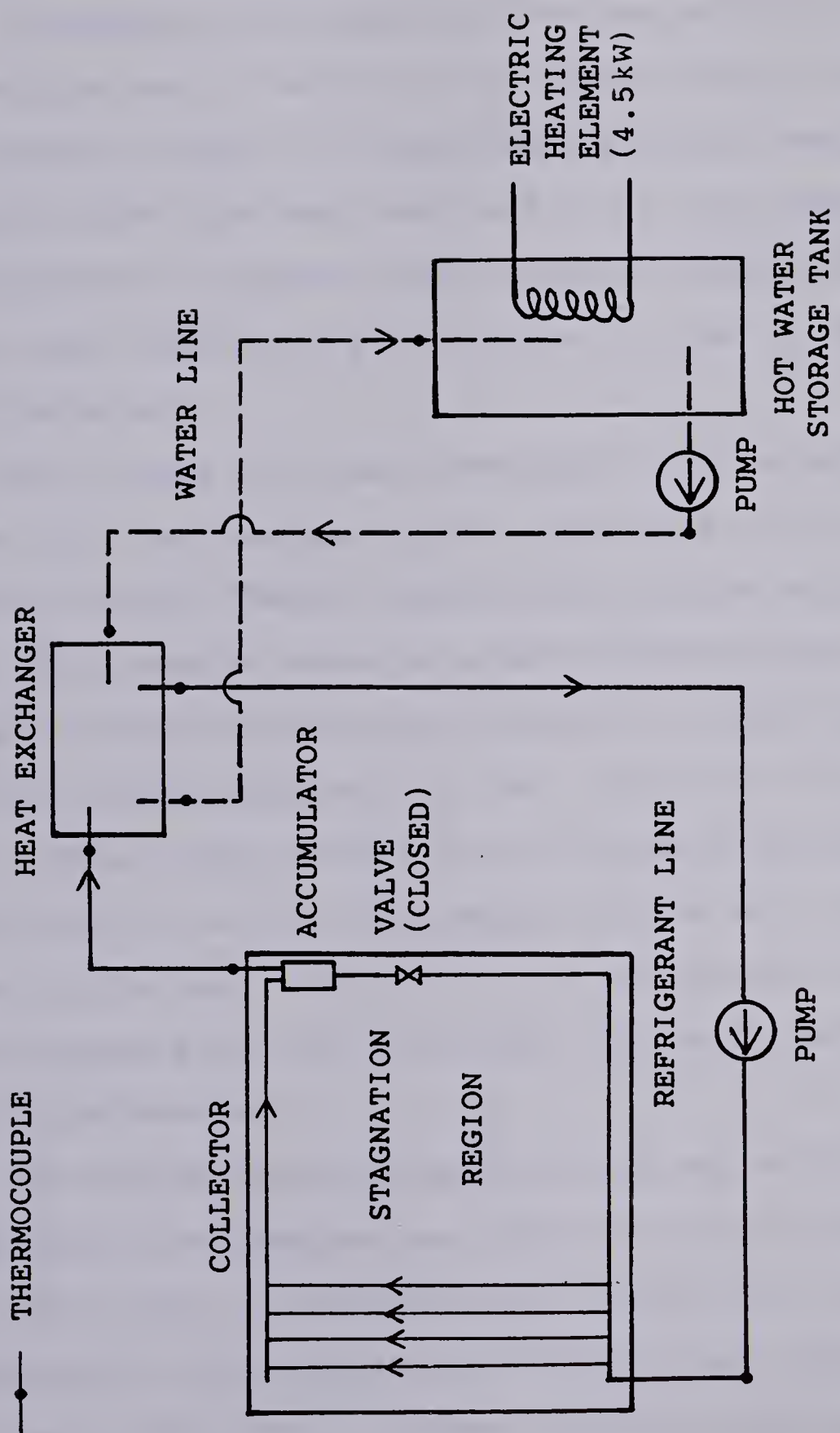


Fig. 2.13 Schematic diagram of experimental apparatus for heat loss test of the thermosyphon system.

2.5 Concluding Remarks

Simultaneous testing of thermal performance of a conventional hydronic system using propylene glycol solution and a two-phase thermosyphon system charged with Freon R-11 was carried out to determine the feasibility of operating the latter in place of single-phase systems. Results obtained under the same test conditions are comparable for both systems, but phase change systems charged with Freon offer other advantages such as totally passive, maintenance free operation.

Heat losses from the thermosyphon system ought to be lower since the absorber plate temperature is lower than the hydronic system tested. Results obtained are contrary to that. The probable causes are the different cover plate and absorber plate materials used resulting in different amount of solar energy absorbed, or poor insulation giving higher heat losses. Tests carried out to determine the heat loss characteristic of the thermosyphon system were unsuccessful. Measuring devices installed in the thermosyphon loop could have increased the flow resistance and contributed to the poorer performance.

The thermosyphon system performed better initially at lower water tank temperature but trails behind later in the day. This again is related to the higher heat losses at high temperature. Higher thermal performance can therefore be realized if hot water is drawn off during the day.

The effects of charge level and closing of the downcomer valve are not conclusive because the solar insolation is not identical in all cases. It is understood that liquid separation at the collector exit is desirable for two reasons: firstly the recirculated hot Freon liquid separated from the accumulator will keep the temperature at the inlet higher, therefore reducing the sensible heat gain required to initiate boiling; secondly higher vapour quality entering the heat exchanger reduces the chances of developing a liquid film on the condensing surface. For the tests carried out, charge level 4 appears to be most effective.

Measuring devices installed in the thermosyphon loop were kept to the minimum for fear of obstructing the Freon flow and affecting the thermal performance. This prevented a detailed analysis of the collector characteristics of the thermosyphon system. Further complication arises because of the uncontrollable solar insolation. An indoor testing facility of a similar phase change thermosyphon collector system heated electrically will overcome these drawbacks. A study of the effects of system components such as accumulator and liquid charge level using an indoor testing facility will be presented in Chapter 3.

**3. Some Operating Characteristics Of A Two-Phase
Thermosyphon Solar Collector System Using Freon R-11 By
Indoor Test**

Summary

The operating characteristics of a two-phase thermosyphon solar collector system with Freon R-11 as the working fluid were examined by electrically heating the absorber plate in an indoor test facility. The effects of the initial liquid Freon charge level, input heat flux to the absorber plate, expansion tank, accumulator for separating liquid and vapour, and cooling water flow rate on thermal performance were studied. Comparison of results between thermosyphon and forced circulation tests are presented. The governing parameters in evaluating the performance of these systems appear to be the vapour generated and the effective mass flow of Freon through the collectors. The vapour quality at the collector exit was evaluated by heat balance at the condenser. The experimental results show favourably the potential of operating phase change thermosyphon solar collector systems.

3.1 Introduction

The refrigerant charged two-phase thermosyphon systems for flat-plate solar collector applications in cold regions for hot water or space heating have received much interest and attention in recent years. Currently in the United States there are several commercial units available. Some thermal performance data on passive, refrigerant charged systems were reported recently [5,11,20,22]. The two-phase thermal processes in the collector tubes and heat exchanger located above the solar collector are of considerable practical and theoretical interest in the designing of such systems. Because of the intermittent nature of the solar radiation depending on weather conditions, it is not practical to study the various operating parameters on the thermal performance of the thermosyphon solar collector using an outdoor test facility. In view of this drawback, an indoor test facility was installed to carry out basic studies of the effects of various parameters on two-phase flow and heat transfer. For these systems, energy is transported in the form of latent heat in contrast to the sensible heat in the conventional solar collector systems, with the collector tubes acting as evaporators and the heat exchanger as a condenser.

This part of the study is concerned with some operating characteristics of the two-phase thermosyphon system with Freon R-11 as working fluid using an indoor test facility. Solar collector panels and heat exchanger developed by the

Solar Research Division of Refrigeration Research, Inc. were utilized in the primary loop.

Only steady state operating conditions considering the effects of the initial liquid refrigerant charge level, power input to the collector panels, expansion tank, accumulator for separating liquid and vapour, and cooling water flow rate in the heat exchanger were examined. The system was designed so that forced circulation tests could also be performed. The forced circulation test results were compared against those of thermosyphon tests.

It should be stressed that the present study is only concerned with the effects of some components on the system operation and not devised for rating collector performance. A proper solar simulator, recently addressed by Streed et al.[23], would require conformity with regards to solar spectral distribution and sky temperature, among others.

3.2 The Thermosyphon Indoor Test Facility

The Experimental Apparatus

A schematic diagram of the indoor test facility is shown in Fig. 3.1. The details of the Refrigeration Research™ two-phase thermosyphon solar collector system can be found in [20,22]. The facility consists of four 0.9 m^2 modules connected in parallel and each cover measures approximately 0.54 m wide by 1.86 m high. Each panel has 8 steel tubes (9.5 mm o.d., length 1.75 m). The heat exchanger has a continuous low-finned copper coil (15.9 mm o.d., linear

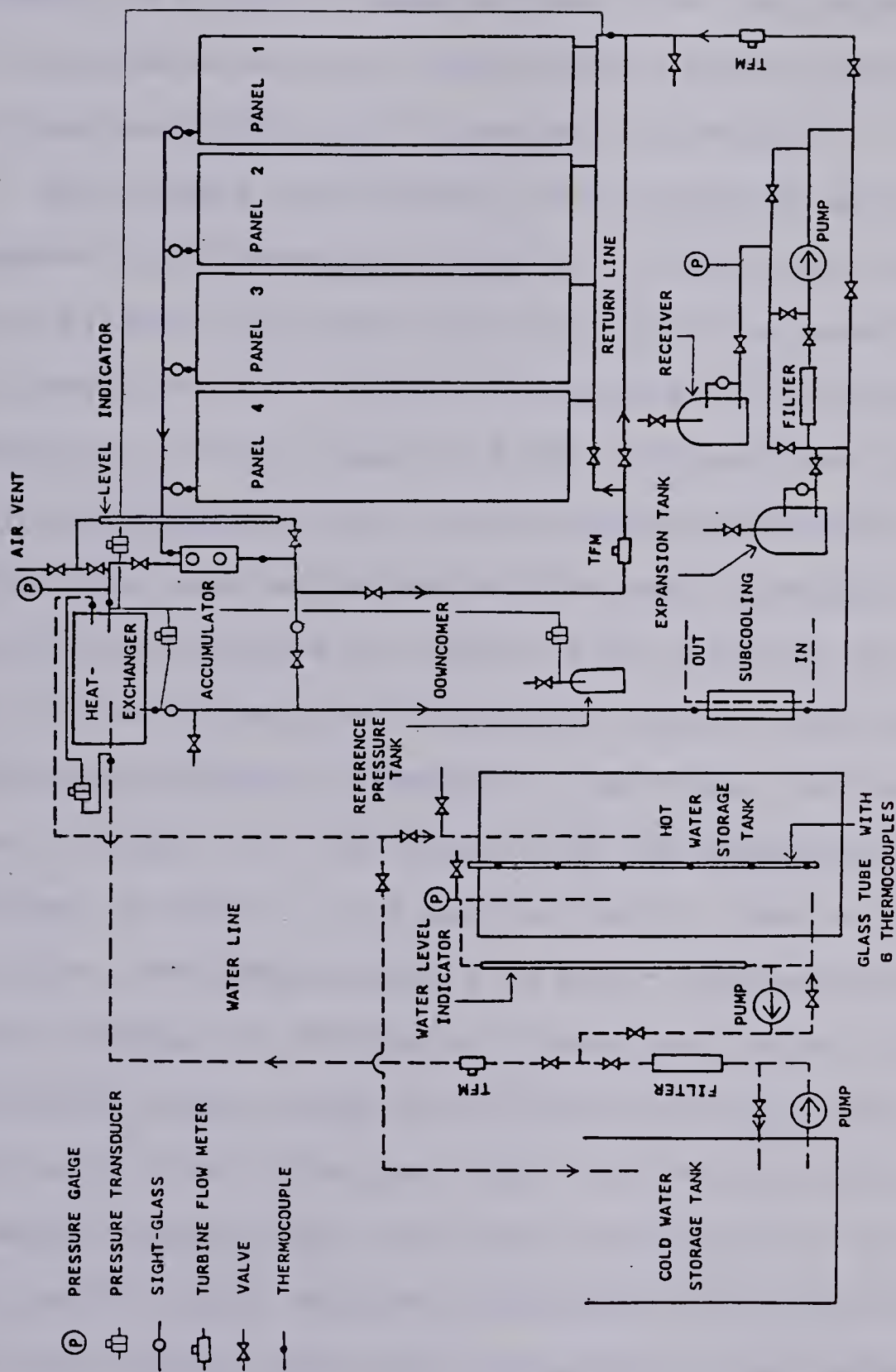


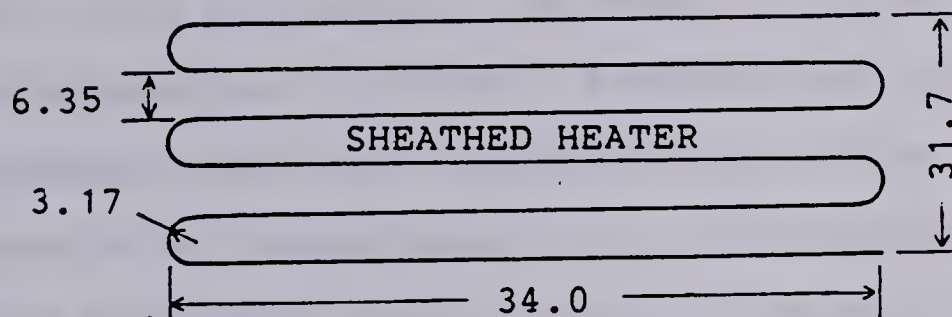
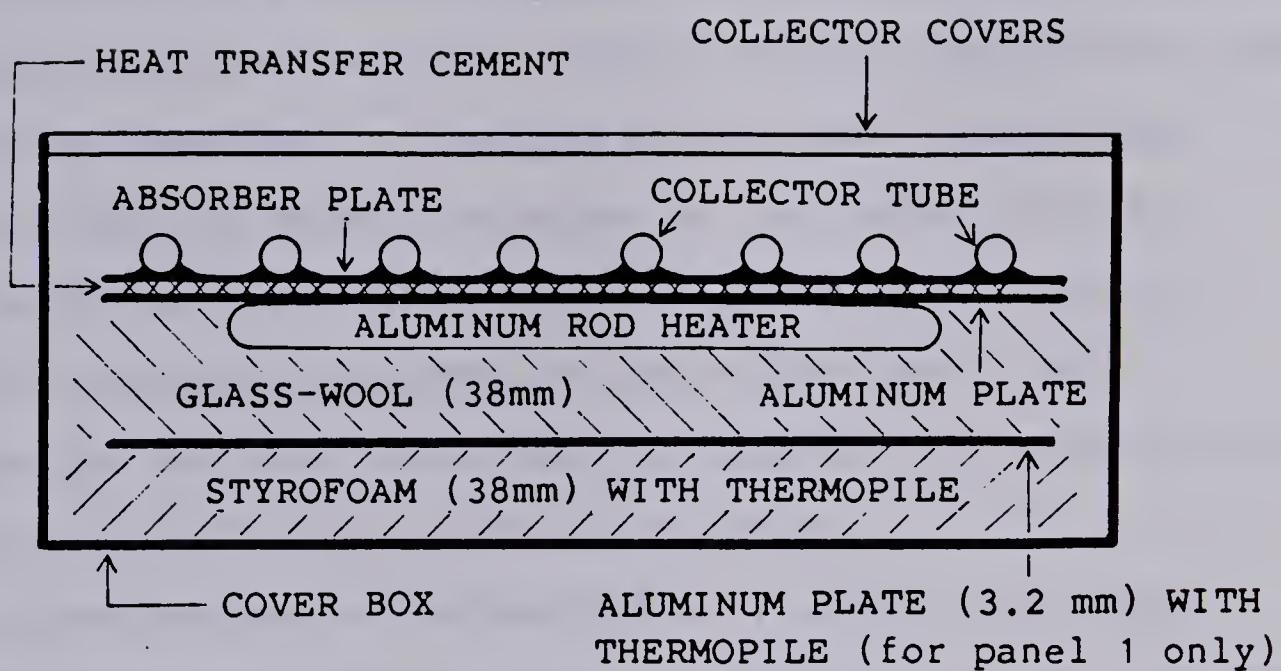
Fig. 3.1 Schematic diagram of two-phase thermosyphon flat plate solar collector indoor testing facility.

length 7.31 m) with an outer surface area of 0.91 m² and inner surface area of 0.25 m². Cooling water was pumped through the inside of the coiled copper tubing (coil diameter of 0.106 m) removing heat from the condensing Freon on the outside surface. The collector panels were set at inclination angle of 68° from the horizontal.

The primary refrigerant loop is passive and a pump is required in the secondary loop to circulate the cooling water between the large cold water tank (volume=1.27 cu.m) or a 248 litres hot water storage tank and the heat exchanger. A Procon pump (1/4 HP, 1725 rpm) was installed in the primary loop so that forced circulation tests (active system) may also be conducted. The heat exchanger was mounted 0.63 m above the top of the collector. As shown in Fig. 3.1 an accumulator with sight glasses was installed above the collector to separate the vapour and liquid as shown in Fig. 3.1. The liquid from the accumulator can be returned to panel 1 or 4 and the return line can be shut off to allow a two-phase mixture to enter the heat exchanger. Copper tubings of 15.9 mm o.d. were used for all the connecting tubes except the bottom manifold of the collector where a 12.7 mm tubing was used. A sight glass was installed at each collector exit for flow visualization. An expansion tank and a liquid receiver each measuring 0.22 m diameter and 0.41 m height were also connected to the primary loop. The cold water storage tank was used when the water temperature at the inlet of the heat exchanger was to be

kept constant. The hot water storage tank was used only for simulation tests under a no-draw condition, as in the tests outlined in Chapter 2. A 6.3 mm o.d. Pyrex tubing was used to indicate the initial liquid refrigerant charge level. All connecting tubes were insulated with Armaflex tubing insulation. System pressure measurements were taken with the help of a small reference pressure tank to provide the necessary differential pressure required.

In each collector panel, five aluminum sheathed rod heaters with a combined heating capacity of 1750 watts were used to heat a 3.2 mm thick aluminum sheet, which in turn heated up the absorber plate. The heaters, each measuring 6.6 mm o.d. and 2.32 m long, were spaced evenly and tied to the back of the aluminum plate. The aluminum plate was then attached to the back of the absorber plate with aluminum rivets and the gap between the plates was filled with heat transfer compound with high thermal conductivity (product of ZESTON®, grade Z-10) to provide uniform heating. The backside of the heaters was insulated with 38 mm thickness each of glasswool and styrofoam as shown in Fig. 3.2. A thermopile with 25 uniformly distributed junctions was attached across a 3.2 mm thick aluminum plate and then inserted between the two layers of insulation in panel 1 to measure heat loss through the back. A similar thermopile was also installed on the styrofoam insulation layer, instead of an aluminum plate, for each of the remaining three panels.



DIMENSIONS IN cm

Fig. 3.2 Cross section of collector and heater arrangement, and plan view of a heating element depicting the dimensions.

Instrumentation

The heating power for each panel was set using a controller with a maximum output of 1500 watts and the total wattage input was measured with two digital wattmeters; one wattmeter measured the heating power input of one fixed panel while the other the inputs of the three remaining panels by using switching devices. There is an error of $\pm 0.5\%$ in wattage measurements due to the power input controller and also a $\pm 2\%$ wattage fluctuation caused by the line voltage fluctuation in the building.

Iron-constantan thermocouples (0.225 mm o.d.) with glass fiber cloth covers were spot welded onto the absorber plate and collector tubes to measure the surface temperature distribution at a total of fourty-nine locations, nineteen on panel 1 and ten each on the remaining three panels. Room temperature and all fluid bulk temperatures in the primary and secondary loops were measured using 0.7 mm o.d. sheathed iron-constantan thermocouples. All thermocouples were initially calibrated using a quartz thermometer (HP-2807A). A maximum error using a linear correlation between output voltage and temperature is $\pm 0.3^\circ\text{C}$.

The thermopile measurements at the back of the collector panel showed that the heat loss through the back is approximately linear with respect to the heat input (0.2 - 1.1 kW) and this heat loss was less than 10 percent of the total heat input.

System pressure was monitored with two pressure gauges; one at the top beside the heat exchanger and another at the bottom on the same level as the Freon circulation pump. Validyne™ differential pressure transducers with sensitive diaphragms were used to measure the system pressure near the heat exchanger as well as pressure drops across the four collector panels and the heat exchanger for the Freon and water loops. For the pressure drop measurement across the four panels, the transducer was located at the top of the collector panel and the connecting tubes were cooled with water during experiments. Sight glasses were installed in the connecting tubes near the pressure taps for visual confirmation of liquid in the lines. Short connecting tubes were used to minimize the static pressure changes on the diaphragms, which affect the initial pressure offset reading, caused by a density change of the liquid in the connecting tubes. All transducers were calibrated using water or mercury manometers depending on the diaphragms used. The maximum error for the transducers is estimated to be 1.1 kPa.

Flow measurements of liquid Freon flow rates from the heat exchanger and the accumulator, and the cooling water flow rate in the heat exchanger were achieved using turbine flow meters. These meters were calibrated using water and Freon R-113 since Freon R-11 vapourizes very easily at room temperature. Rotameters (flow rate 0.05 - 0.40 Water GPM) installed initially to measure flow distribution to each

collector panel were subsequently discarded due to severe flow restrictions and lower accuracy. The turbine flow meters measure liquid flow rates in the range of 3 - 60 ml/s with a ± 0.5 percent error.

Experimental Procedure

The evacuation of air, leakage test, pressure testing at 500 kPa (72 psig) and the charging of the liquid refrigerant into the two-phase system followed the usual refrigeration practice. The system was occasionally charged fully with liquid Freon in order to purge any air trapped in the system before the experiment. The experimental conditions such as the system pressure and the initial liquid charge level were set a day before the experiment. The large cold water tank was filled just before the experiment with cold tap water.

Data under the set initial conditions were taken at the start of each experiment to ensure proper functioning of all electronic devices and to obtain the initial readings. The water circulation pump was then turned on with the heating power set at a pre-assigned value. Data were subsequently taken every five minutes until reaching steady state. The heating power input for each panel was set at the same value. Steady state was confirmed by a constant system pressure at the collector outlet. At least ten readings were taken for each measurement to obtain the average value. A HP-85 micro-computer and a HP-3497A data acquisition system

were used for data collection. All the readings are stored on magnetic tapes for further analysis. The above procedure was repeated up to a heating power input of 1.1 kW per panel or until the experiment was terminated when the heater surface temperature exceeded 130°C in order to operate within the safe range of the electric heaters. Measurements, such as liquid Freon and cooling water flow rates and system pressure, were recorded on strip chart recorders for observations on transient behaviour and the confirmation of steady state during the experiment.

Two series of tests were carried out. The first series involved constant cooling water flow rate while varying the heating power input to the collector panels. The effects of the initial liquid refrigerant charge level, expansion tank, downcomer from the accumulator and the liquid Freon returning to panel 1 or 4 from the accumulator were studied. Only thermosyphon condition was considered in these tests. The second series of tests was performed with a constant heating power input while varying the cooling water flow rate for both natural and forced circulation conditions. The initial charge level was maintained constant except for the cases where superheating at the collector tube exit was desired. Forced flow operation required that the downcomer from the accumulator be closed off and the by-pass valve shown on Fig. 3.1 was used to control the Freon volume flow rate through the heat exchanger.

3.3 System Characteristics And Efficiency

Under steady state condition, the total heat transfer rate Q_c to the Freon in the collector tubes is given by

$$Q_c = \bar{m}_l [Cp_l(T_s - T_{ci}) + x_0 h_{fg} + Cp_v(T_{co} - T_s)] \quad (3.1)$$

The terms on the right-hand side represent sensible heat of liquid, latent heat of vapourization and sensible heat of superheated vapour, respectively. Since the true value of the vapour mass quality x_0 at the exit of the collectors cannot be determined readily in the experiments due to liquid entrainment in the vapour flow, an approximated value of Q_c can be obtained by considering the heat transfer rate Q_w to the cooling water in the heat exchanger, defined as

$$Q_w = \bar{m}_w \cdot Cp_w \cdot (T_{wo} - T_{wi}) \quad (3.2)$$

Noting that the total heat input is $Q_i \cdot A_c$, a system efficiency η_s of the two-phase thermosyphon system can be defined as

$$\eta_s = Q_w / (Q_i \cdot A_c) \quad (3.3)$$

The absolute error in calculating η_s depends on the temperature drop of the water flowing across the heat exchanger, ΔT_w . For $\Delta T_w = 10^\circ\text{C}$, the error is ± 9 percent; for $\Delta T_w = 20^\circ\text{C}$, the error is ± 6 percent.

In this study, the liquid Freon mass flow rates from the heat exchanger and accumulator, \bar{m}_{l1} and \bar{m}_{l2}

respectively, were obtained from measurements using turbine flow meters. Thus, the experimentally determined vapour quality at the collector exit could be evaluated by

$$x'_0 = \bar{m}_{\ell 1} / (\bar{m}_{\ell 1} + \bar{m}_{\ell 2}) \quad (3.4)$$

A better approximation is desirable because some liquid was expected to be carried over from the collector to the heat exchanger, especially when the liquid level is high. By neglecting the heat loss from the heat exchanger and all preceding connecting tubes, the vapour quality x_1 at the entrance of the heat exchanger was estimated by

$$x_1 = [Q_w / \bar{m}_{\ell 1} - C_p \ell (T_{hi} - T_{ho})] / h_{fg} \quad (3.5)$$

Considering the liquid entrainment part, $\bar{m}_{\ell 1}$, can be written as

$$\bar{m}_{\ell 1} = \bar{m}_{\ell 1, v} + \bar{m}_{\ell 1, l}$$

where the subscripts v and l signify the vapour and liquid entrainment part, respectively, resulting in a better approximation for x_0 given as

$$x_1 = \bar{m}_{\ell 1, v} / \bar{m}_{\ell 1}$$

$$x_0 = \bar{m}_{\ell 1, v} / (\bar{m}_{\ell 1} + \bar{m}_{\ell 2}) = x'_0 \cdot x_1 \quad (3.6)$$

The true quality therefore lies between x'_0 and x_0 , with x_0 approaching x'_0 when the collector exit vapour quality is

high.

The average heat transfer coefficient in the collector tubes may be defined as

$$\bar{h} = Q_c / (A_t \cdot \Delta T) \quad (3.7)$$

where the logarithmic mean temperature difference ΔT is defined as

$$\Delta T = \frac{(\bar{T}_t - T_{ci}) - (\bar{T}_t - T_{co})}{\ln [(\bar{T}_t - T_{ci}) / (\bar{T}_t - T_{co})]}$$

For the shell and coil heat exchanger, the overall heat transfer coefficient, U , is given as

$$U = Q_w / (A_w \cdot \Delta T) \quad (3.8)$$

where

$$\Delta T = \frac{(T_{ho} - T_{wi}) - (T_{hi} - T_{wo})}{\ln [(T_{ho} - T_{wi}) / (T_{hi} - T_{wo})]}$$

The initial Freon charge level was taken as a percentage of the vertical distance between the bottom manifold of the collector and the horizontal axis of the heat exchanger. A 100 percent charge therefore means the shell of the heat exchanger was half filled with liquid Freon.

3.4 Results And Discussion

Some Experimental Observations

The present experimental set-up was designed so that the liquid separated at the accumulator can be returned to the manifold near panel 4 or be merged with liquid return line from the heat exchanger to the bottom manifold entrance near panel 1 as shown in Fig. 3.1. When the hot Freon liquid from the accumulator was returned near panel 4, an uneven flow distribution for each panel and system pressure fluctuation at higher heating power input was observed; the higher vapour quality can also be seen through the sight glasses at the collector exit, and in some cases, dry out condition in panels 3 and 4. The pressure fluctuation may be caused by the top-heavy situation due to the higher temperature, and hence lower density, of the separated hot liquid returning to the bottom of the collector tubes. The higher temperature of the returned liquid from accumulator also resulted in higher exit vapour quality in these panels. When the hot Freon liquid from the accumulator was mixed with condensed cold liquid from the downcomer of the heat exchanger, the observed instability problem was seldom encountered.

A small amount (140 gm) of internal refrigerant leak detector Trace™ was added to the primary loop to facilitate visual observation through the sight glass installed at the exit of each collector panel. With the addition of dye, the liquid refrigerant appears reddish in colour. Since the dye

has a higher boiling point than the refrigerant, one expects that only small amount of dye, due to liquid entrainment, will be carried over to the heat exchanger and most dye will be separated at the accumulator. Thus, when the separated hot Freon liquid was returned to the lower manifold near panel 4, a deep red colour showing highly concentrated dye was seen through the sight glass at the exit of panel 4 and occasionally through the sight glass of panel 3 as compared to the clear bubbling liquid seen in the remaining sight glasses. When hot Freon liquid was returned to the manifold near panel 1, this phenomenon was seldom observed. However, when it did occur, the red dye concentration could occur in any of the four panels. The exact cause of this seemingly erratic phenomenon is not well understood at present. With higher dye concentration in one panel, one may expect the increase of collector tube wall temperature and superheating of Freon at the top section of the tubes. The phenomenon of thermal instability is beyond the scope of this study.

Effect of Initial Liquid Refrigerant Charge Level

Referring to Fig. 3.1, a charge level of 75 percent corresponds to the level of the sight glasses above the collector panels, 71 percent corresponds to half way between the two sight glasses of the accumulator, 67 percent represents the level of the bottom sight glass of the accumulator and 59 percent represents a level below the accumulator.

Fig. 3.3 shows the effect of initial charge level on the axial temperature distributions along the top surface of one representative collector tube for three wall heat fluxes to the absorber plate. Although the tube circumferential temperature is not uniform since heating was done from the back of the absorber plate, measurements show that the difference in temperature between the top of the steel collector tube and the pure copper bond near the absorber plate is less than 1.5°C . Thus, the axial temperature distributions provide a good indication of the two-phase flow patterns and heat transfer regions inside the collector tubes. The tube wall temperature increases from the bottom manifold up to the beginning of bubbly flow, and reaches a fairly uniform temperature in the saturated nucleate boiling regime. Since the fluid pressure decreases axially, the wall temperature also decreases axially signifying the decreasing saturation temperature of the Freon. A large portion of the heat transferred occurred isothermally as seen by the relatively constant temperature over two thirds of the collector surface. At higher charge level, the system pressure increases for a given heating power input, hence the saturation temperature and the wall temperature increase accordingly. It is noted that higher collector tube wall temperature leads to higher heat losses. Apparently, the effect of the initial liquid charge level also depends on the value of the input heat flux, Q_i .

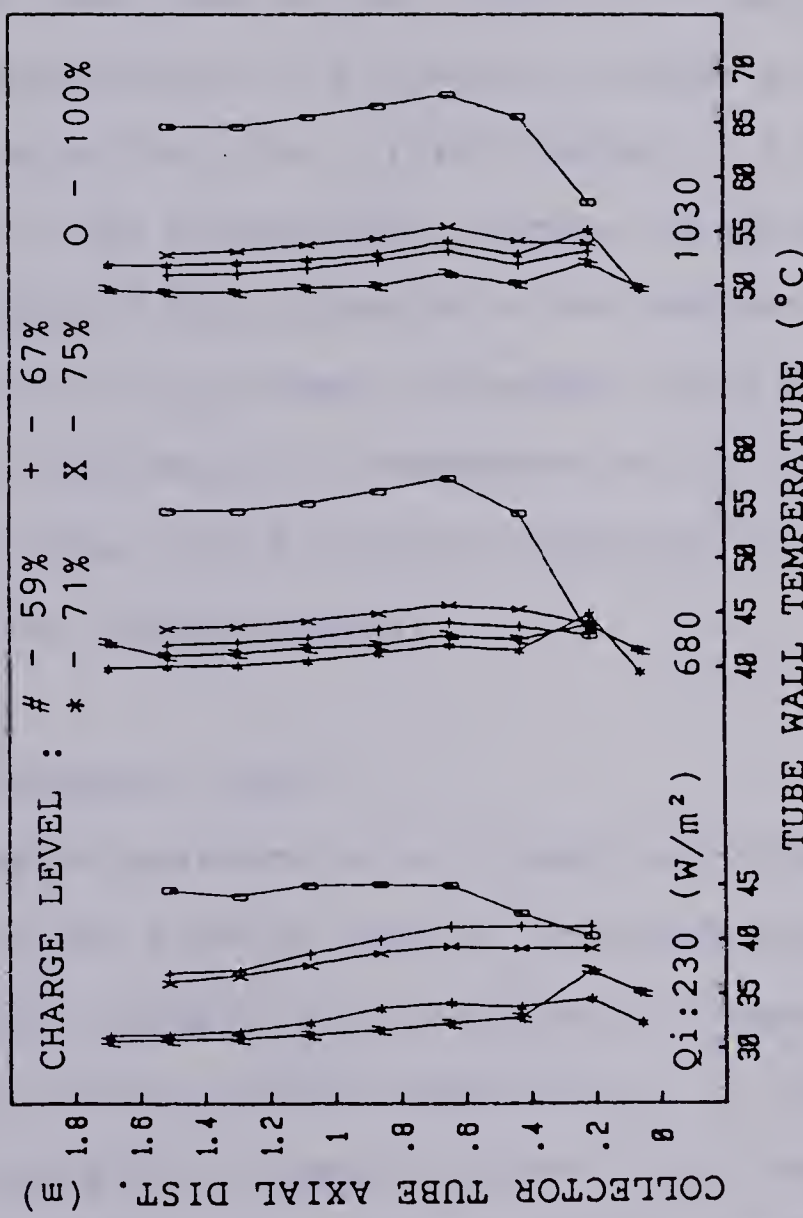


Fig. 3.3 Effect of heat input and charge level upon the collector tube wall axial temperature distribution (cooling water flow rate at 40 ml/s).

The effect of charge level on system efficiency, η_s , is shown in Fig. 3.4. It is seen that at 71 percent charge level, η_s is fairly uniform over a range of input heat fluxes. Above the value of $Q_i = 0.8 \text{ kW/m}^2$, 67 percent charge level gives better performance up to a tested value of $Q_i = 1.15 \text{ kW/m}^2$. At 100 percent charge level, the heat exchanger is flooded and η_s is lower as expected. A change of the liquid level upon heating and evaporation may have caused the higher efficiency of 67 percent charge at high Q_i . Keeping in mind that the initial charge of 71 percent is at the middle of the accumulator, vapour volume may have pushed this level beyond the accumulator and reduced the vapour quality going into the heat exchanger. This suggests that the thermal performance is dependent on the location of the accumulator, the liquid thermal expansion and the specific latent heat of vapourization.

Effect of Expansion Tank

The system pressure of a closed loop thermosyphon is dependent on the cooling rate at the condensing end. The pressure will increase until saturation temperature, T_s , exceeds the cooling medium temperature, T_w . An ideal situation would be to keep T_s close to T_w , and this may be achieved by adding an expansion tank to the system. Fig. 3.5 shows the results for η_s and system pressure of the system operating with and without an expansion tank at 100 percent charge. At high input heat flux, higher boiling rate causes

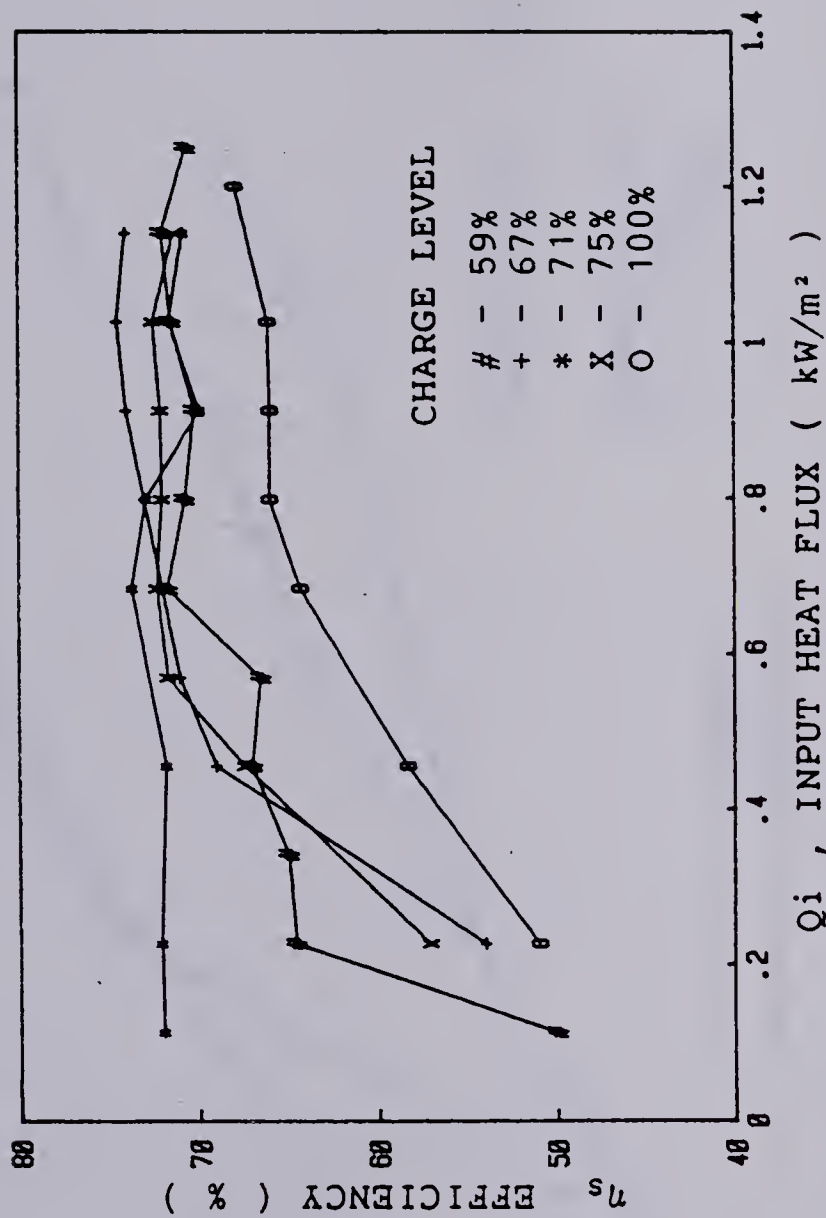


Fig. 3.4 Effect of charge level on the system efficiency at different heat input (cooling water flow rate at 40 ml/s).

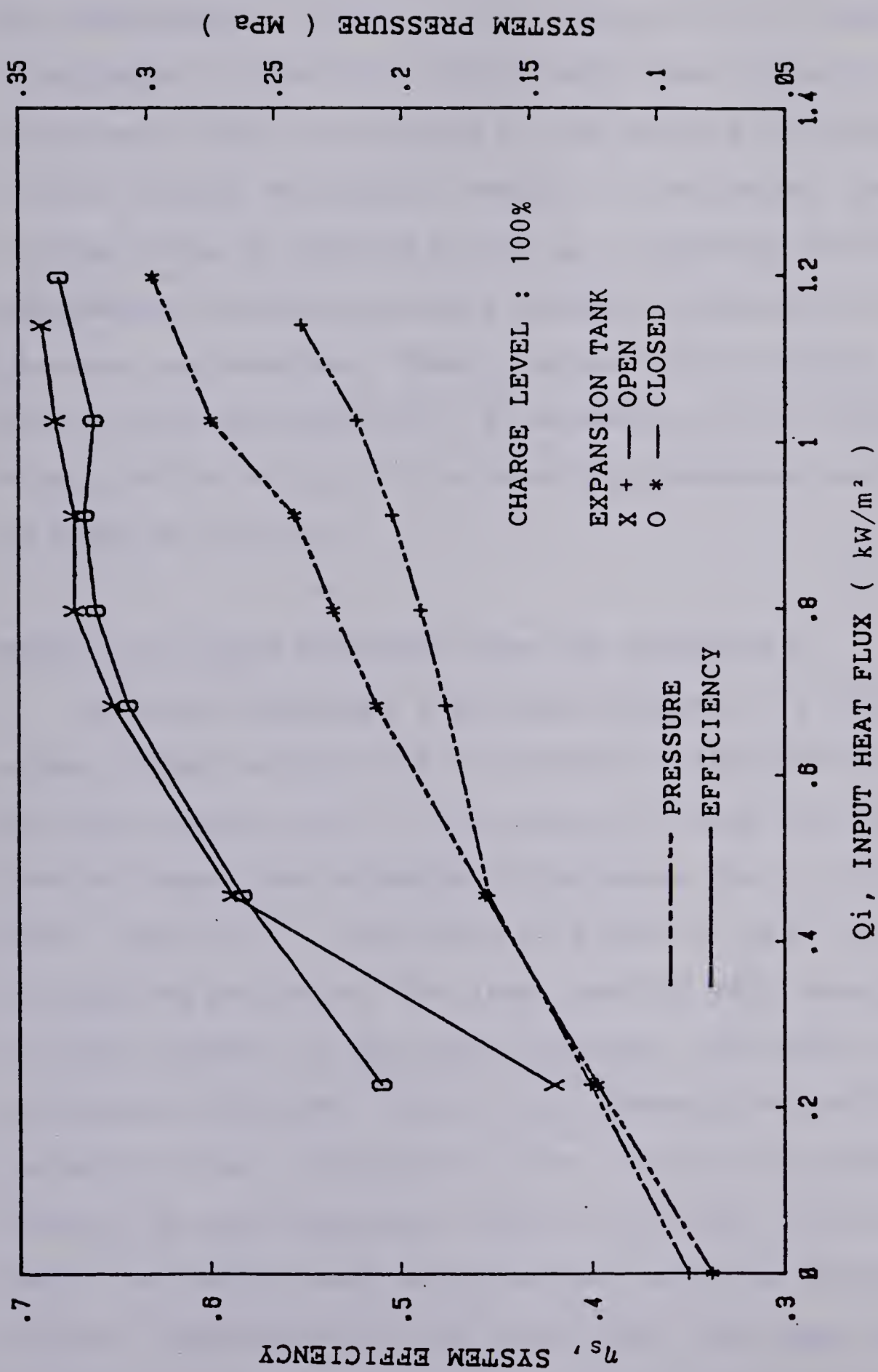


Fig. 3.5 Effect of expansion tank on system efficiency and pressure at 100 percent charge (cooling water flow rate at 34 ml/s).

the pressure to rise and η_s increases to an asymptotic value. The lowering of pressure in the former case is due to the compressible volume in the expansion tank, resulting in a decrease in effective liquid charge when pressure increases. This is analogous to the effects of different initial liquid refrigerant charge in the system. During the initial stage of heating at low Q_i , a periodic bursting phenomenon characterized by a sudden increase of the system pressure was observed. These fluctuations are damped to some extend with the addition of an expansion tank. The flow visualization study of this bursting phenomenon was reported by Cheng et al.[24].

Effect of Liquid Downcomer From the Accumulator

When the downcomer from the accumulator is closed, the vapour-liquid mixture will be forced up the heat exchanger and the pressure drop in the connecting tube between the heat exchanger and accumulator increases due to two-phase flow, resulting in a decrease in effective mass flow rate through the collector. The lower quality will cause a drop in heat transfer in the heat exchanger. The effect of the accumulator downcomer on the axial temperature profiles of a collector tube is depicted in Fig. 3.6 for two charge levels, 59 and 75 percent, with Q_i at 0.228, 0.684 and 1.026 kW/m^2 . At charge level of 59 percent and with downcomer closed, superheating in the region near the upper manifold is clearly shown. The tube wall temperature near the bottom

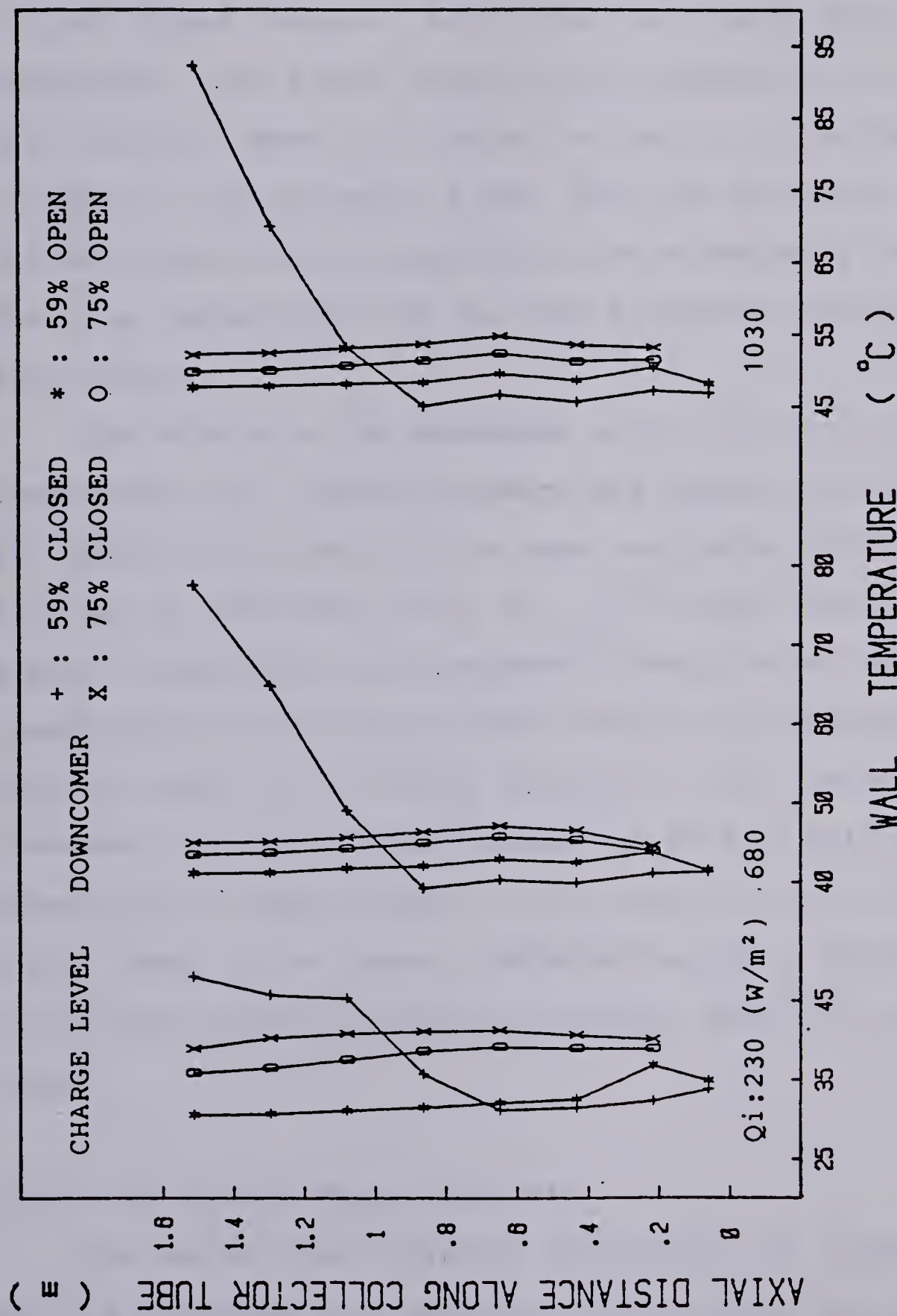


Fig. 3.6 Effect of liquid separation at collector exit, with an accumulator, upon the collector tube wall axial temperature distribution (cooling water flow rate at 40 ml/s).

manifold is lower with the downcomer closed because of higher subcooling in the heat exchanger in this case. This effect is less prominent at 75 percent charge because the initial liquid charge at this level is already above the accumulator. The higher subcooling of liquid at the inlet of the collector leads to a longer section of single phase heat transfer in the collector tubes. With the downcomer open, the hot liquid Freon separated at the accumulator increases the inlet temperature and the liquid therefore reaches T_s much sooner.

The effects of the downcomer on the collector exit temperature, T_{co} , system pressure and system efficiency, η_s , are shown in Fig. 3.7 for the same two charge levels as a function of input heat flux, Q_i . It is noted that at 59 percent charge and with downcomer closed, the collector exit temperature is relatively higher because of superheating. This is caused by the higher pressure in the system when the downcomer is closed. This reduces the rate of boiling and generation of vapour, and in turn lowers the effective liquid level in the tubes. The behaviour of η_s depends also on Q_i which directly affects the vapour quality in the tubes.

Effect of Cooling Water Flow Rate

The overall heat transfer coefficient, U , computed from Eq.(3.8) was used as a parameter to determine the efficiency of the test unit at different operating conditions. The U

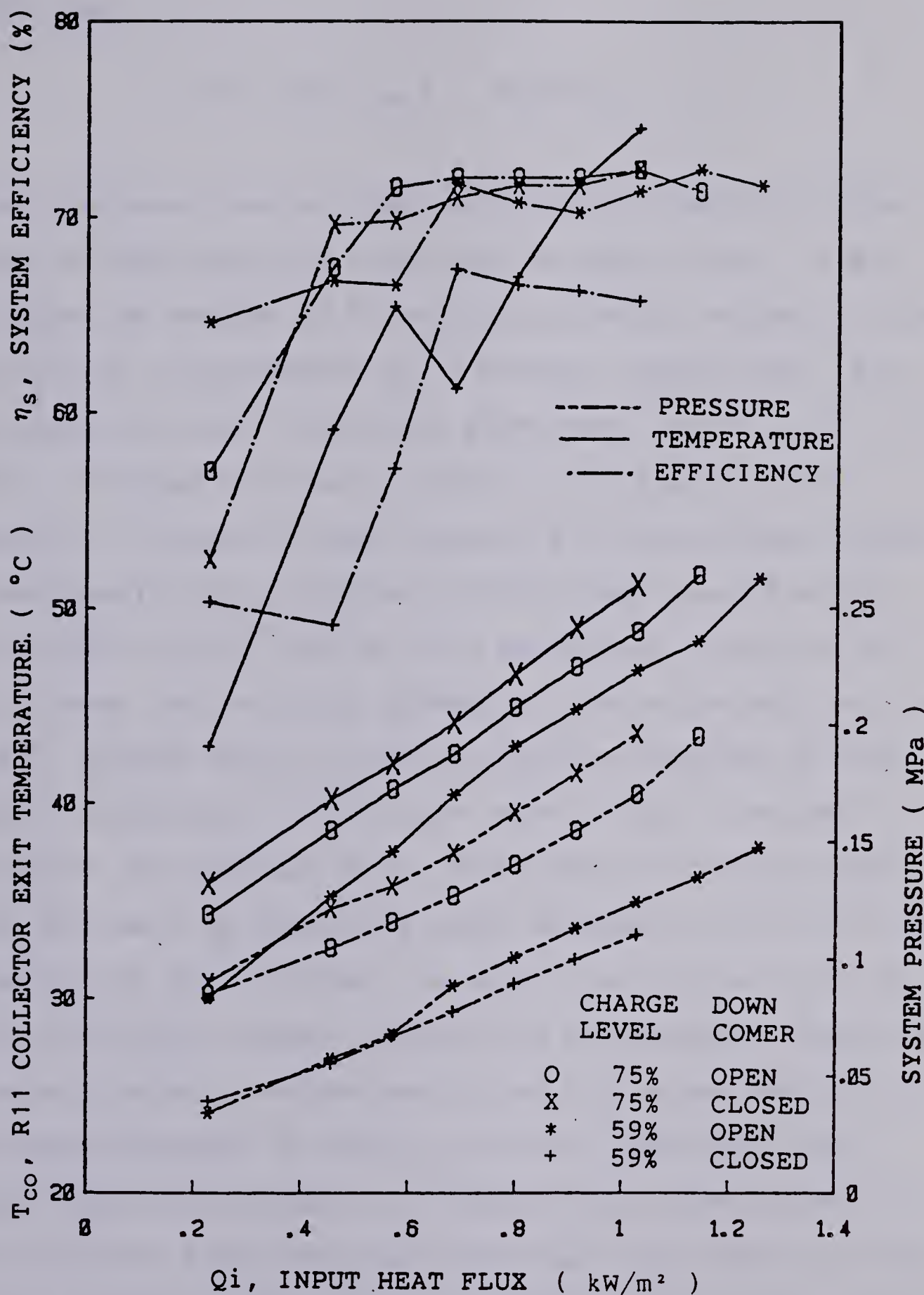


Fig. 3.7 Effect of liquid separation at collector exit, with an accumulator, upon the system performance (cooling water flow rate at 40 ml/s).

value computed using the arithmetic mean temperature difference

$$\Delta T = [(T_{hi} + T_{ho}) - (T_{wi} + T_{wo})] / 2$$

gives the same trend as that of Eq.(3.8), therefore either value is sufficient for comparison purpose. Figs. 3.8 and 3.9 show the results of U with cooling water volumetric flow rate and Q_i as parameters at 71 percent charge level. Fig. 3.8 shows that some transition phenomenon occurs at $Q_i \approx 0.7 \text{ kW/m}^2$. Although the cause of this is not clear, it is apparently related to heat transfer and flow pattern regime caused possibly by a change in liquid level upon heating. The initial liquid level at this particular charge is half way between the two sight glasses of the accumulator and the rise in liquid level at high Q_i may have resulted in more liquid entrainment in the Freon vapour flow to the heat exchanger. For $Q_i < 0.29 \text{ kW/m}^2$, the effect of cooling water flow rate on U is relatively small as shown on Fig. 3.9. The behaviour of U with respect to water flow rate at $Q_i = 1.15 \text{ kW/m}^2$ is rather unusual; temperature measurements along the tube wall reveal no superheating and the vapour quality at the heat exchanger is close to unity at high water flow rate. This could be due to a change in the flow pattern in the collector tubes resulting from the higher quality, and hence a change in heat transfer characteristic. Pressure measurement showed a steady reading at water flow rate greater than 40 ml/s, as opposed to a decreasing trend at

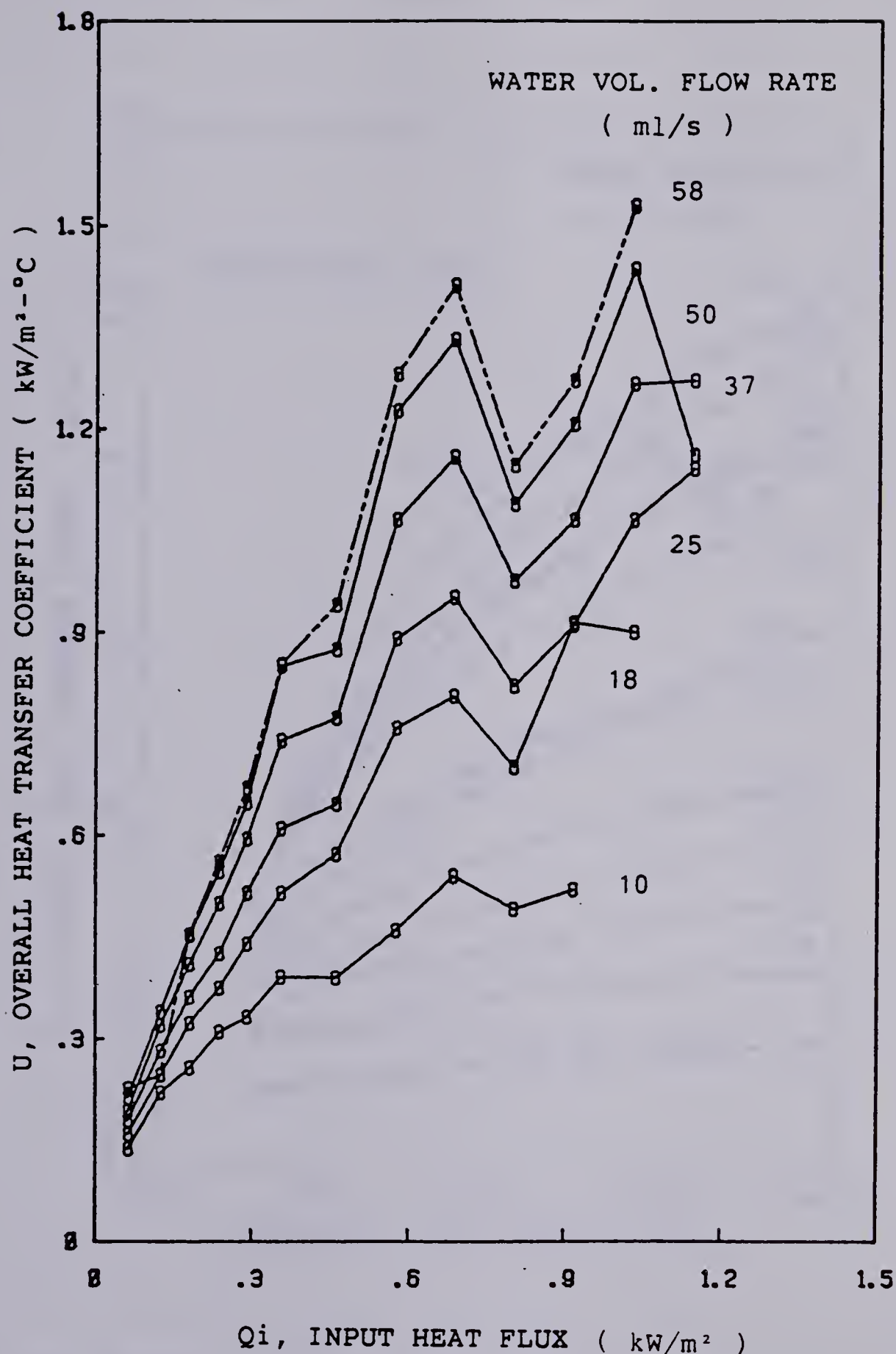


Fig. 3.8 Dependence of overall heat transfer coefficient on the cooling water flow rate at 71 percent charge.

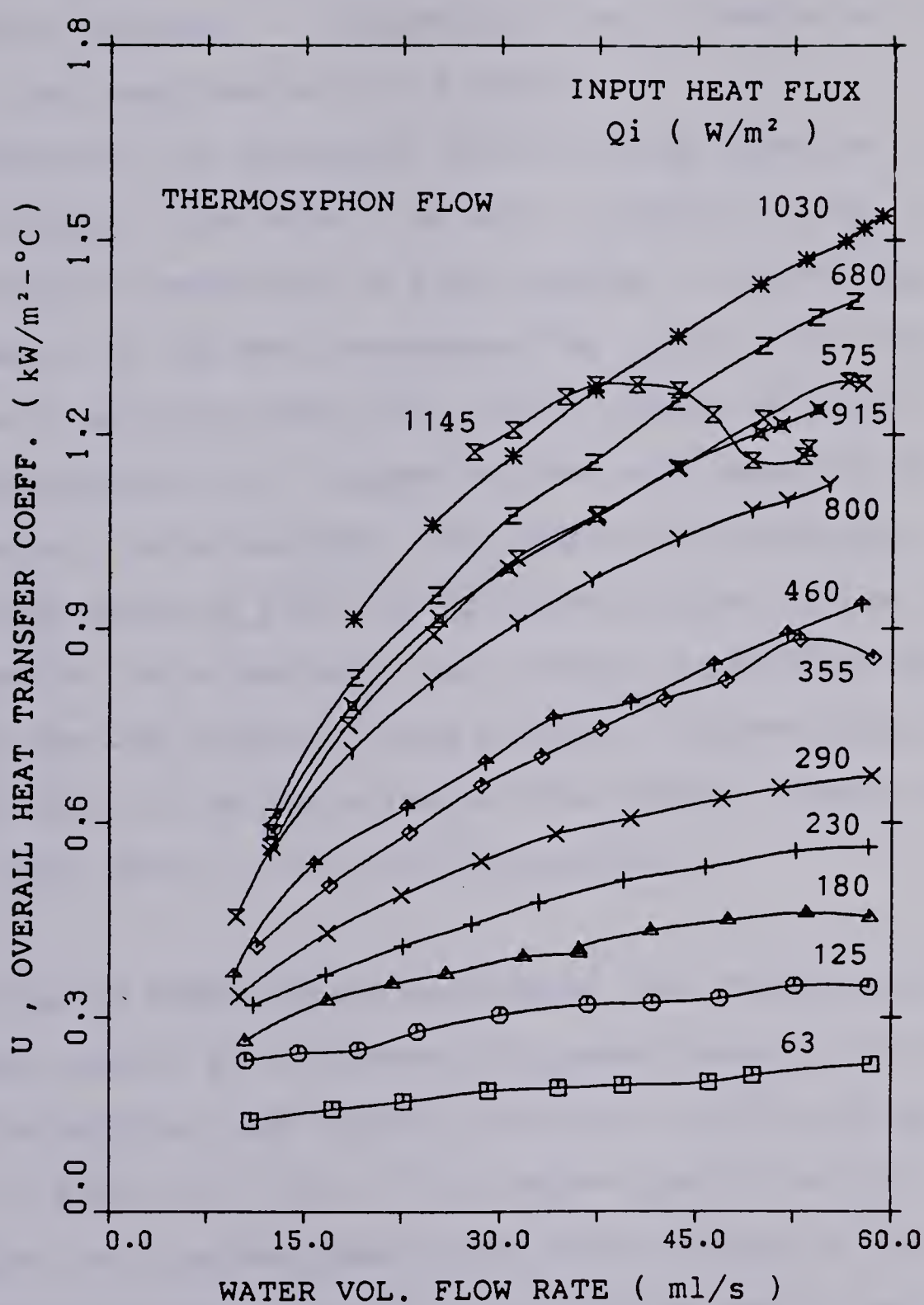


Fig. 3.9 Effect of cooling water flow rate and input heat flux upon the overall heat transfer coefficient at 71 percent charge.

other heat input. Results show that U tends to a maximum value at all Q_i , where the amount of heat gained will not increase with increasing water flow. These results are of particular interest for determining the optimum water flow rate if the magnitude of Q_i is known.

The effect of different initial charge level on U at constant water flow rate of 40 ml/s is shown in Fig. 3.10, depicting the importance of Freon charge on the thermal performance of the heat exchanger. The results show the value of U decreases when the initial charge is above or below the accumulator, suggesting the importance of the location of the accumulator. The speculation that the transition shown on Fig. 3.8 is caused by the rise in liquid level above the accumulator upon heating is further shown here by the dip in the U value at only 71 percent charge. For the rest of the curves shown, the initial charge levels were either above or below the accumulator.

Comparison of Thermosyphon and Forced Flow Circulation Tests

The results at a constant 71 percent charge level for both thermosyphon and forced circulation conditions are shown in Figs. 3.11 to 3.15 for vapour quality at the collector exit, axial temperature distributions of the collector tube wall, overall heat transfer coefficient, U , average collector tube wall heat flux to Freon, Q_c/A_t , and the average heat transfer coefficient of the collector tubes, \bar{h} , as defined by Eq.(3.7).

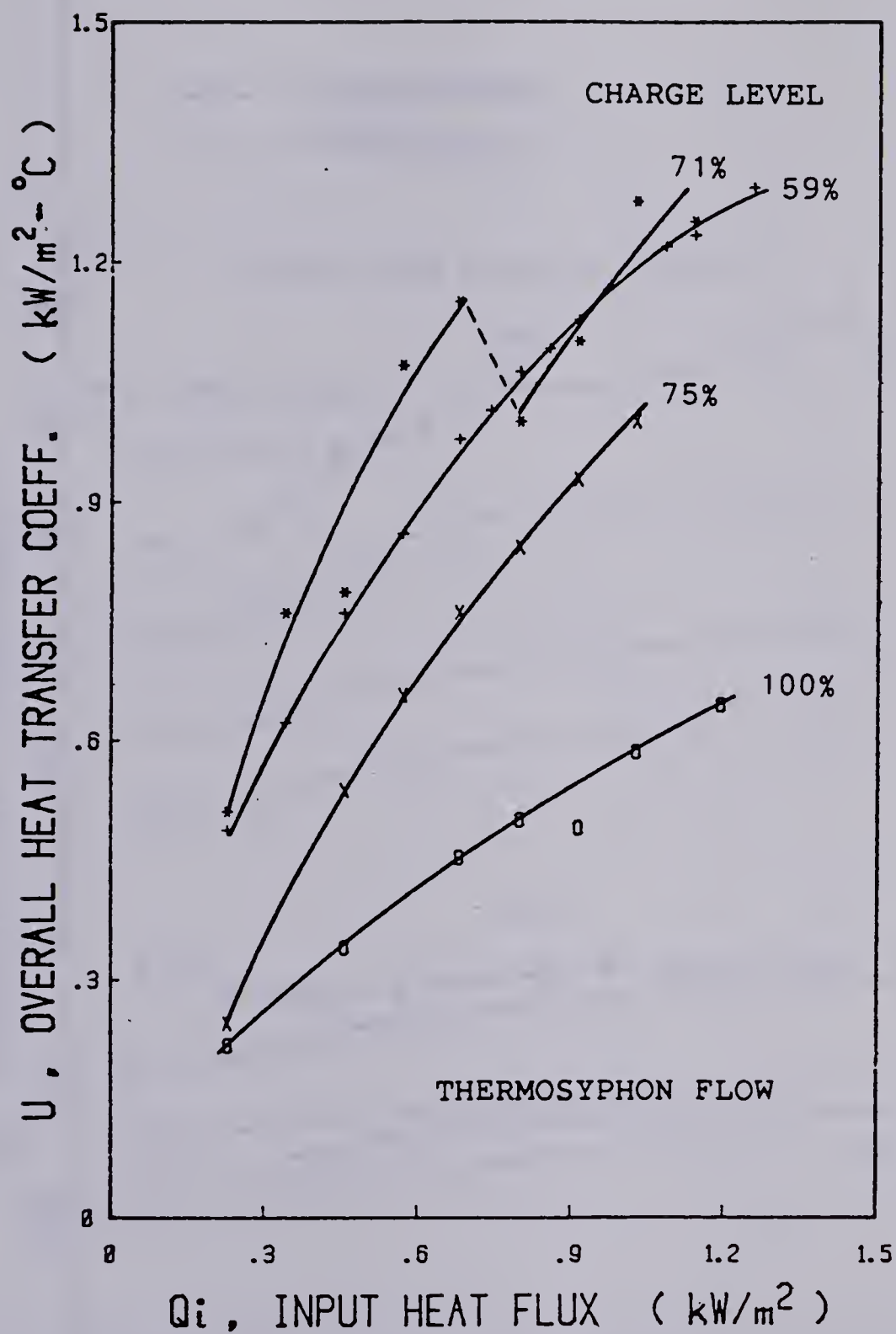


Fig. 3.10 Effect of charge level upon the overall heat transfer coefficient showing the transition at 71 percent charge.

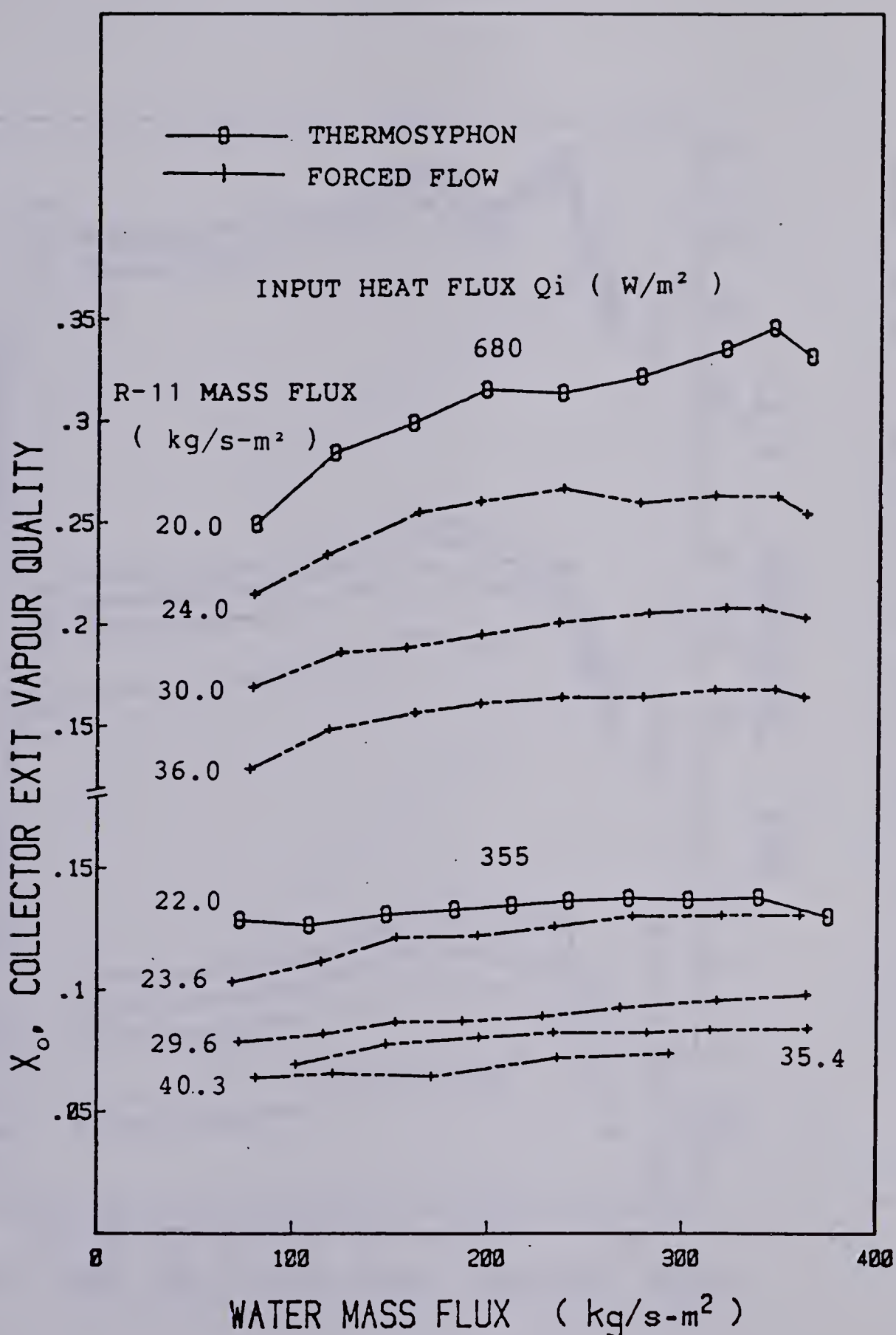


Fig. 3.11 Effect of cooling water and Freon flow rates upon the vapour quality at two representative input heat flux.

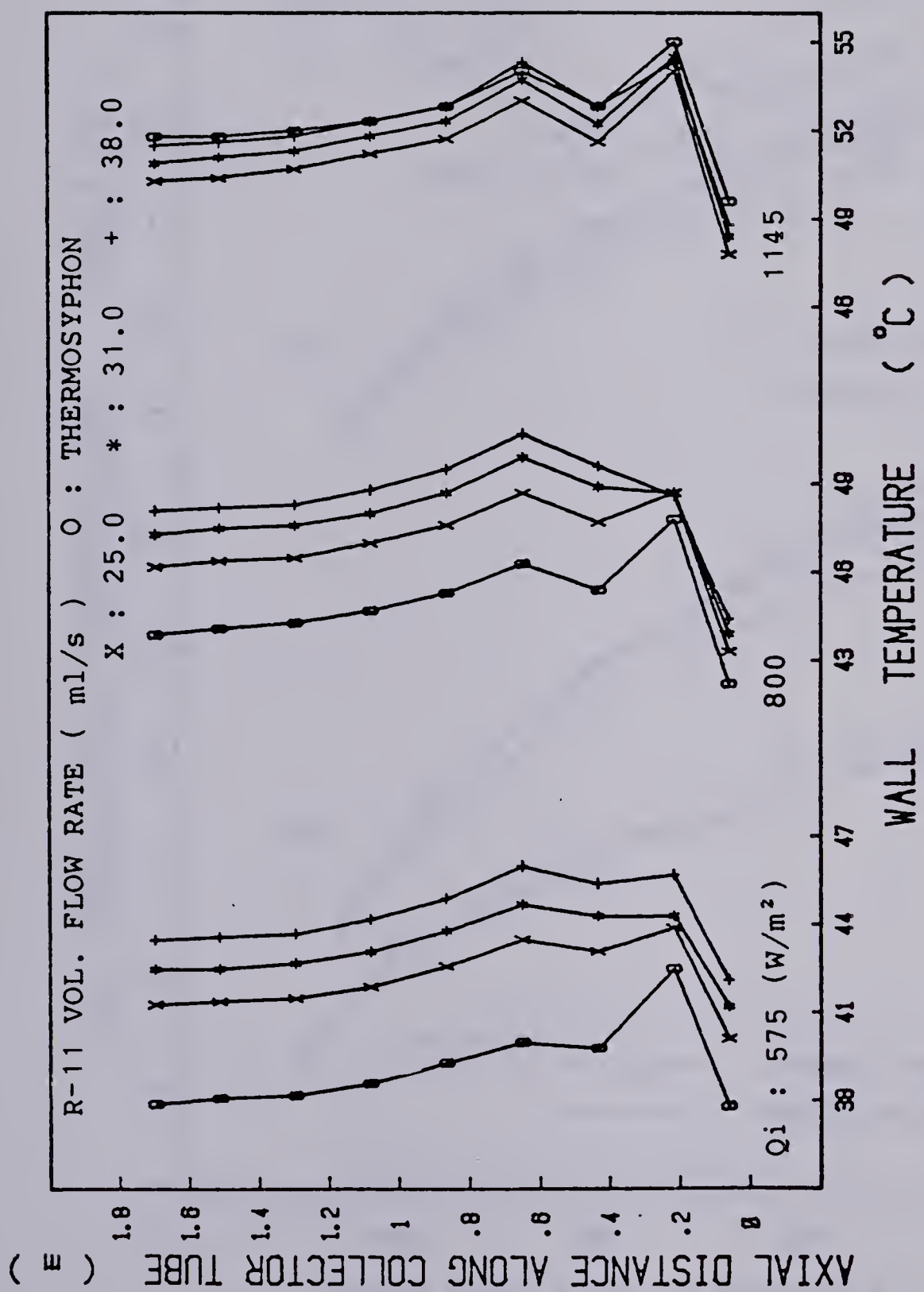


Fig. 3.12 Effect of liquid Freon flow rate on collector tube wall axial temperature distribution.

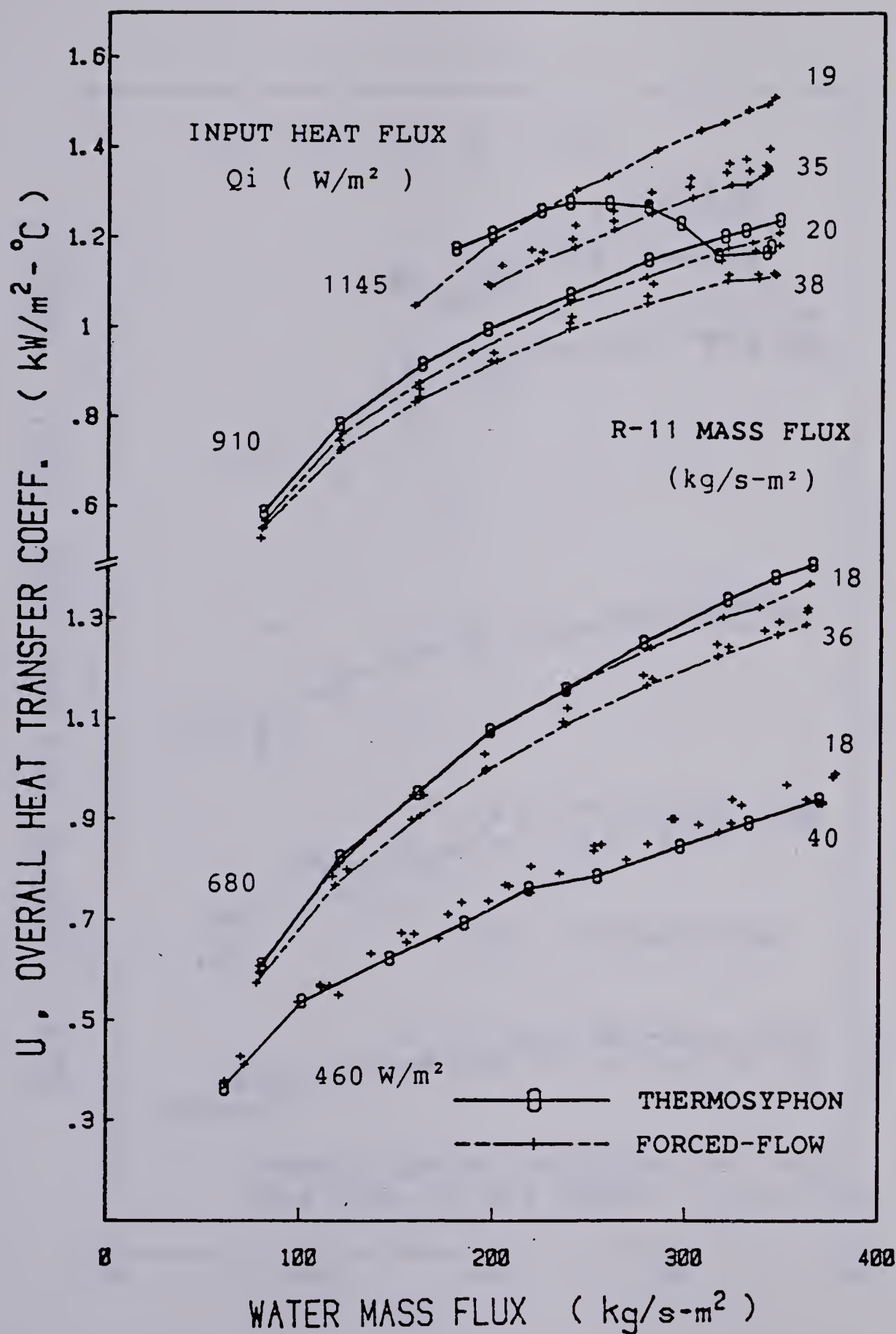


Fig. 3.13 Overall heat transfer coefficient at different Freon flow rates, along with the effects of input heat flux and cooling water flow rate.

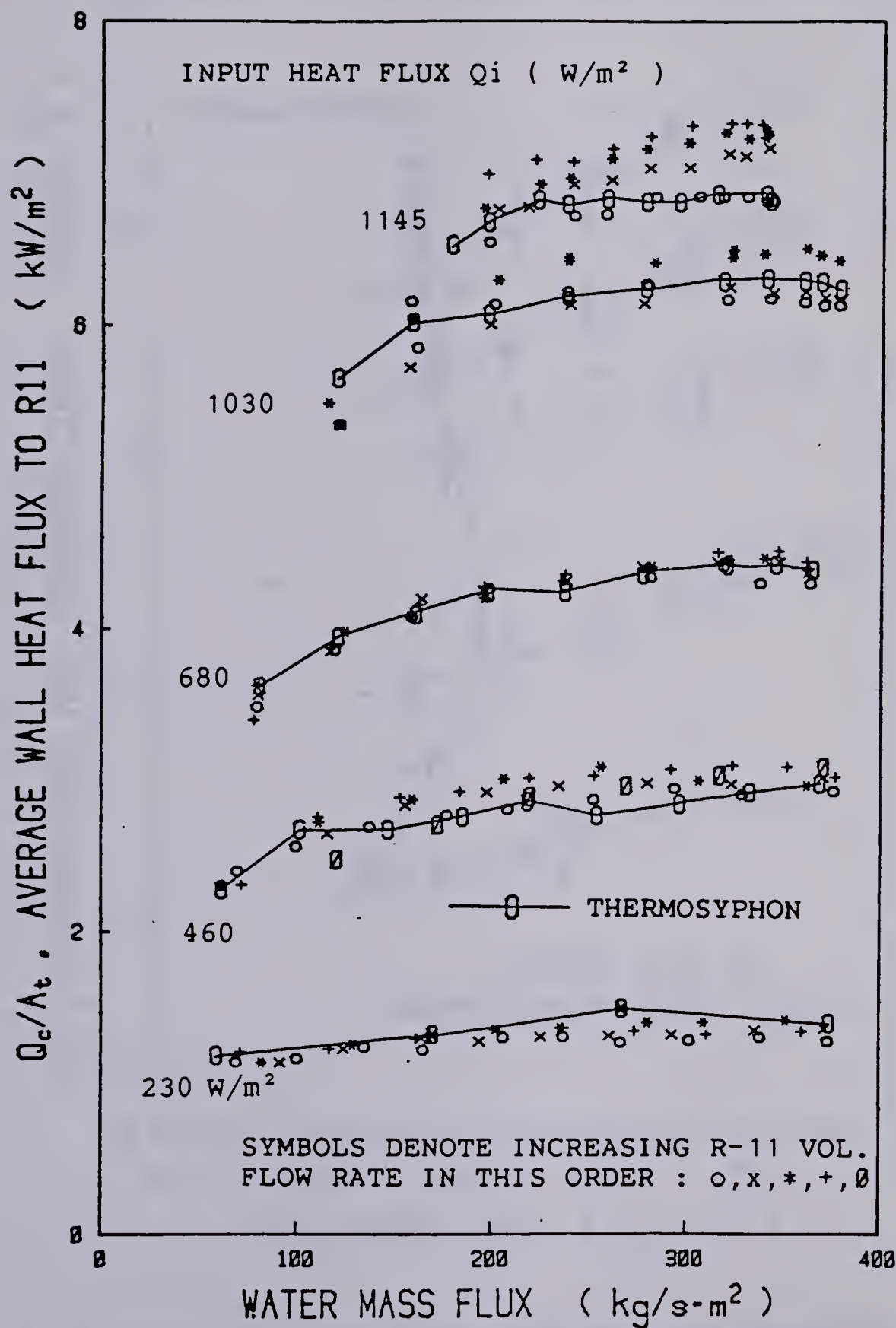


Fig. 3.14 Effect of cooling water and Freon flow rates upon the average tube wall heat flux at different input heat flux.

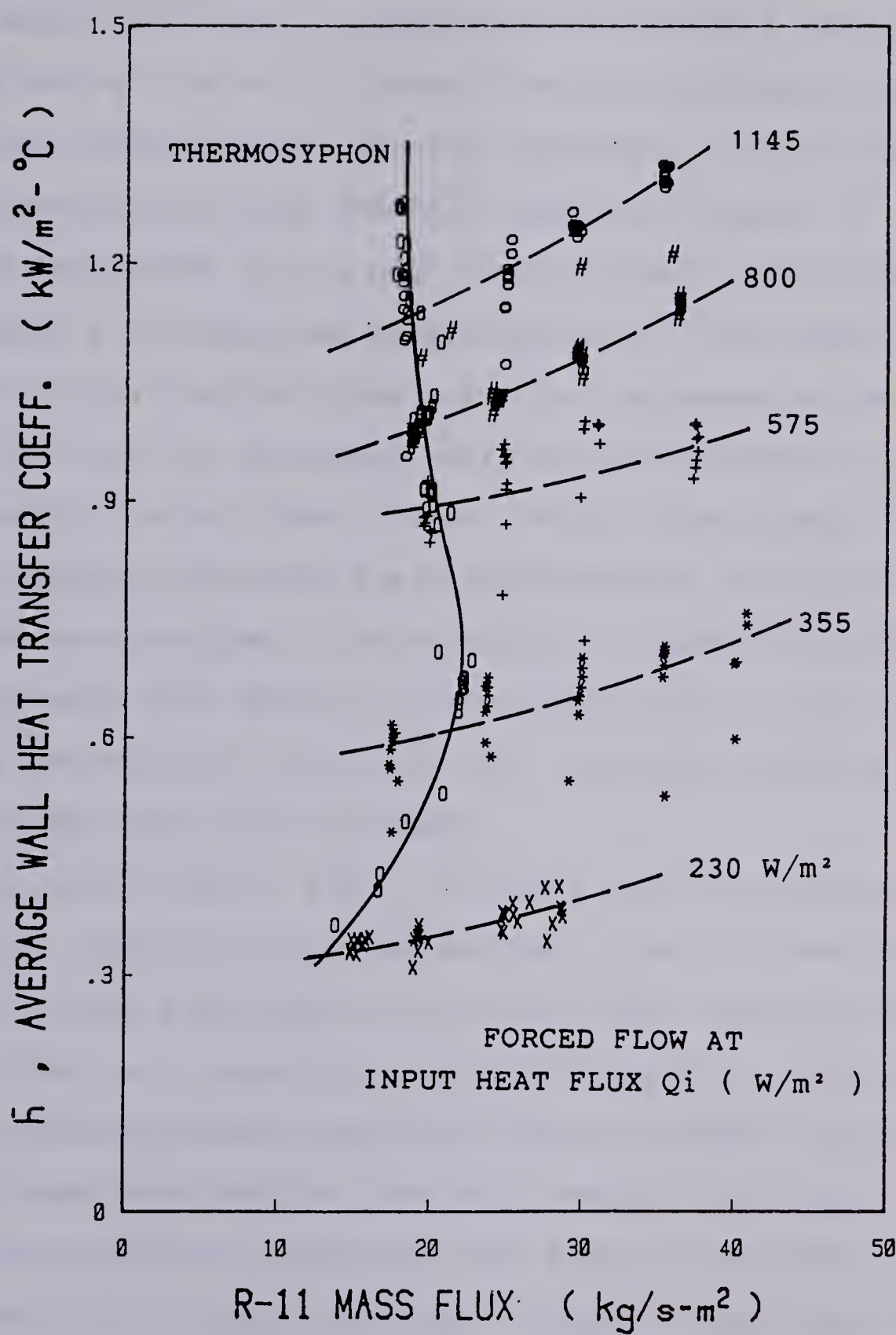


Fig. 3.15 Effect of Freon flow rate upon the collector tubes average heat transfer coefficient at various input heat flux.

Fig. 3.11 shows that for forced circulation, the collector exit vapour quality decreases with increasing Freon mass flux. This is expected since sensible heat plays an increasing role as the Freon flow rate increases, along with less nucleation as the wall superheat is diminished. The vapour quality does not vary much with respect to cooling water flow at low heat input. However, at higher heat input as represented by $Q_i=0.68 \text{ kW/m}^2$, the vapour quality as well as the Freon mass flow increases as the water flow rate is increased. This can be explained by considering the fact that higher cooling rate causes a system pressure decrease due to condensation of vapour, which in turn results in more boiling. It should be noted that the mass flux shown for thermosyphon flow is only an average value since the actual flow increases slightly as the cooling water flow increases.

For $Q_i<0.8 \text{ kW/m}^2$, Fig. 3.12 shows that the collector tube wall temperature for thermosyphon flow is lower than that of forced flow tests. At $Q_i=1.15 \text{ kW/m}^2$, the relatively higher tube wall temperature for thermosyphon is caused by higher system pressure resulting from the higher vapour quality mentioned earlier. One may conclude from this figure that system pressure increases with higher Freon mass flow. Pressure in the forced flow case is greater than that of the thermosyphon flow up to a certain Q_i value, beyond which the higher vapour volume in the latter case may cause a higher system pressure.

The overall heat transfer coefficient, U , as a function of cooling water flow rate is shown in Fig. 3.13 for several Q_i values with the range of liquid forced mass fluxes shown for reference. The liquid mass flux for thermosyphon flow is not shown here but some idea can be gained from Fig. 3.15. The U values for both cases are roughly equal at comparable flow rates for the range of Q_i tested, with U assuming a decreasing value for further flooding of the heat exchanger at increasing Freon flow rate. Forced circulation at $Q_i=1.15 \text{ kW/m}^2$ does not exhibit the same trend as that of thermosyphon flow because the higher mass flow resulted in lower quality and pressure. It appears that thermal performance compared on the basis of U evaluated at the condenser alone is not sufficient at high heat input since there is a change in heat transfer and flow characteristics at the heat source. The fact that forced flow shows no adverse effect suggests this behaviour is not caused by a change in condensation characteristic in the heat exchanger.

The average tube wall heat flux, Q_c/A_t , calculated using Eqs.(3.5), (3.6) and (3.1) is shown in Fig. 3.14 as a function of cooling water flow rate for several Q_i values for both flow conditions. The effect of forced flow rate is seen to be rather small and results for both thermosyphon and forced flow tests are nearly identical for $Q_i < 1.0 \text{ kW/m}^2$. The Average heat transfer coefficient, \bar{h} , for collector tubes as a function of liquid Freon mass flux in the tube is shown in Fig. 3.15 as a function of Q_i . For thermosyphon

flow the mass flux increases initially due to boiling which forces the liquid upwards and later decreases at high Q_i with higher vapour quality. For forced flow h increases with liquid Freon flow rate for a given heat input as expected.

A plot of collector efficiency η versus $\Delta T/I$ based on the Hottel-Whillier [25] equation is widely used in characterizing the efficiency of a collector. The equation is given as

$$\eta = F'[\tau\alpha - U'[(T_{ci} + T_{co})/2 - T_a]/I] \quad (3.9)$$

The parameters F' , $\tau\alpha$ and U' represent the collector efficiency factor, product of the collector transmittance and absorptance, and overall conductance, respectively. In the present study, a plot of η_s against $\Delta T/Q_i$, i.e., replacing η versus $\Delta T/I$ of Eq.(3.9), is shown on Fig. 3.16. The large scattering is believed to be caused by the changing of various parameters being investigated. It appears that Eq.(3.9) may not be adequate for rating phase change collector systems. Soin et al.[12] intuitively suggested a modified Hottel-Whillier equation by introducing the liquid height fraction, L' , into Eq.(3.9), giving

$$\eta = F'[\tau\alpha - U'[(T_{ci} + T_{co})/2 - T_a]/I]/L' \quad (3.10)$$

This modification would require that L' , identical to the percentage liquid charge used in this study, be known and equal to 1.0 at the optimum position. Results obtained with

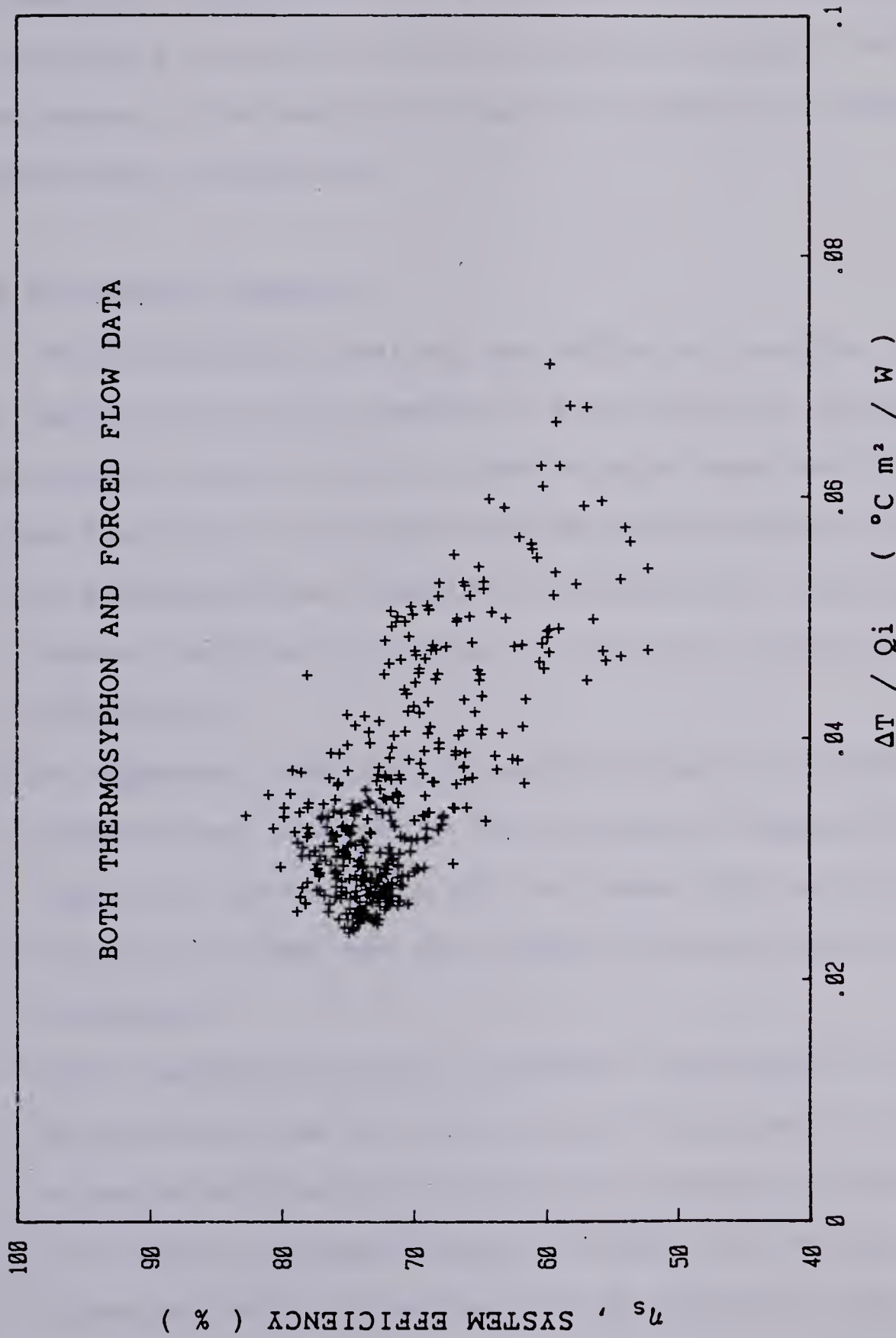


Fig. 3.16 Plot of all data according to the Hottel-Whillier equation showing the scattering of results with changing parameters.

charge levels above this optimum will not conform to Eq.(3.10). Furthermore, a low charge value will give a misleadingly high collector efficiency value. Identification of governing parameters here is clearly required for the development of an analytical model to predict or rate phase change solar collectors.

3.5 Concluding Remarks

By electrically heating the collector absorber plate, the operating characteristics of a refrigerant charged thermosyphon solar collector system were examined using an indoor facility. The results can be summarized as follows

1. An accumulator is essential in separating liquid and vapour completely in order to achieve a high system efficiency.
2. An expansion tank may be used to control the system pressure and indirectly the saturation temperature. The expansion tank affects the two-phase flow and heat transfer regimes and the amount of Freon circulating in the system.
3. Flow instability in the collector tubes may be induced by returning the hot Freon liquid separated at the accumulator directly to the panel instead of mixing with the colder condensed liquid drained from the heat exchanger before returning to the collector tubes. This problem can also be caused by the presence of impurity such as leak detector dye or mixture of working fluid

with different boiling point.

4. The initial amount of Freon charged plays a significant role in the thermal performance of the system. The optimum charge level depends on the relative locations of the accumulator and heat exchanger with respect to the top of the collector as well as input heat flux. An excess amount will tend to flood the heat exchanger and an insufficient amount will lead to dry-out and subsequent superheating of vapour in the collector tubes. The system pressure varies with the cooling capacity of water in the system and the onset of convective boiling and two-phase flow patterns in the tubes are related to this pressure.
5. Increasing the cooling water flow rate raises the overall heat transfer coefficient of the heat exchanger but the additional pumping power required must be weighted against the gain in thermal performance.

Operation of a phase change thermosyphon system appears to be a viable alternative to single-phase active system. The complexity of boiling and two-phase flow in the collector tubes is further compounded by the many variables present. The major effects of the changing parameters on the performance of the test system are the system pressure, the amount of vapour generated and flowing into the heat exchanger, and the Freon mass flow through the collectors. Identification of the governing parameters is essential in rating of these collectors. A detailed study of the pressure

drop and heat transfer characteristics is in order and will be presented in the next chapter.

4. Pressure Drop And Heat Transfer Characteristics Of Freon R-11 In Solar Collector Under Thermosyphon And Forced Flow Conditions

Summary

A closed loop phase change collector system with Freon R-11 as the working fluid was tested indoors to study the pressure drop and heat transfer characteristics. The pressure drops across the collector and heat exchanger were successfully correlated with the Lockhart-Martinelli parameter. Simplification was achieved by treating the entire collector construction, including all the bends and joints, as a unit and the inclusion of the accelerational component. Saturated boiling predominates within the operating range of phase change solar collectors. An average two-phase heat transfer coefficient has been correlated in terms of single-phase flow using the Dittus-Boelter equation, Boiling number and the Lockhart-Martinelli parameter. Results obtained are in good agreement with Shah's correlation. The experiments include changing input heat flux, Freon and cooling water mass fluxes.

4.1 Introduction

Unlike single-phase flow, there is as yet no exact analytical solution to the pressure drop and heat transfer in two-phase flow. The difficulties arise from the unknown vapour-liquid interaction, thermodynamic and hydrodynamic inequilibrium, and in the case of heating the changing mass ratio of the two phases. However, experimental data on vapourization of refrigerants are available in the saturated boiling and critical heat flux regions because of the wide spread applications in air conditioning, heating industries and as a modelling fluid for steam-water mixture. This leads to empirical or semi-empirical correlations to predict pressure drops and heat transfer coefficients essential in the designing process and simulation studies.

Boiling of Freon in phase change collectors occurs mainly in the saturated boiling regime if sufficient working fluid is charged into the system to avoid superheating of the vapour. Natural circulation depends on the buoyancy force to overcome pressure drops for energy transport. Pressure drops across the whole collector will be affected by the tilt angle, θ , vapour quality generated, x , Freon mass flow, \dot{m}_f , the number of bends and joints, tube sizes as well as the flow pattern in the collector tubes. It is obvious an iterative procedure is required to arrive at a predicted flow rate in the collector, and it is impractical to do so by using just a single collector tube. A study was carried out to identify the dominant factors from the large

number of variables that characterize the flow. The use of dimensionless numbers such as Lockhart-Martinelli parameter, X_{L} , and Boiling number, Bo , reduces the number of changing parameters to be dealt with in both the pressure drop and heat transfer analyses.

The experimental set-up is as described in Chapter 3. The present analyses will only deal with those data taken at a fixed initial liquid refrigerant charge level of 71 percent. The changing parameters are the Freon and cooling water flow rates, \bar{m}_f and \bar{m}_w , respectively, and the input heat flux, Q_i .

4.2 Governing Equations

4.2.1 Pressure Drop Analysis

Most studies on pressure drops of boiling flow in circular pipes are concerned with only horizontal and vertical positions, with both upwards and downwards flow. Inclined tube configuration is usually approximated by correlations derived from horizontal or vertical tube studies. Two models – the homogeneous model and the separated flow model – are widely used in evaluating two-phase flow pressure gradients. The homogeneous theory assumes a well-mixed vapour-liquid flow with a mean density, $\bar{\rho}$, and viscosity, $\bar{\mu}$, to characterize the flow, given as

$$1/\bar{\rho} = \bar{v} = [x/\rho_v + (1-x)/\rho_f] \quad (4.1)$$

$$1/\bar{\mu} = [x/\mu_v + (1-x)/\mu_l] \quad (4.2)$$

Other proposed definitions of $\bar{\rho}$ and $\bar{\mu}$ are outlined in Collier[26, p.33]. The separated flow model, as its name implies, assumes the two phases are flowing separately with independent velocities. A further assumption is the non-interaction between the two phases, leading to discrepancy in results when the void fraction is derived using this model, as reported by Chisholm[27]. The accuracy of these two models is limited by flow pattern but their simplicity in application makes them attractive choices in modelling. Interaction between the two phases in the latter model is accounted for in some semi-empirical correlations. These are described in details by Wallis[28].

Following Collier[26], the frictional, accelerational and gravitational components are given, respectively, as

$$-dp/dz|f = 2 \cdot f_t G^2 \bar{v}/D \quad (4.3)$$

$$-dp/dz|a = G^2 \cdot d\bar{v}/dz \quad (4.4)$$

$$-dp/dz|g = g \cdot \sin\theta / \bar{v} \quad (4.5)$$

The two-phase friction factor, f_t , taken to remain constant over the tube length may be expressed by the Blasius equation where the boiling flow is always assumed to be in turbulence

$$f_t = 0.079[G \cdot D / \bar{\mu}]^{-0.25} \quad (4.6)$$

The use of homogeneous model will be shown to be valid for most cases where Freon mass flux, \dot{m}_ℓ , is high and sufficient vapour is generated to cause turbulent flow; it fails, on the other hand, at low vapour quality, x , when the input heat flux, Q_i , is low.

Martinelli et al.[29,30] successfully correlated their results by introducing a two-phase friction multiplier, Φ^2 , defined as

$$\Phi_{j0}^2 = \frac{dp/dz|_t}{dp/dz|_{s0}} \quad (4.7)$$

or

$$\Phi_j^2 = \frac{dp/dz|_t}{dp/dz|_s} \quad (4.8)$$

where Φ_{j0}^2 represents the total flow being taken as liquid flow and Φ_j^2 represents when only the liquid phase alone is assumed to flow inside the tube. The subscripts t and s denote two-phase and single-phase flow, respectively. The parameter Φ^2 is further given as a function of X_{tt} , defined as the ratio of pressure gradients of the liquid and vapour flowing alone in the tube

$$X_{tt} = (\frac{dp/dz|_\ell}{dp/dz|_v})^{0.5}$$

$$= (1/x - 1)^{0.9} (\mu_\ell/\mu_v)^{0.1} (\rho_v/\rho_\ell)^{0.5} \quad (4.9)$$

Two pressure drop readings will be considered here: one across the four collectors, ΔP_c , where heat was added and the other across the heat exchanger, ΔP_e , where heat was extracted. ΔP_c represents the total collector pressure drop and the gravitational component is subtracted using Eq.(4.5). A constant wall heat flux, Q_c/A_t , is assumed and the collector tube length, l_s , where only single-phase exists is approximated by heat balance between the wall heat flux and the sensible heat gained by the Freon, giving

$$l_s = \bar{m}_f C_p f (T_{co} - T_{ci}) / (\pi \cdot D \cdot Q_c / A_t) \quad (4.10)$$

where

$$Q_c = \bar{m}_f [C_p f (T_{co} - T_{ci}) + x_0 \cdot h_{fg}] \quad (4.11)$$

The single-phase length, l_s , was found to be close to 3.5 cm at maximum \bar{m}_f for a total tube length of 1.72 m. The actual length would be higher since slight superheating was required to initiate boiling, along with higher saturation temperature at the bottom of the tube. For a linear change in x ($dx/dz = \text{constant} = x_0/(L-l_s)$) along the rest of the tube, $L-l_s$, the gravitational component is obtained by integration of Eqs.(4.5) and (4.1) over the length

$$\int_{l_s}^L 1/\bar{v} dz = \int_0^{x_0} 1/[v_f (1+x \cdot v_{fg}/v_f)] \cdot [(L-l_s)/x_0] dx$$

and

$$\Delta P_c | g = \frac{g \cdot \sin\theta \cdot (L-l_s)}{v_{fg} \cdot x_0} \ln[1+x_0(v_{fg}/v_f)] \quad (4.12)$$

Since the heat exchanger was in a horizontal position, no $\Delta P_{e|g}$ correction is necessary.

The accelerational component of ΔP_c was found to be less than 0.02 percent of the frictional part using the homogeneous model, hence it is assumed to be negligible and not excluded from ΔP_c . This assumption was also done by Schrock and Grossman[31], and they used a simple model to show the insignificant improvement achieved when the accelerational component is subtracted. It should be noted, however, that Lockhart and Martinelli[29] correlated only the frictional component.

The two-phase collector pressure gradient is therefore calculated from

$$\int (\frac{dp}{dz}|_t) dz = \Delta P_c - \Delta P_{c|g} \quad (4.13)$$

The single-phase frictional pressure drop, $\frac{dp}{dz}|_s$, was measured by pumping the Freon through the collectors isothermally.

4.2.2 Heat Transfer Analysis

Simple correlations for flow boiling in the saturated nucleate region have been proposed by Schrock and Grossman[31] and others in the form

$$\psi = N_u_t / N_u_s = A(B_o + C \cdot X_t^n) \quad (4.14)$$

where the single-phase Nusselt number, N_u_s , is given by the

Dittus-Boelter equation with the total flow being taken as the liquid part only

$$Nu_s = 0.023 Re^{0.8} Pr^{1/3} (1-x)^{0.8} \quad (4.15)$$

$$Bo = \frac{Q_b / A_t}{G \cdot h_{fg}} \quad (4.16)$$

where

$$Q_b = \bar{m}_f \cdot x_0 \cdot h_{fg}$$

The Boiling number, Bo , is interpreted physically as the vapour generated per unit heated surface area flowing through the collector tube cross sectional area. The term Q_b represents the latent heat gained by the flowing Freon in the collector tubes. At low quality or large X_{tt} , the two-phase convective effect is negligible and ψ is dependent only on Bo . At low X_{tt} , e.g., in the case of annular flow where the surface is fully wetted with a thin layer of liquid and bubble nucleation suppressed, ψ becomes less dependent on Bo . In between the pure nucleate and pure convective regimes, both the parameters Bo and X_{tt} govern. This is similar to Chen's[32] effective two-phase Reynolds number, F , and bubble-growth suppression function, S . Chen has given F as a function of X_{tt} and S in terms of F in his paper. However, Eq.(4.14) appears to be more attractive than the superposition equation by Chen or Bjorge et al.[33], where the convective and boiling parts of heat transfer are assumed to be additive, given as

$$q = q|c + q|b$$

because the latter correlation for $q|b$ requires accurate evaluations of physical properties of the mixture.

Schrock and Grossman[31] correlated their results using Eq.(4.14) with $A=7400$, $C=0.00015$ and $n=-2/3$ to within ± 35 percent. Shah[34] proposed a chart correlation and introduced a Convection number, Co , defined as

$$Co = (1/x - 1)^{0.8} (\rho_v/\rho_\ell)^{0.5} \quad (4.17)$$

For vertical flow, Shah divided the correlation according to different flow regimes and gave the following equations and conditions for ψ

For $Co > 1.0$

$$\psi' = 230 \cdot Bo^{0.5}, \quad Bo > 0.00003 \quad (4.18)$$

$$\psi' = 1 + 46 \cdot Bo^{0.5}, \quad Bo < 0.00003 \quad (4.19)$$

For $0.1 < Co \leq 1.0$

$$\psi' = F \cdot Bo^{0.5} \exp(2.74 \cdot Co^{-0.1}) \quad (4.20)$$

For $Co \leq 0.1$

$$\psi' = F \cdot Bo^{0.5} \exp(2.47 \cdot Co^{-0.15}) \quad (4.21)$$

where

$$F = 14.7, \quad Bo \geq 0.0011$$

$$F = 15.43, \quad Bo < 0.0011$$

In all values of Co , ψ is equal to the larger of ψ' or ψ'' , where ψ'' is given as

$$\psi'' = 1.8/Co^{0.8} \quad (4.22)$$

4.3 Results And Discussion

4.3.1 Pressure Drops Results

It is felt that separate consideration of the collector and heat exchanger pressure drops is required because one involves boiling with positive quality change and the other involves condensation where heat is extracted. Furthermore, the Freon flow has a higher vapour quality, x_1 , and experiences a sudden large expansion and then contraction when entering and leaving the heat exchanger.

The total collector pressure drop, ΔP_C , is shown plotted against x_0 in Fig. 4.1. It is interesting to note that the pressure drop during thermosyphon operation remains relatively constant at all input heat flux, Q_i . The increase in x_0 , which should also increase the pressure drop, is accompanied by a slight decrease in Freon mass flow, \bar{m}_f , tending to keep ΔP_C constant regardless of flow conditions. Also depicted on the figure are the effects of \bar{m}_f and Q_i . The downward turns of the lines of constant \bar{m}_f at low x_0 values are caused by the reduction in static pressure head upon initial heating, where the frictional effect is less. Changing cooling water flow rate at the condenser resulted in increased quality and higher pressure loss as shown by the close to vertical variation at each specific Q_i and \bar{m}_f .

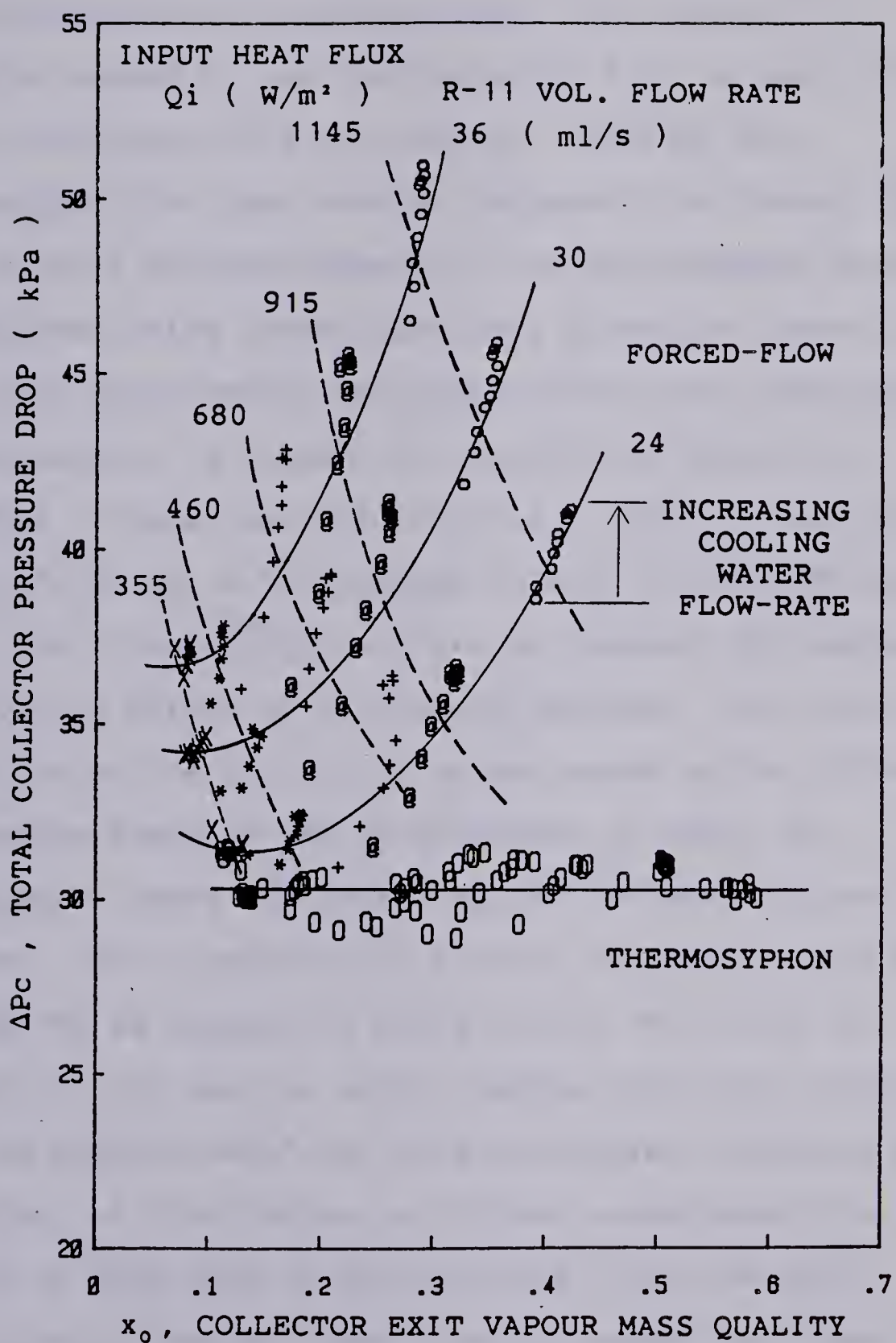


Fig. 4.1 Total collector pressure drop as a function of the collector exit vapour mass quality showing the effects of Freon flow rate and input heat flux.

Fig. 4.2 shows ΔP_c plotted against $1/X_{t,i}$, of Eq.(4.9). The improvement over Fig. 4.1 achieved here is the better correlated curves of constant Freon flow rates. The variation caused by the cooling water flow is seen to be better correlated with $X_{t,i}$ than x_0 , although the thermosyphon flow data remains isolated from forced flow data. It will be advantageous if the thermosyphon data can be predicted using forced flow data since the latter case needs less measurements and computations; the downcomer from the accumulator is closed for forced flow operation.

This is made possible when the pressure gradients ratio, Φ_j^2 of Eq.(4.7), instead of ΔP_c , is plotted against $1/X_{t,i}$. The lines on Fig. 4.3 are of constant Q_i instead of \bar{m}_f , with the effect of Q_i clearly depicted. The larger scattering at low Q_i is felt to be caused by the different flow regime where it may be erroneous to apply the homogeneous theory in correcting for the gravitational component. This reasoning is further reinforced with Fig. 4.4 when Φ_j^2 is plotted in place of Φ_j^2 . The lines of constant Q_i are seen to merge together with the exception of those of $Q_i \leq 0.46 \text{ kW/m}^2$ for this particular collector design. The effect of flow regime is further established from the merging of some data at $Q_i = 0.46 \text{ kW/m}^2$ with the rest, particularly those at higher quality caused by higher cooling water mass flow, and those at higher Freon mass flux (lower $1/X_{t,i}$ due to the lower quality).

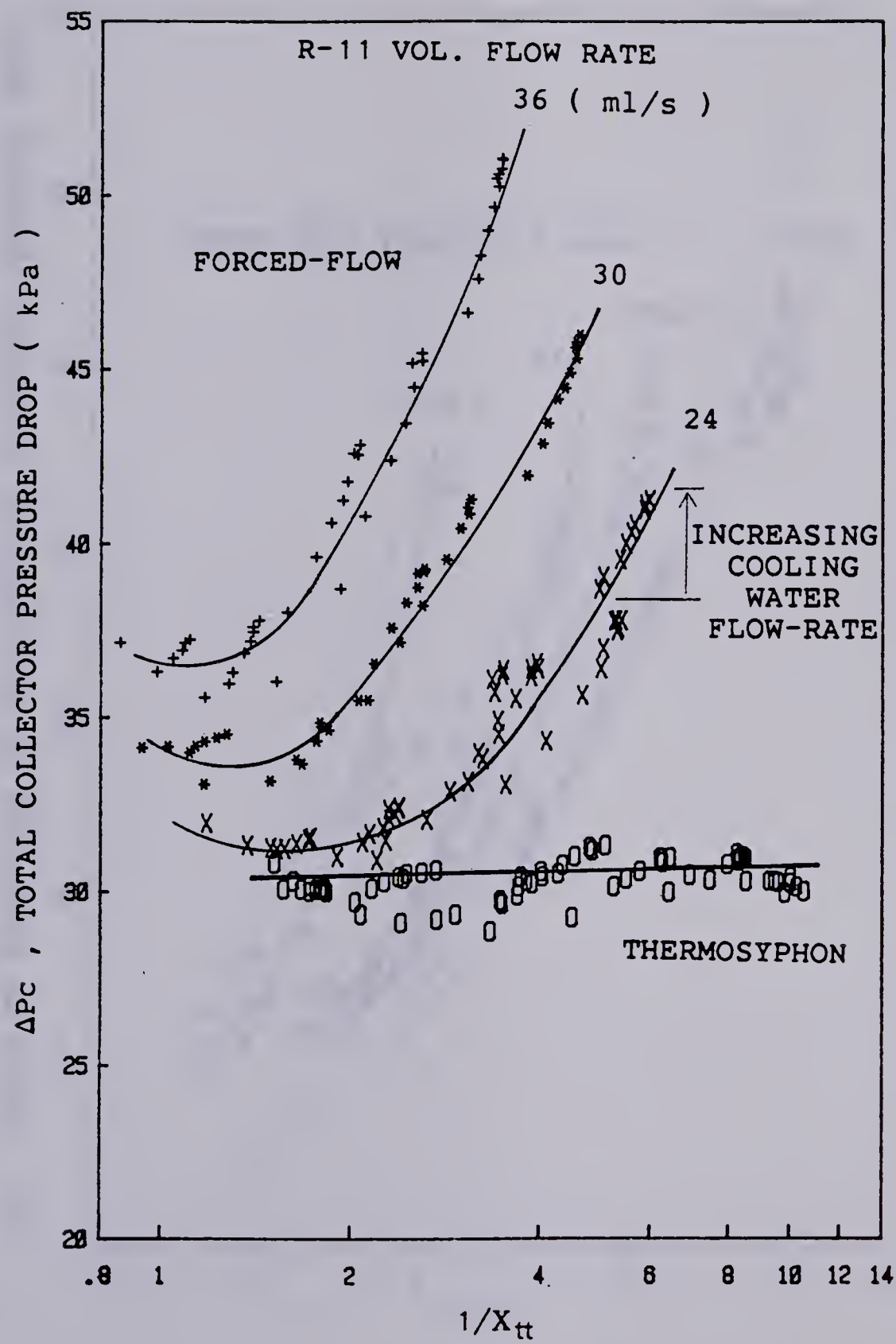


Fig. 4.2 Total collector pressure drop as a function of the Lockhart-Martinelli parameter showing the effects of Freon flow rate and input heat flux.

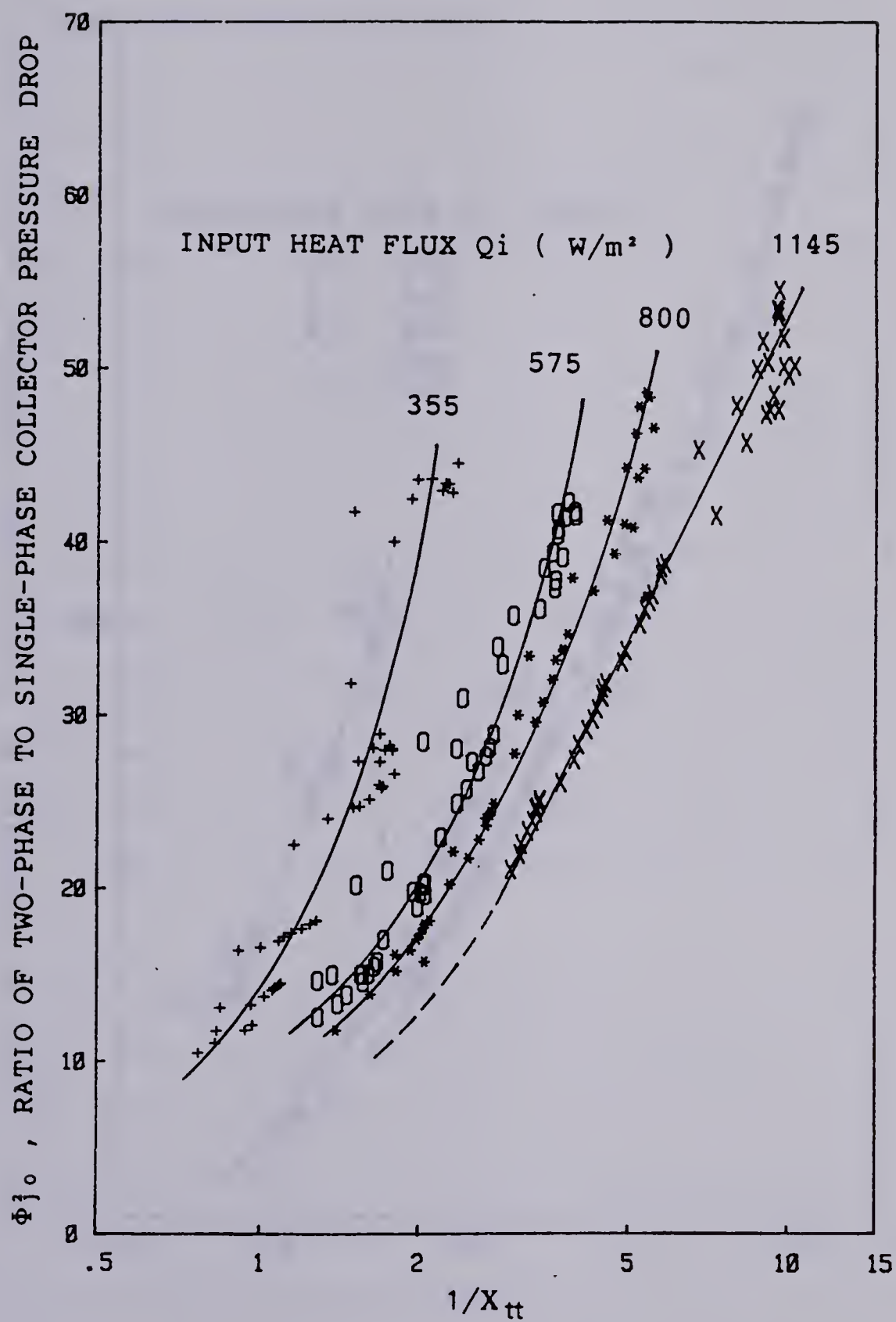


Fig. 4.3 Correlation of the ratio of two-phase to single-phase pressure drops (assuming total flow as liquid phase) across the collectors in terms of the Lockhart-Martinelli parameter.

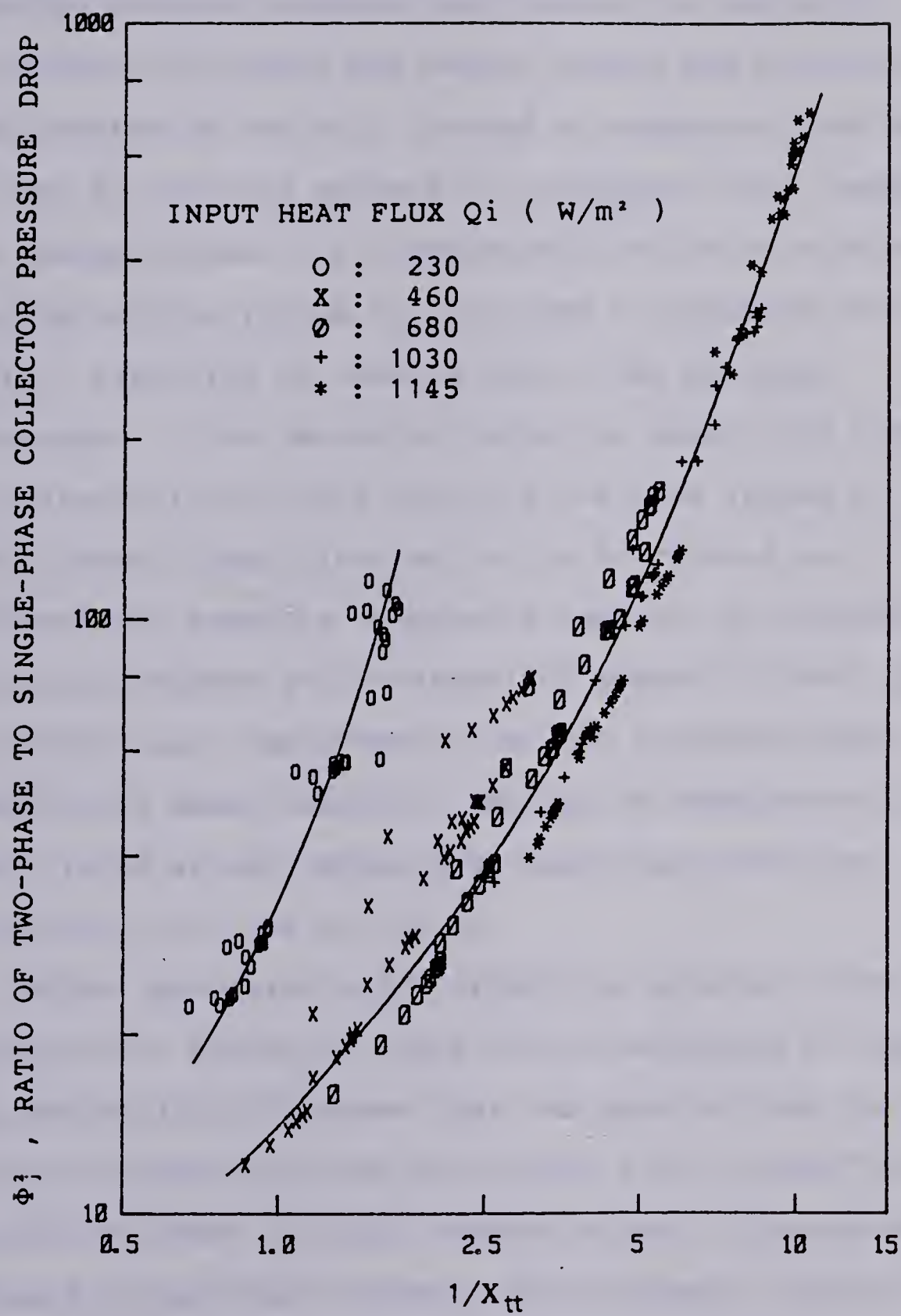


Fig. 4.4 Correlation of the ratio of two-phase to single-phase pressure drops (assuming liquid phase flowing alone) across the collectors in terms of the Lockhart-Martinelli parameter.

The significance of Fig. 4.4 is its usefulness in design and the simplification involves. Firstly, the successful attempt suggests that the entire collector construction, including the bends, joints and accumulator, can be treated as one unit instead of separate tubes as have been done by previous workers in two-phase flow. Designs of phase change systems will undoubtedly strive to attain the saturated boiling regime in the tubes to maximize heat transfer, resulting in needing only a few pressure measurements in the saturated region to obtain the pressure drop characteristic while ignoring the flow regime at low Q_i . The second simplification is the frictional and accelerational pressure components need not be treated separately. Schrock and Grossman[31] showed in their paper the insignificant improvement when the accelerational correction is made. Moreover, the use of homogeneous theory is only valid at well-mixed high mass flux condition, which is evidently not true at low Q_i .

Another parameter which affect the pressure drop is the collector tilt angle, θ , which is not accounted for by X... Beggs and Brills[35] showed that for upwards flow the liquid hold-up increases from the horizontal $\theta=0^\circ$ to $\theta \approx 50^\circ$ where the gravity effect is high, causing higher slippage velocity and hence higher shear between the two phases. Above $\theta \approx 50^\circ$ the liquid is concentrated at the bottom, leading to reduction in liquid hold-up. This factor will alter the pressure drop characteristics. However, it is not known if

boiling flow will exhibit similar trend since Beggs and Brills experimented with air-water mixture flowing isothermally, ruling out phase change along the tube.

Chisholm[36] proposed a frictional pressure drop correlation of the form

$$\Phi_j^2 = 1 + C/X_{t,t} + 1/X_{t,t}^2, \quad (4.23)$$

Collier[26] recommends a value of 20 for C for turbulent-turbulent flow, although Lazarek and Black[37] used C=30 to fit their data of boiling Freon R-113 in small diameter vertical tube. An attempt to obtain a curve fit for most data on Fig. 4.4 resulted in

$$\Phi_j^2 = 1 + 13/X_{t,t} - 0.6/X_{t,t}^2 + 0.5/X_{t,t}^3,$$

A fit similar to Eq.(4.23) is unattainable because the large number of bends and joints included has resulted in a higher pressure drop.

Fig. 4.5 shows the heat exchanger pressure drop, ΔP_e , exhibiting the same characteristics as ΔP_c when plotted against the heat exchanger inlet vapour quality, $x_{t,t}$. ΔP_e remains, similarly, relatively constant for the thermosyphon case. It increases sharply at higher mass flux, probably due to the large momentum change at entry and exit. Three separate curves emerge when Φ_j^2 is plotted against $1/X_{t,t}$ as shown in Fig. 4.6. The parameter Φ_j^2 in this case is calculated using Eq.(4.8) with $\Delta P_{e,t}$ and $\Delta P_{e,s}$, and $X_{t,t}$ using

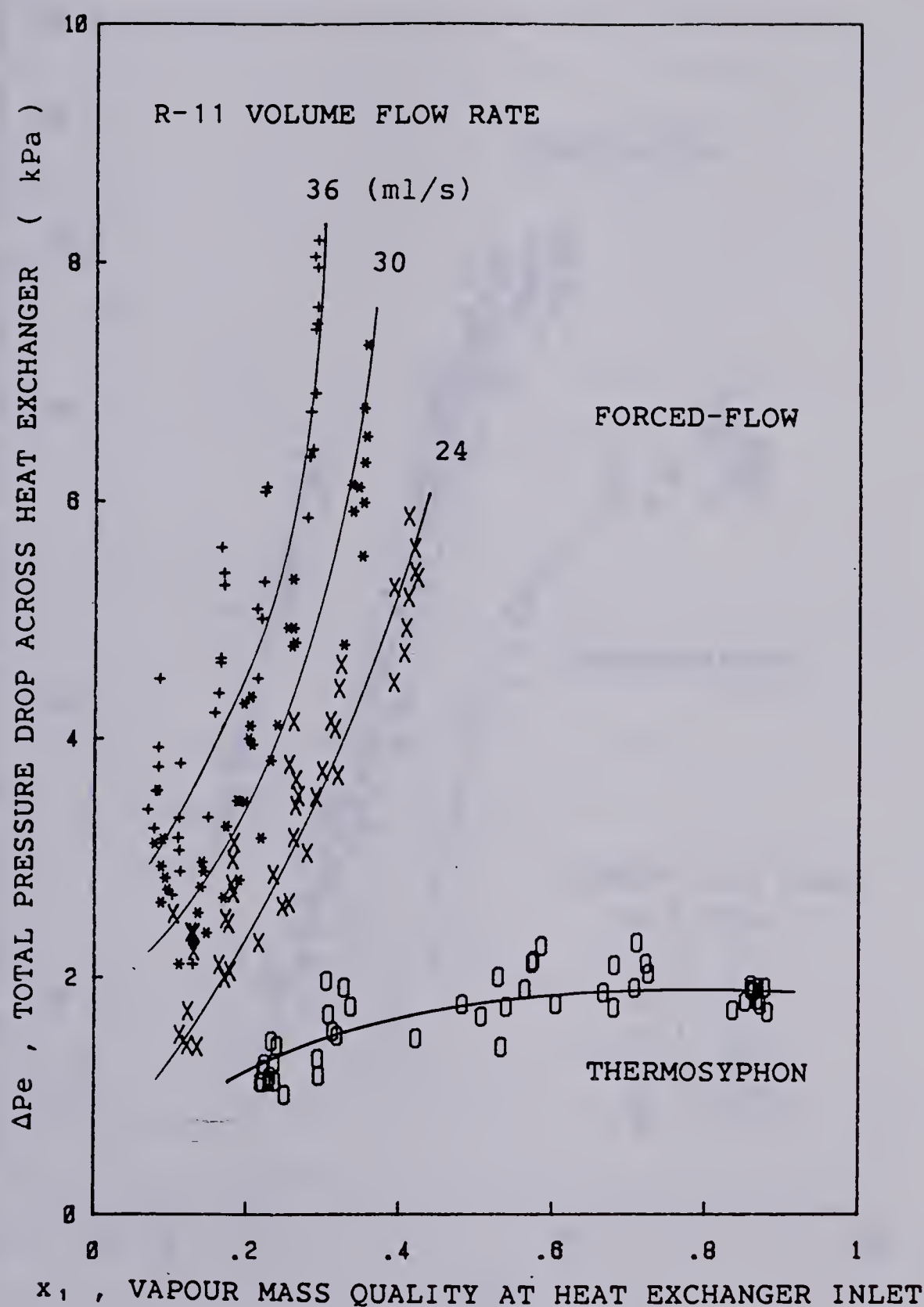


Fig. 4.5 Pressure drop across the heat exchanger as a function of the vapour mass quality at the heat exchanger inlet.

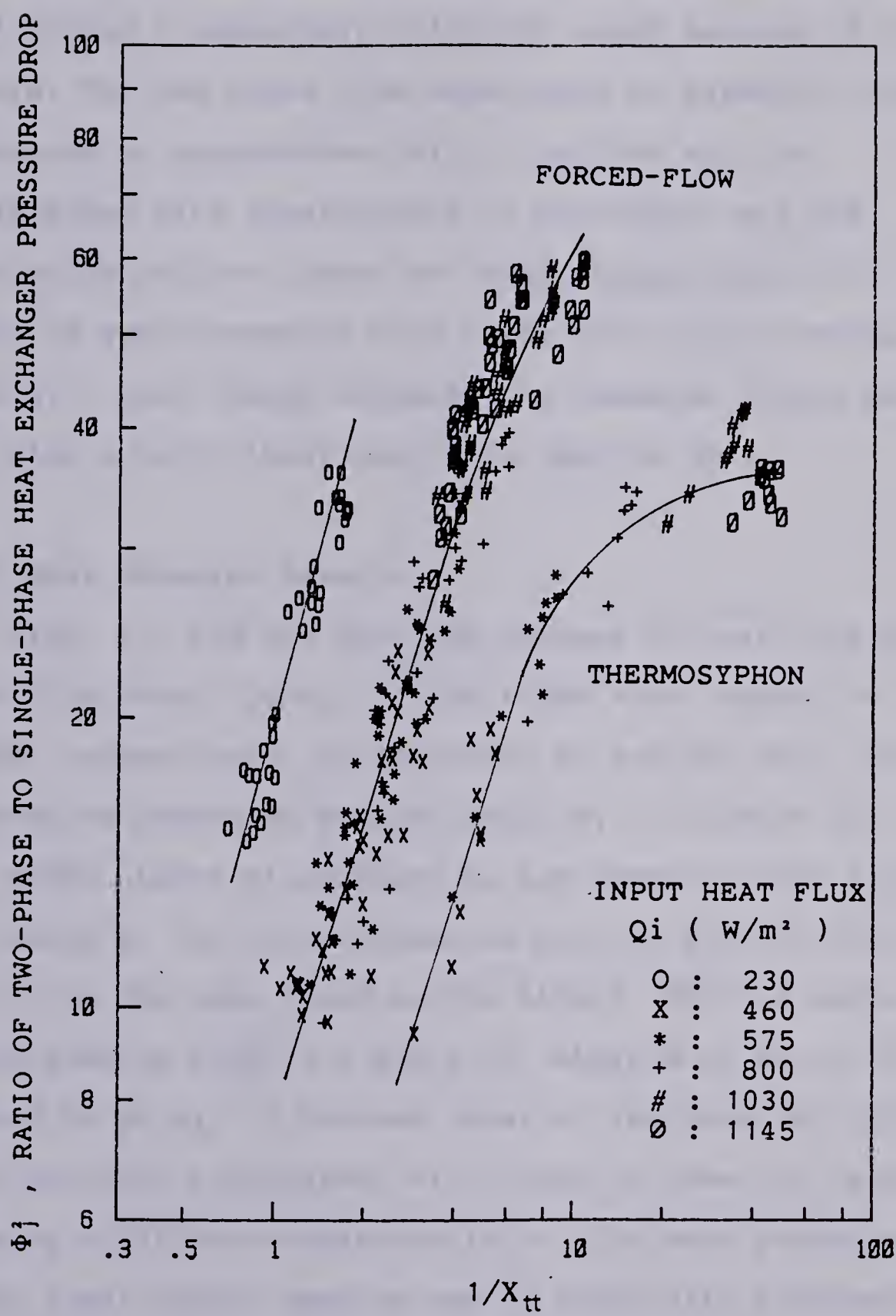


Fig. 4.6 Ratio of two-phase to single-phase pressure drops across the heat exchanger as a function of the Lockhart-Martinelli parameter.

Eq.(4.9) with x_1 replacing x_0 . Thermosyphon data gave a separate curve from forced flow data, and those at $Q_i=0.23 \text{ kW/m}^2$ taking a completely different trend because of flow pattern. The two curve fits shown tend to asymptotic values because as x_1 approaches unity, the flow will be single-phase with superheating of the vapour and the correlation will no longer be valid. Simplification in design is again possible with these fortuitous correlations using X_{tt} , even though arguably the momentum change here does play a more significant role than in ΔP_c .

4.3.2 Heat Transfer Results

Figs. 4.7 and 4.8 show the changes of heat flux gained by boiling Freon, Q_c/A_t , in the tubes with respect to $1/X_{tt}$ and B_o , respectively, at different \bar{m}_f and Q_i . Q_c/A_t is observed to depend on both B_o and $1/X_{tt}$ in almost all the data taken. Lines of constant \bar{m}_f are drawn on both figures but values at low Q_i , represented here by $Q_i=0.23 \text{ kW/m}^2$, do not follow the same trend as the others. This is better illustrated by Figs. 4.9 and 4.10, where ψ of Eq.(4.14), instead of Q_c/A_t , is plotted. Most of the data for $Q_i>0.3 \text{ kW/m}^2$ are well correlated, with those at lower Q_i values assuming a different characteristic. The most probable cause is the lower vapour quality and \bar{m}_f along with different flow pattern, resulting in different heat transfer characteristic. The dependence on both parameters used suggests that saturated boiling regime is dominant.

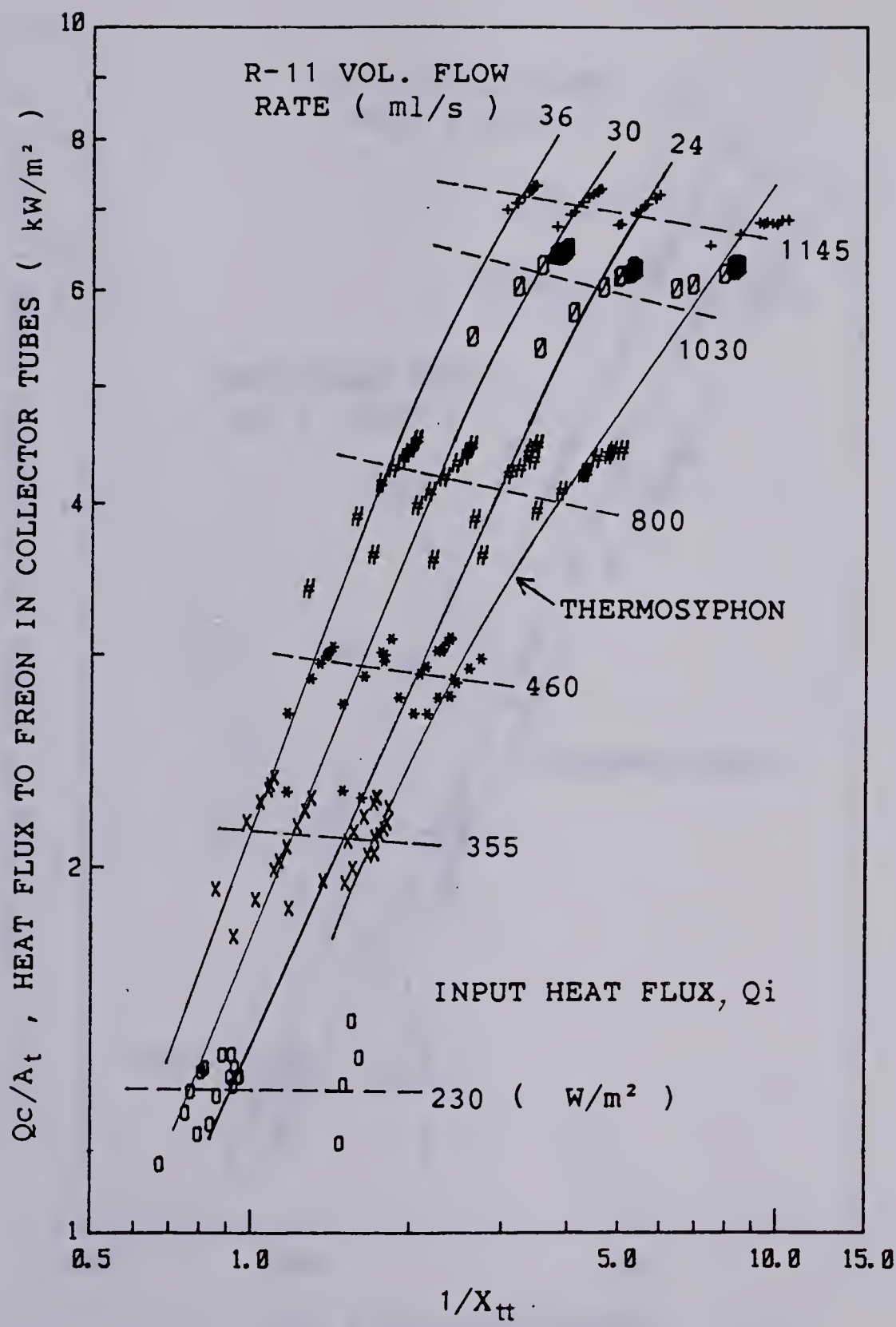


Fig. 4.7 Heat flux to flowing Freon in the collector tubes as a function of the Lockhart-Martinelli parameter.

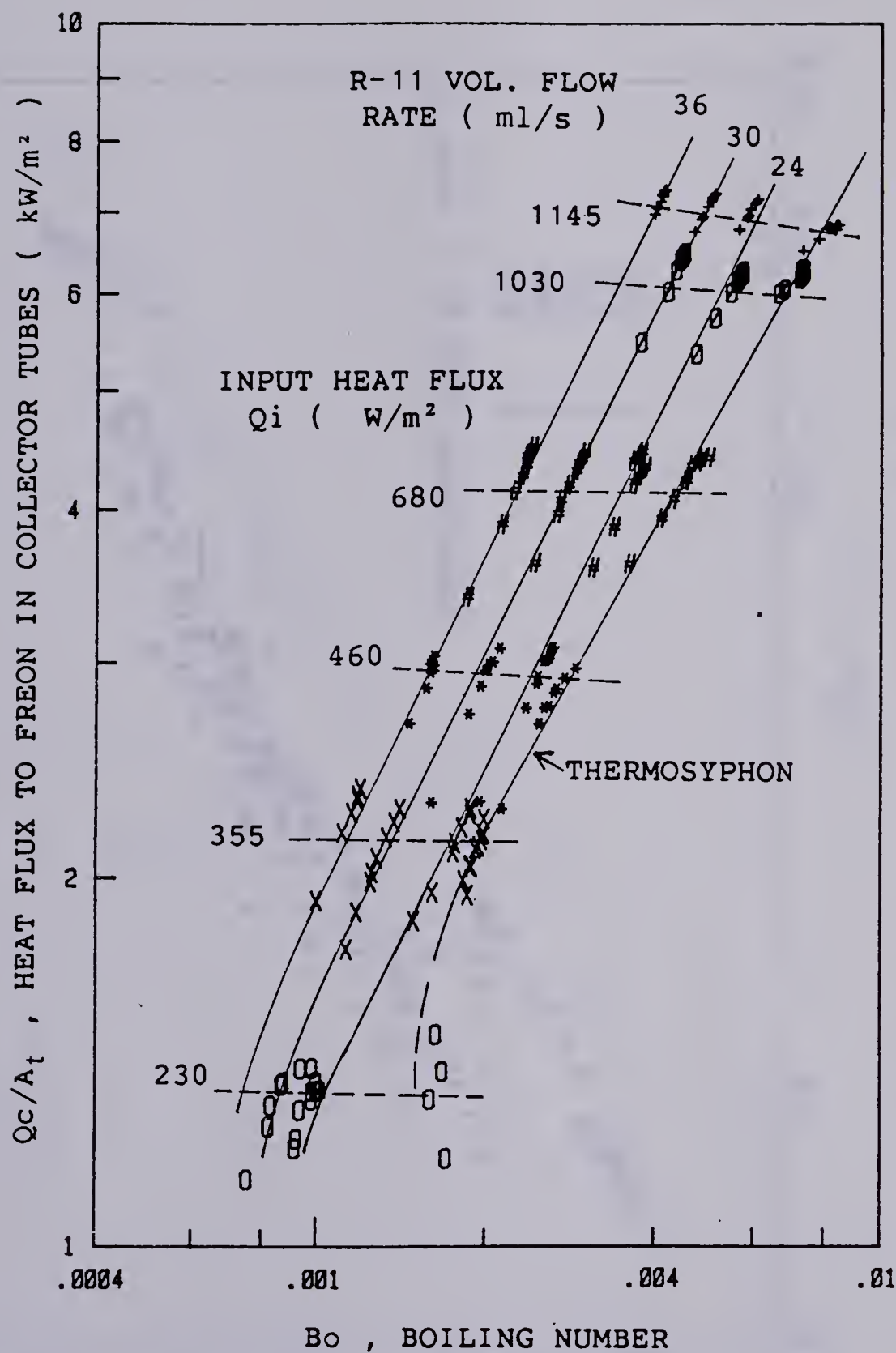


Fig. 4.8 Heat flux to flowing Freon in the collector tubes as a function of Boiling number.

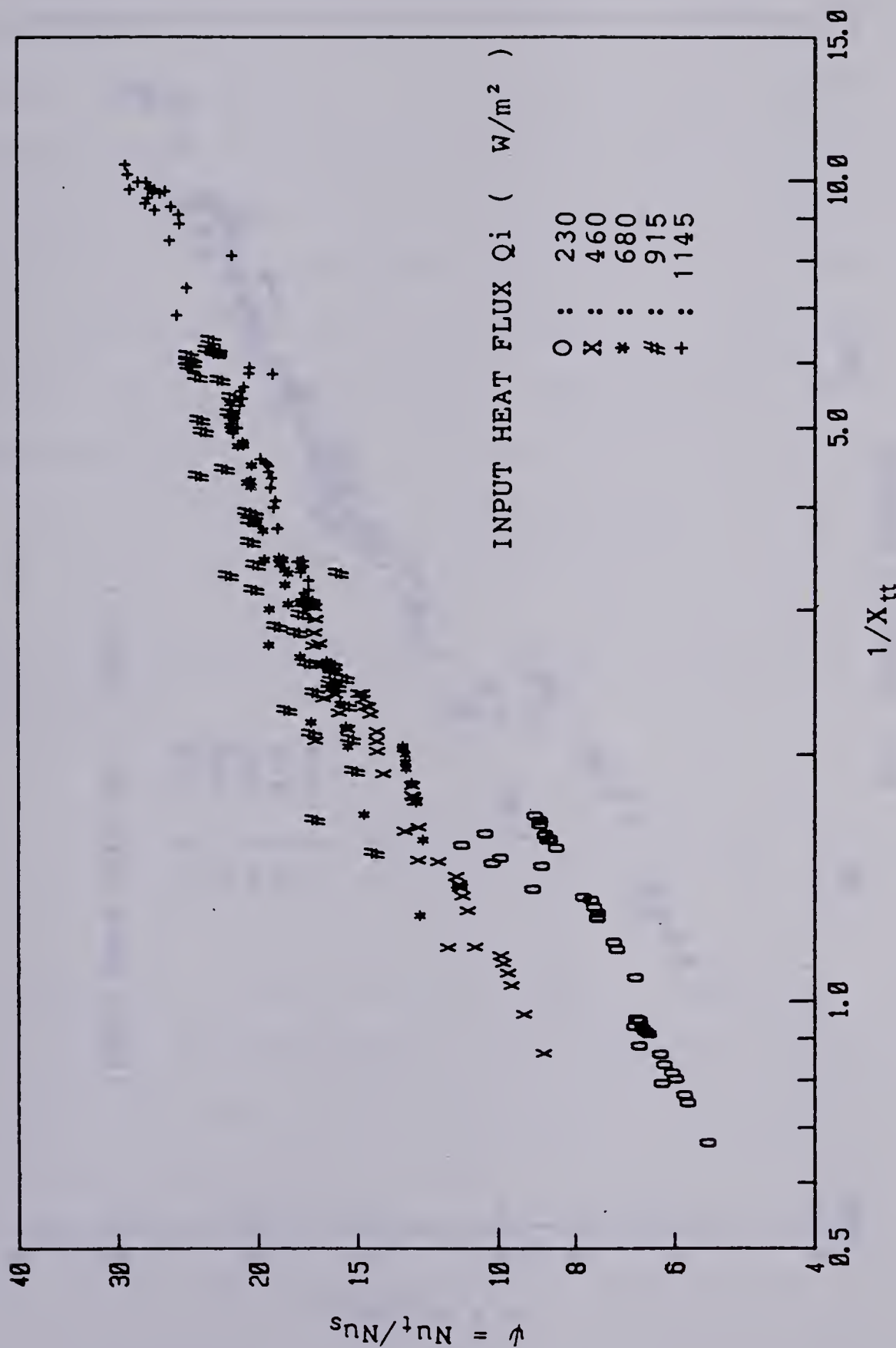


Fig. 4.9 Ratio of experimental two-phase to single-phase Nusselt numbers as a function of the Lockhart-Martinelli parameter.

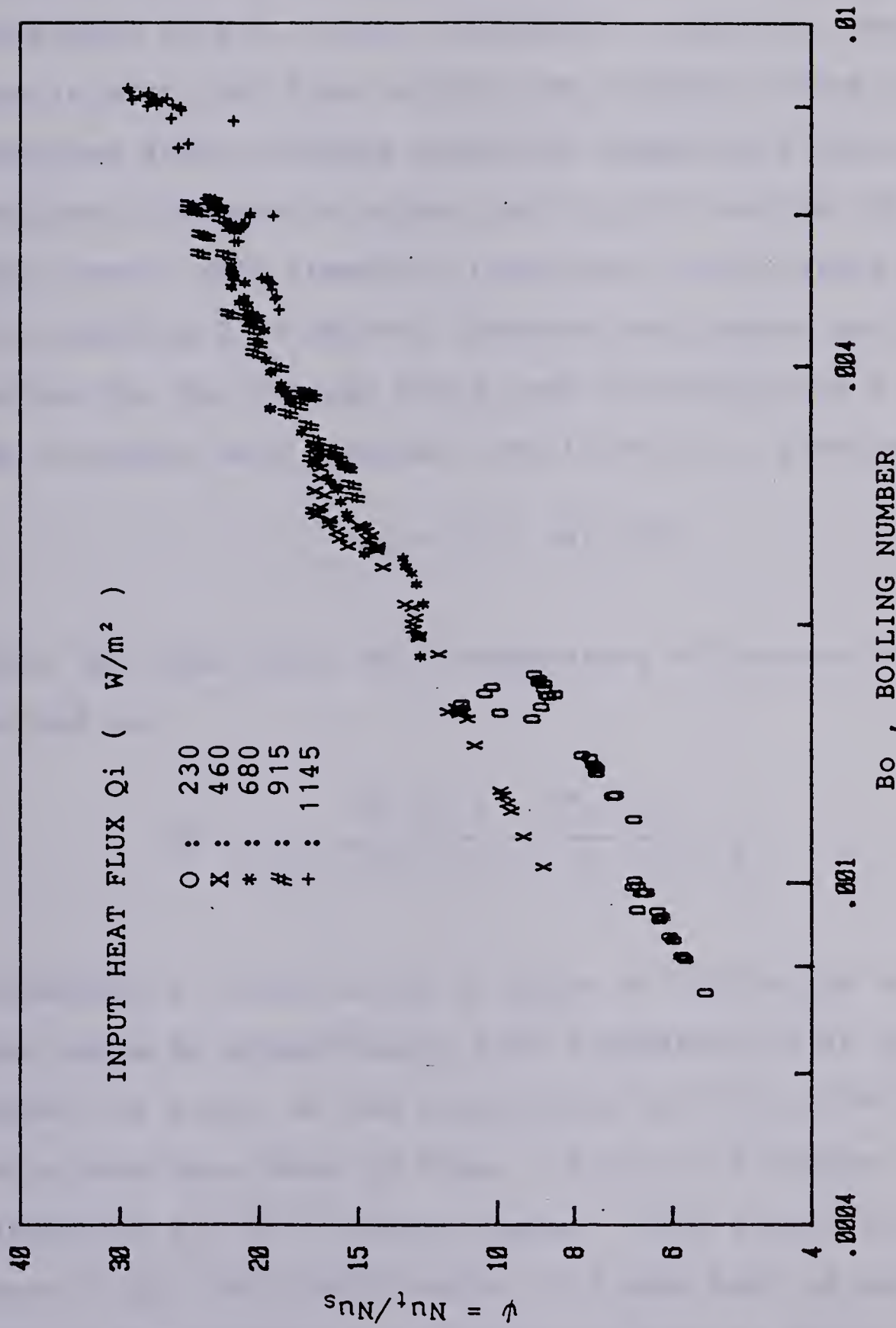


Fig. 4.10 Ratio of experimental two-phase to single-phase Nusselt numbers as a function of the Boiling number.

At low heating and consequently low quality, nucleate boiling predominates with ψ being a function of Bo alone; at high heat flux, pure convective regime reigns with ψ well correlated with $X_{t,i}$ alone (Shah[34]). However, one must keep in mind that Freon enters the collector tubes at a subcooled state, reaches saturated temperature state quickly and then increases in vapour quality for the rest of the tube length. Heat transfer, therefore, varies along the tube with changing flow pattern, pressure and vapour quality. An average Nu_t has thereby being used in calculating ψ , with the two-phase heat transfer coefficient, \bar{h}_t , given as

$$\bar{h}_t = Q_c / (A_t \cdot \Delta T) \quad (4.24)$$

where the logarithmic mean temperature difference ΔT is defined as

$$\Delta T = \frac{(\bar{T}_t - T_{ci}) - (\bar{T}_t - T_{co})}{\ln [(\bar{T}_t - T_{ci}) / (\bar{T}_t - T_{co})]}$$

Consequently, there exists a region at the bottom of the tube where Bo predominates, with a possibility of pure convective region at the top at high heat flux. The well correlated data shown on Figs. 4.9 and 4.10 suggest that the assumption is, to a certain degree, valid within the tested range of Qi . The simplification in ψ used here is merely for ease in computations and application such as designing.

Comparisons of experimentally obtained ψ with those calculated from the empirical correlations of Schrock and Grossman(Eq.(4.12)) and Shah(Eqs.(4.16-4.20)) are presented in Figs. 4.11a and 4.11b, respectively. Measured values at $Q_i=0.23 \text{ kW/m}^2$ are seen to be lower in both cases; it may be assumed that at such low input heat flux, boiling probably occurs in the subcooled region. Shah's method appears to correlate the data much better, and over a wider range. The tapering at the higher end shown on both graphs is likely caused by the estimation of Q_c of Eq.(4.11), where heat losses to the surrounding are neglected (see Chapter 3). An improvement can certainly be achieved if the heat loss characteristic is known, thereby correcting the heat gain by Freon to Q'_c where

$$Q'_c = Q_c + U'A (\bar{T} - T_a)$$

with U' , A , \bar{T} and T_a as the overall collector conductance, total collector surface area, average absorber surface temperature and ambient temperature, respectively. It should be noted that heat gain in phase change collectors occurs isothermally in a large section of the tubes, therefore the heat losses in relation to heat flux is different to that of the liquid phase systems.

The design of phase change collectors can be greatly simplified if simple correlations similar to those used here are utilized for the prediction of overall heat transfer coefficients in the collector tubes. Neglecting single-phase

Fig. 4.11b
Comparison of correlation by Shah with experimental results.

Fig. 4.11b

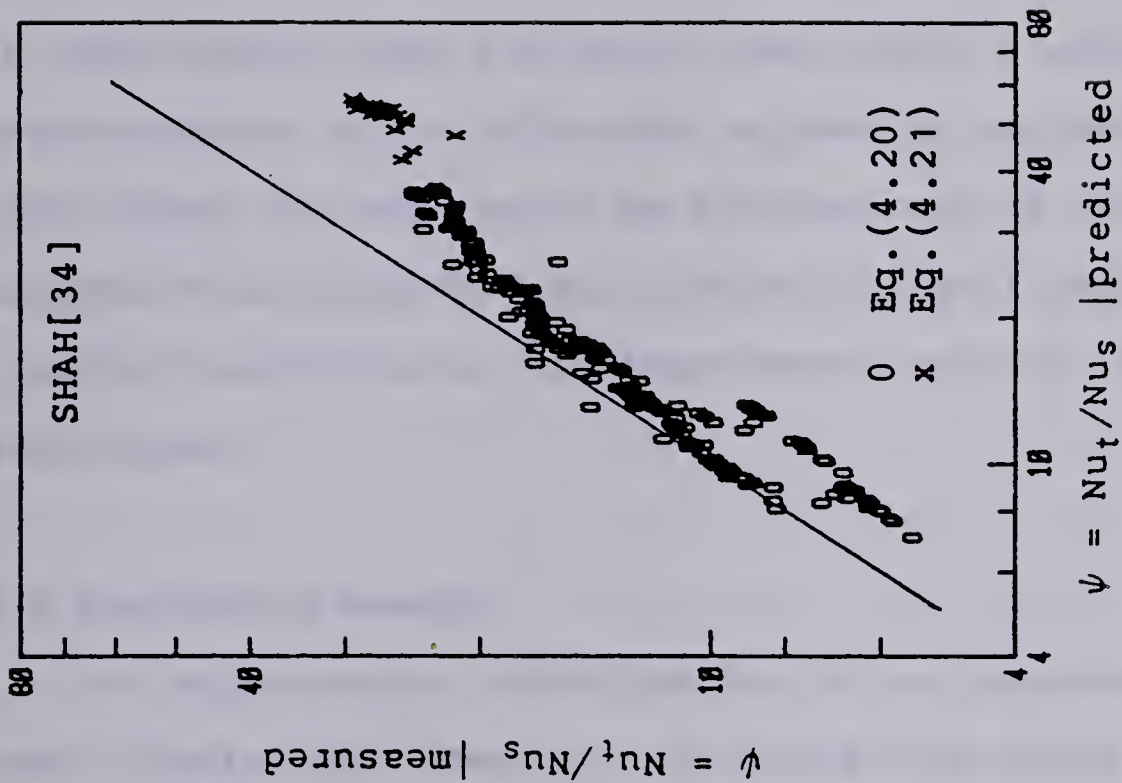
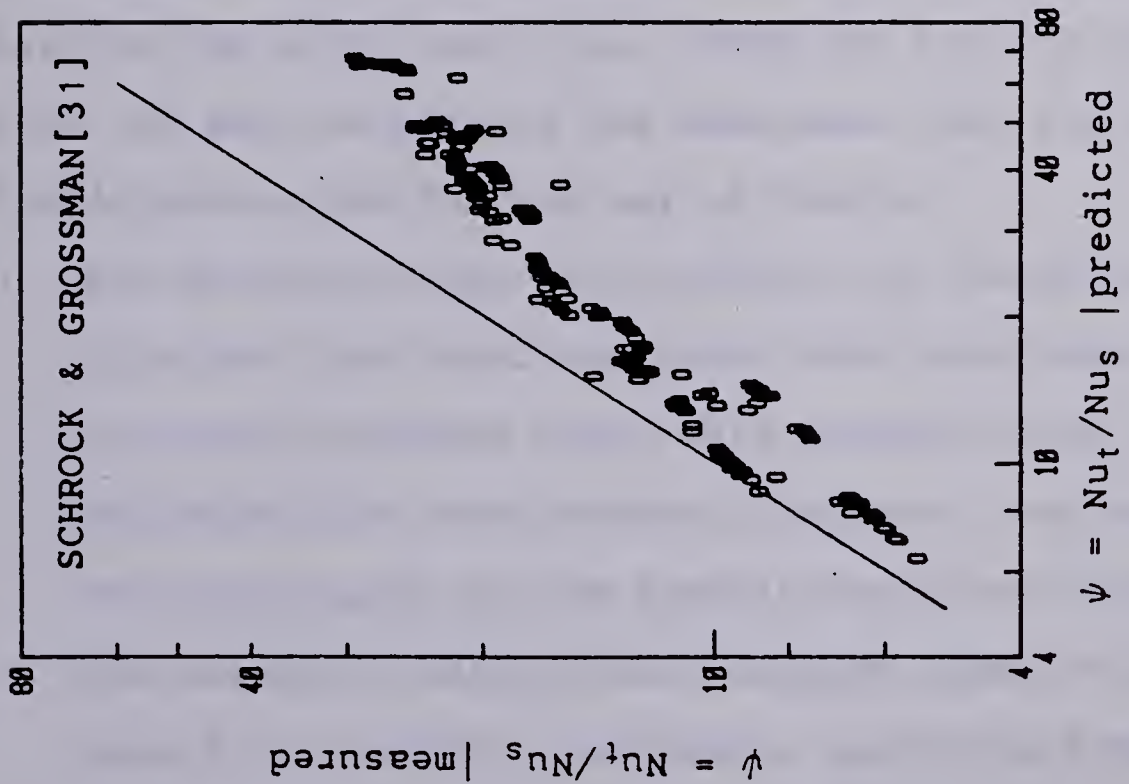


Fig. 4.11a
Comparison of correlation by Schrock and Grossman with experimental results.

Fig. 4.11a



region at the lower section of the tubes should not introduce any significant error since heat balances show that this length is rather short and the sensible heat gain is much smaller than the latent heat gain. A separate determination of the different regimes by estimating the tube length for each would be tedious, and in view of the uncertainties regarding calculating the boiling heat transfer coefficients, the improvement may not be significant.

4.4 Concluding Remarks

An experimental investigation of the pressure drop and heat transfer performance of a closed loop phase change collector system undergoing thermosyphon and forced flow conditions has been described. The experiments involved a fixed amount of Freon liquid charge in the collectors, while varying the input heat flux, Freon and cooling water mass flow, as well as closing the downcomer from the accumulator. The following conclusions may be drawn:

1. The accelerational part need not be treated separately from the frictional component when examining the collector pressure drop. This pressure drop, after excluding the gravitational component, was found to be well correlated by the Lockhart-Martinelli parameter. The exception being those readings taken at low input heat flux, yeilding low vapour quality and mass flux where correction for the gravitational part using the

- homogeneous theory is invalid.
2. The analysis of pressure drop across the heat exchanger yeilds three curves, one being the results at low heat flux, another for forced flow condition and the third for thermosyphon flow. The accelerational component is felt to be the cause of the separate curves for forced and thermosyphon flows, since the latter has a higher vapour quality.
 3. Saturated boiling was found to be the dominant regime, and the results were found to be sensitive to both the Boiling number and Lockhart-Martinelli parameter. The use of an overall heat transfer coefficient, instead of estimating the local values at different sections of the tube, is presented with the results being in good agreement with the saturated boiling heat transfer correlation developed by Shah and, to a less extent, with that of Schrock and Grossman.

The possibility of treating the entire collector construction as a whole, rather than taking into account of each tube, would simplify the designing of phase change collectors. The knowledge of a single parameter, the Lockhart-Martinelli parameter, appears to be sufficient to characterize the pressure drops across the collector and the heat exchanger. An average heat transfer coefficient can be predicted with some simple correlations, although the heat loss characteristics must be known to obtain an accurate solution at higher heat flux. The governing dimensionless

numbers used here only require two flow variables to be known, the Freon mass flux and the vapour mass quality.

5. Two-Phase Flow Patterns In A Heated Inclined Tube -- A Preliminary Study

Summary

Flow visualization study of the vapour-liquid mixture in a heated inclined Pyrex tube was carried out. Heating was achieved electrically at the bottom half of the test tube. Under thermosyphon condition, the effect of the liquid Freon charge level was found to delay the transition to annular flow at high charge level, and to cause slug flow with bursting of the vapour bubble at low charge level. Intermittent annular flow was attained, but cannot be sustained continuously, within the operating range of the present experiments. Forced circulation tends to prolong the bubbly flow regime and prevents coalescence of bubbles.

5.1 Introduction

The formation of two-phase mixture by vapour generation in a heated tube is most easily studied via flow visualization using a transparent tube. The heat flux added alters the vapour quality along the tube length and subsequently the flow regime varies axially too. The change in flow regime induces variations in the local heat transfer coefficients. Identification of the two-phase flow patterns therefore allows one to know which regime predominates under given conditions and thus one may check if assumptions made in computations are valid.

Small jets of bubbles grow from preferred sites on the tube surface when the suface temperature exceeds saturation temperature and conditions for bubble nucleation are satisfied. These bubbles grow larger as they rise because of the addition of heat as well as decreased pressure. The larger bubbles interact with one another and with the liquid phase, causing a churning turbulent motion. As the vapour quality increases at the upper section, annular flow occurs where the vapour flows in the centre core with some small entrained liquid droplets, and a thin liquid film being sheared along the tube wall. Dry-out can be avoided if sufficient liquid is charged into the system or if heating is done below the critical heat flux. In cases where high superheating of the liquid is required to initiate boiling, slug flow may occur instead of bubbly flow. This is characterized by a single bullet shaped bubble expanding

along the tube. When the expansion rate is high, a bursting type of boiling is observed.

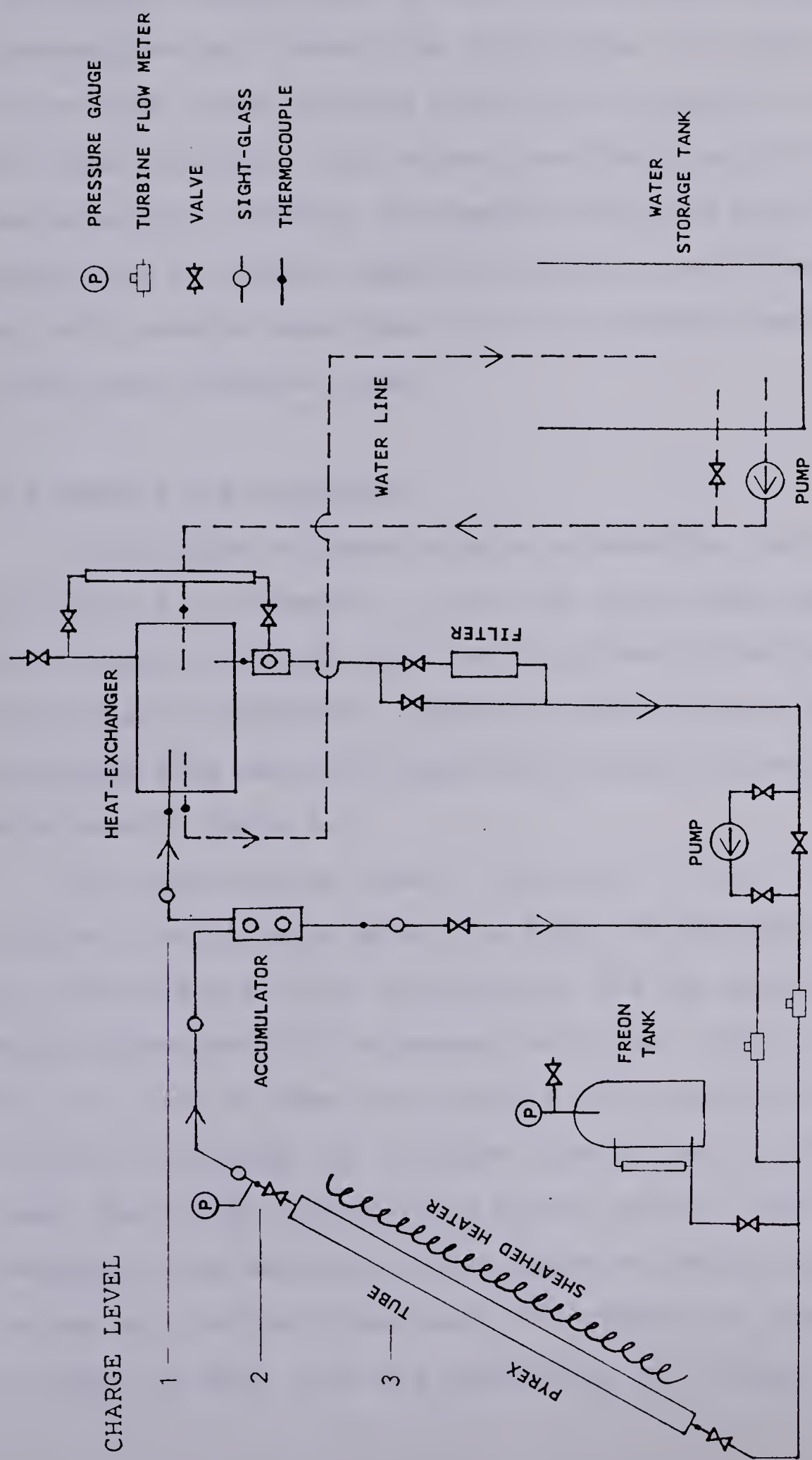
Boiling in the collector tubes is similar to the description outlined above. This part of the study was concerned with the flow patterns in the tubes and the effects of liquid charge level and forced flow on the boiling.

5.2 Experimental Apparatus

The experimental apparatus is similar to that reported in Cheng et al.[24] with the replacement of the Packless™ condenser by Refrigeration Research™ condenser and also the addition of an accumulator after the test section. The schematic diagram of the thermosyphon loop is shown in Fig. 5.1. The bottom half of the 1.22 m long Pyrex tube (31.5 mm o.d. and 23 mm i.d.) was heated using eight steel and incoloy sheathed heating elements. These elements were insulated, leaving the upper half exposed for flow visualization. Only 1.1 m of the tube length was heated and the tube was inclined at 68° to the horizontal.

Freon R-11 was used as the working fluid. The cooling water flow rate was kept constant throughout this series of experiments. The liquid charge level was adjusted using the expansion tank and sight glasses. The Freon pump was used for forced circulation of the working fluid.

Temperature, flow rate and pressure were measured using devices described in Chapter 3 (§3.2 - Instrumentation).



5.1 Schematic diagram of the thermosyphon loop for flow visualization study.

The use of a single heated tube here only provides a preliminary visual study of the flow patterns under thermosyphon and forced flow conditions, but does not reflect the actual boiling occurring in parallel tubes in the solar collector unit since flow distribution is not accounted for. However, the results obtained here will be applicable to similar apparatus used for waste heat recovery and will provide some ideas of the two-phase phenomena inside the collector tubes.

5.3 Results And Discussion

A multitude of names exists to describe the various two-phase flow patterns. In view of this, terms used here will conform to those descriptions given in Collier[26, pp. 8-9] to avoid confusion. Operating conditions of the two-phase flow patterns depicted in Figs. 5.2 to 5.6 are tabulated in Table 5.1.

At liquid charge level 1 indicated in Fig. 5.1, the typical flow patterns along the tube are depicted in Fig. 5.2. Boiling was first initiated at the top section and moved downwards with increasing heat flux. Figs. 5.2(a), (b), (c) and (d) show the changing flow patterns from bubbly flow at the bottom (a) to churn flow at the top (d) of the tube. The vapour travels in a spiral motion (see (d)) because of the secondary flow caused by heating only the bottom half of the Pyrex tube. The transition between bubbly to churn is shown with the photograph of a longer section of

Fig. 5.2 Flow patterns along tube at high heat flux
and high charge level.

(e)



(d)



(c)



(b)



(a)



Fig. 5.3 Transition from churn flow to annular flow at high heat flux.

(a)



(b)



(c)



(d)



(e)



Fig. 5.4 Slug flow with bursting of the vapour bubble at low charge level and low heat flux.

(a)



(b)



(c)



(d)



(e)



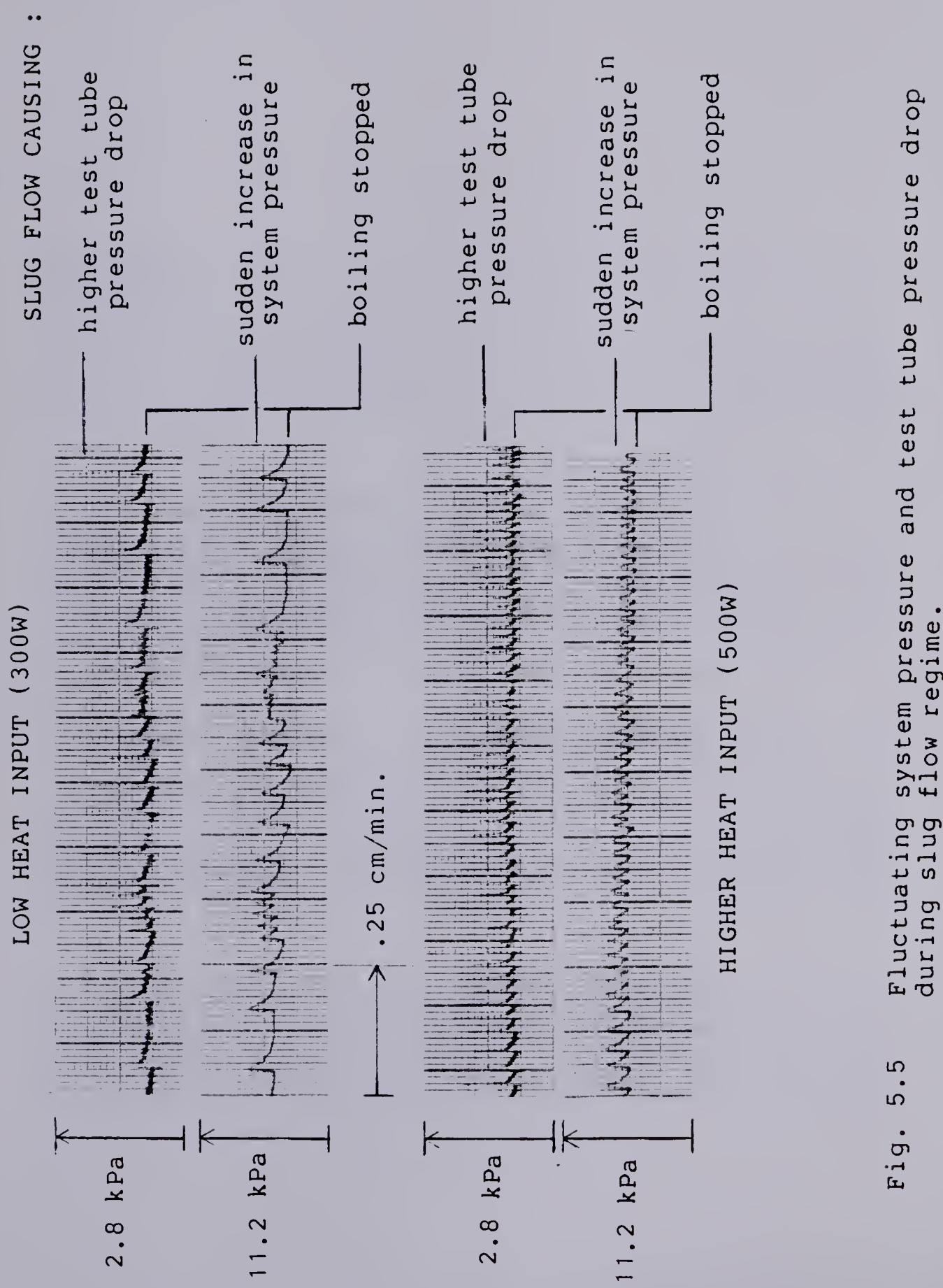


Fig. 5.5 Fluctuating system pressure and test tube pressure drop during slug flow regime.

Fig. 5.6 Prolonged bubbly flow under forced flow condition.

(d)



(c)



(b)



(a)



Table 5.1 Operating conditions of the flow patterns depicted in Figs. 5.2 to 5.6.

		Fig. 5.2	Fig. 5.3	Fig. 5.4	Fig. 5.6
(a)	Tube inlet temp. (°C) Tube outlet temp. (°C) System pressure at top of tube (kPa) Freon flow rate (kg/s)	28.7 39.1 75 0.025	27.7 31.1 40 0.031	21.45 21.7 17 not detected	23.2 33.7 40 0.02
(b)	Tube inlet temp. (°C) Tube outlet temp. (°C) System pressure at top of tube (kPa) Freon flow rate (kg/s)	28.7 39.1 75 0.025	27.7 31.1 40 0.031	pressure fluctuates as shown in	23.2 33.5 65 0.036
(c)	Tube inlet temp. (°C) Tube outlet temp. (°C) System pressure at top of tube (kPa) Freon flow rate (kg/s)	28.7 39.1 75 0.025	27.7 31.1 40 0.031	Fig. 5.5	23.9 39.1
(d)	Tube inlet temp. (°C) Tube outlet temp. (°C) System pressure at top of tube (kPa) Freon flow rate (kg/s)	28.7 39.1 75 0.025	27.7 31.1 40 0.031		24.9 44.0
(e)	Tube inlet temp. (°C) Tube outlet temp. (°C) System pressure at top of tube (kPa) Freon flow rate (kg/s)	28.7 39.1 75 0.025	27.7 31.1 40 0.031		27.7 31.1 40 0.031

the tube in (e). Within the range of heat fluxes possible for these experiments, annular flow was not observed.

When the charge level was reduced to level 2 (see Fig. 5.1), annular flow was attained intermittently. Fig. 5.3 shows the transition of the flow pattern from turbulent-churn (a) to wispy-annular (c), and finally to annular flow (d). This sequence of events will later collapse and the whole process will be repeated. It is apparent the maximum wall heat flux possible here cannot sustain a steady annular flow regime. The spiral motion is present just downstream of the annular flow regime as shown in (e). Annular flow is possible in this case because a reduction in liquid charge level also reduces the pressure, along with a shorter liquid column above the tube.

A further reduction of the liquid charge level to level 3 caused slug flow instead of small bubble jets when boiling was initiated at low heat flux. The probable cause is the much lower static pressure, due to the shorter liquid column, which causes the vapour bubble generated to expand quickly. Figs. 5.4(a) to (e) show the bubbles generated expanding upwards, pushing the liquid column above it higher as it rises. A wake region with many small vapour bubbles was created because of the lower pressure behind the slug. Bursting occurs when the bubble reaches the top, follows by the liquid column falling back. This is shown in (e). Nucleation then stops momentarily until sufficient superheat is reached at the bottom. This process (slug) is then

repeated and causes a fluctuation in pressure. Slug flow is absent in the first two cases mentioned. Fig. 5.5 shows the fluctuating system pressure and pressure drop across the Pyrex tube section during the slug flow regime. The frequency of the slug formation increases with higher input wall heat flux as shown.

Forced circulation makes use of sensible heat change more and prevents the coalescence of bubbles generated, as shown in Figs. 5.6(a) and (b), for thermosyphon and forced flow, respectively, under the same conditions. More tiny bubbles are formed with increased heating, again without coalescence. This is depicted in (c) and (d).

5.4 Concluding Remarks

Under thermosyphon condition, the charge level is seen to affect the type of flow regime in the heated tube. A high charge level tends to delay the transition to annular flow when compared to a lower charge level. As the charge level is lowered much further, slug flow with bursting of the vapour bubble occurs at initial boiling. This is associated with fluctuation of pressure in the system. Forced flow prolongs the bubbly flow regime and prevents the coalescence of bubbles, i.e., the flow remains in the laminar region till a higher wall heat flux when compared to thermosyphon flow.

The assumption of homogeneity of the vapour-liquid mixture in these experiments will be valid for most cases

with the bubbly and churn flow regimes. The exception is when annular flow appears near the top section under high wall heat flux or during slug flow at low charge level and low heat flux.

It is expected that the flow patterns will depend on tube size, inclination angle and heating arrangement. In order to study the convective boiling process in the collector tubes, it is necessary to construct an apparatus with parallel tubes to account for non-uniform flow distribution, if any.

6. Conclusions

6.1 Scope Of Results

Results obtained from outdoor testing of the two-phase thermosyphon collector system show that the system is a viable alternative to the conventional hydronic system. Problems regarding the stability of Freon R-11 are being studied by Downing[15] and Farrington et al.[11].

The important parameters in evaluating the thermal performance of a Freon charged two-phase thermosyphon flat plate solar collector system are the vapour quality generated in the collector tubes and the Freon mass flow rate through the collector system. These two parameters are affected by the liquid charge level in the collector, wall heat flux, liquid separation at the collector exit using an accumulator and the cooling water flow rate.

Boiling in the collector tubes was found to occur mainly in the saturated boiling regime. An average collector tube heat transfer coefficient calculated compares well with Shah's[34] correlation using the Boiling number and the Convection number. The use of an average value simplifies computations by not having to account for varying local heat transfer coefficient along the collector tube length. The correlation fails at low wall heat flux because boiling has not reached the saturated state. Combinations of different liquid charge level and wall heat flux to the Freon produce different flow regimes in the collector tubes, and

consequently the heat transfer coefficient varies. The accuracy of the predictions can be improved if the heat loss characteristic of the system is known.

Pressure drops across the collector panel and the heat exchanger are well correlated with the Lockhart-Martinelli parameter [29]. Predictions of pressure drop can be simplified by treating all the bends and joints along the collector panel as a single unit, and the accelerational component need not be treated separately. The assumption of homogeneity of the vapour-liquid mixture was found to be valid, the exception being at low wall heat flux where slug flow regime may occur. Annular flow regime may exist in only the upper section of the collector tubes at high wall heat flux, thus neglecting this should not incur a significant error in assuming homogeneous flow.

6.2 Future Studies

Outdoor testing throughout the year needs to be carried out to ascertain the feasibility of operating these thermosyphon systems in cold regions on a year round basis.

The successful correlations of the average heat transfer coefficients and pressure drops data must be checked with results obtained from outdoor test since heat loss characteristics are different for the unit tested indoors. The simplifications involved in correlating the indoor test results need to be validated for outdoor test results.

Flow visualization studies on the two-phase flow patterns in parallel collector tubes will provide further insights into the boiling phenomena as well as flow distribution in the tubes.

The ability of the thermosyphon system to transfer heat with a small temperature difference suggests the feasibility of using these systems to recover low temperature waste heat.

References

1. H.T. Whitehouse, "Draindown freeze protection for thermosyphon water heaters", *Solar Engineering*, pp.14-18, December, 1981
2. B. Doron, a technical note on Testing of Collectors, *Solar Energy*, Vol. 9, pp. 103-104, 1965
3. S.C. Bhattacharya and V.K. Kapur, "Investigation on the feasibility of using a two-phase thermosyphon for solar storage, space heating and cooking", *Sun, Mankind's Future Source of Energy* (eds. F. de Winter and M. Cox), Proc. of the ISES Congress, New Delhi, India, 1978, Vol. 1, pp.579-582
4. R.C. Downing and V.H. Waldin, "Phase-change heat transfer in solar hot water heating using R-11 and R-114", *ASHRAE Trans.*, Vol. 86, Part 1, pp. 848-856, 1980
5. F. Kissner and P.Seydlik, "Performance and energy management analysis of a passive phase change solar water heating system", Proc. of the 1980 Annual Meeting, AS/ISES, Phoenix, Az., 1980, Vol. 3.2, pp. 860-864
6. F. Kissner, "A passive, refrigerant-driven, solar domestic water heating system -- the ultimate in efficiency and freeze protection for cold climate", Proc. of the National Conference on Solar Energy, SESCI - Montreal, Canada, 1981, pp. 201-205
7. M. DeAngelis and D. Nordham, "Design and installation considerations for refrigerant charged thermosyphoning solar dhw systems", Proc. of the 1980 Annual Meeting, AS/ISES, Phoenix, Az., 1980, Vol. 3.2, pp. 779-783
8. J.M. Schreyer, *Residential applications of refrigerant-charged solar collectors*, Technical report of the Solar Research Division of Refrigeration Research, Inc., Brighton, MI., 1978
9. F.K. Manasse and J.A. O'Leary, "Heliophase™ solar hot water heating system", Proc. of the 1978 Annual Meeting, AS/ISES, Denver, Colorado, 1978, Vol. 2.2, pp.36-40
10. F. Kissner, "Field testing of a passive, phase-change solar domestic water heating system", Proc. of the 4th National Passive Solar Conference, AS/ISES, Kansas City, MO., 1979, pp. 615-616
11. R. Farrington, M. DeAngelis, L. Morrison and D. Dougherty, "Performance evaluation of a refrigerant

- charged thermosyphon solar dhw system", Proc. of the 1981 Annual Meeting, AS/ISES, 1981, Vol. 4.1, pp. 676-680
12. R.S. Soin, K. Sangameswar Rao, D.P. Rao and K.S. Rao, "Performance of flat plate solar collector with fluid undergoing phase change", Solar Energy, Vol. 23, pp. 69-73, 1979
13. B.W. Davis and K.B. Bol, "Using two-phase working fluids to greatly improve passive solar water heating", Proc. of the 1978 Annual Meeting, AS/ISES, Denver, Colorado, 1978, Vol. 2.1, PP. 599-602
14. D.P. Rao and K.S. Rao, "Solar water pump for lift irrigation", Solar Energy, Vol. 18, pp. 405-412, 1976
15. R.C. Downing, "Thermal stability of R-114 and R-11 in solar applications", Proc. of the ASME Solar Energy Division 4th Annual Meeting, Albuquerque, New Mexico, 1982, pp. 76-81
16. N.D. Kaushika, S.C. Bharadwaj and S.C. Kaushik, "Analysis of a flat plate collector with fluid undergoing phase change", Applied Energy, Vol. 11, pp. 233-242, 1982
17. S.K. Chaturvedi, Y.F. Chiang and A.S. Roberts, Jr., "Analysis of two phase flow solar collectors with application to heat pumps", (Journal of Solar Energy Engineering) Trans. of ASME, Vol. 104, pp. 358-365, 1982
18. D. Best, "What you should know about phase-change water heaters", Solar Age, pp.22-25, December, 1981
19. K.C. Cheng, *Application of boiling and condensation heat transfer to flat plate solar collectors in cold region*, Final report submitted to Alberta/Canada Energy Resources Research Fund (ERRF) Universities Program under Contract U-79-9, June, 1982
20. E.W. Bottum, "Refrigerant charged phase change solar water and space heating systems", ASHRAE Trans., Vol. 87(2), pp. 397-404, 1981
21. J.A. Duffie and W.A. Beckman, *Solar engineering of thermal processes*, Wiley-Interscience, 1980
22. J.M. Schreyer, "Residential application of refrigerant charged solar collectors", Solar Energy, Vol. 26, pp. 307-312, 1981
23. E. Streed, D. Waksman, A. Dawson and A. Lunde, "Comparison of solar simulator and outdoor ASHRAE

Standard 93 thermal performance tests", Proc. of the 1980 Annual Meeting, AS/ISES, 1980, Vol. 3.1, pp. 405-409

24. K.C. Cheng, I. Morioka, K. Ichimiya and G.W. Sadler, "Experimental study of a two-phase thermosyphon system", *Alternative Energy Sources IV*, Vol. 1, 1982, pp. 151-170, Ann Arbor Science
25. F. Kreith and J.F. Kreider, *Principles of Solar Engineering*, McGraw-Hill, 1978, p. 221
26. J.G. Collier, *Convective boiling and condensation*, McGraw Hill, 2nd Edition, 1981
27. D. Chisholm, "Void fraction during two-phase flow", *J. Mech. Eng. Sci.*, Vol. 15(3), pp. 235-236, 1967
28. G.B. Wallis, *One dimensional two-phase flow*, McGraw Hill, 1969
29. R.W. Lockhart and R.C. Martinelli, "Proposed correlation of data for isothermal two-phase two-component flow in pipes", *Chem. Eng. Prog.*, Vol. 45, pp. 39-48, 1949
30. R.C. Martinelli and D.B. Nelson, "Prediction of pressure drop during forced circulation boiling of water", *Trans. ASME*, Vol. 70, pp. 695-702, 1948
31. V.E. Shrock and L.M. Grossman, "Forced convective boiling in tubes", *Nuclear Science and Engineering*, Vol. 12, pp. 474-481, 1962
32. J.C. Chen, "Correlation for boiling heat transfer to saturated fluids in convective flow", *I&EC Process Design and Development*, Vol. 5(3), pp. 322-329, 1966
33. R.J. Bjorge, G.R. Hall and W.M. Rohsenow, "Correlation of forced convection boiling heat transfer data", *Int. J. Heat Mass Transfer*, Vol. 25(6), pp. 753-757, 1982
34. M.M. Shah, "Chart correlation for saturated boiling heat transfer: equations and further study", *ASHRAE Trans.*, Vol. 88(1), pp. 185-196, 1982
35. H.D. Beggs and J.P. Brill, "A study of two-phase flow in inclined pipes", *J. Petroleum Technology*, Vol. 25, pp. 607-617, 1973
36. D. Chisholm, "A theoretical basis for the Lockhart-Martinelli correlation for two-phase flow", *Int. J. Heat Mass Transfer*, Vol. 10, pp. 1767-1778, 1967
37. G.M. Lazarek and S.H. Black, "Evaporative heat transfer,

pressure drop and critical heat flux in small vertical tube with R-113", Int. J. Heat Mass Transfer, Vol. 25(7), pp. 945-960, 1982

Appendix A : Flow Chart For Experimental Instrumentation

The flow chart of the data acquisition system and the associated instrumentation is shown in Fig. A.1.

Measuring devices, e.g., flow meters and thermocouples, are connected to the HP-3497A D/A unit, and triggering of the unit is done via a HP-85 micro-computer. Signals that are required to be monitored continuously are connected to chart recorders.

Data collected are stored on magnetic tapes in the HP-85 and printed out on paper through the printer as well. Results obtained at the end of the experiment are then plotted.

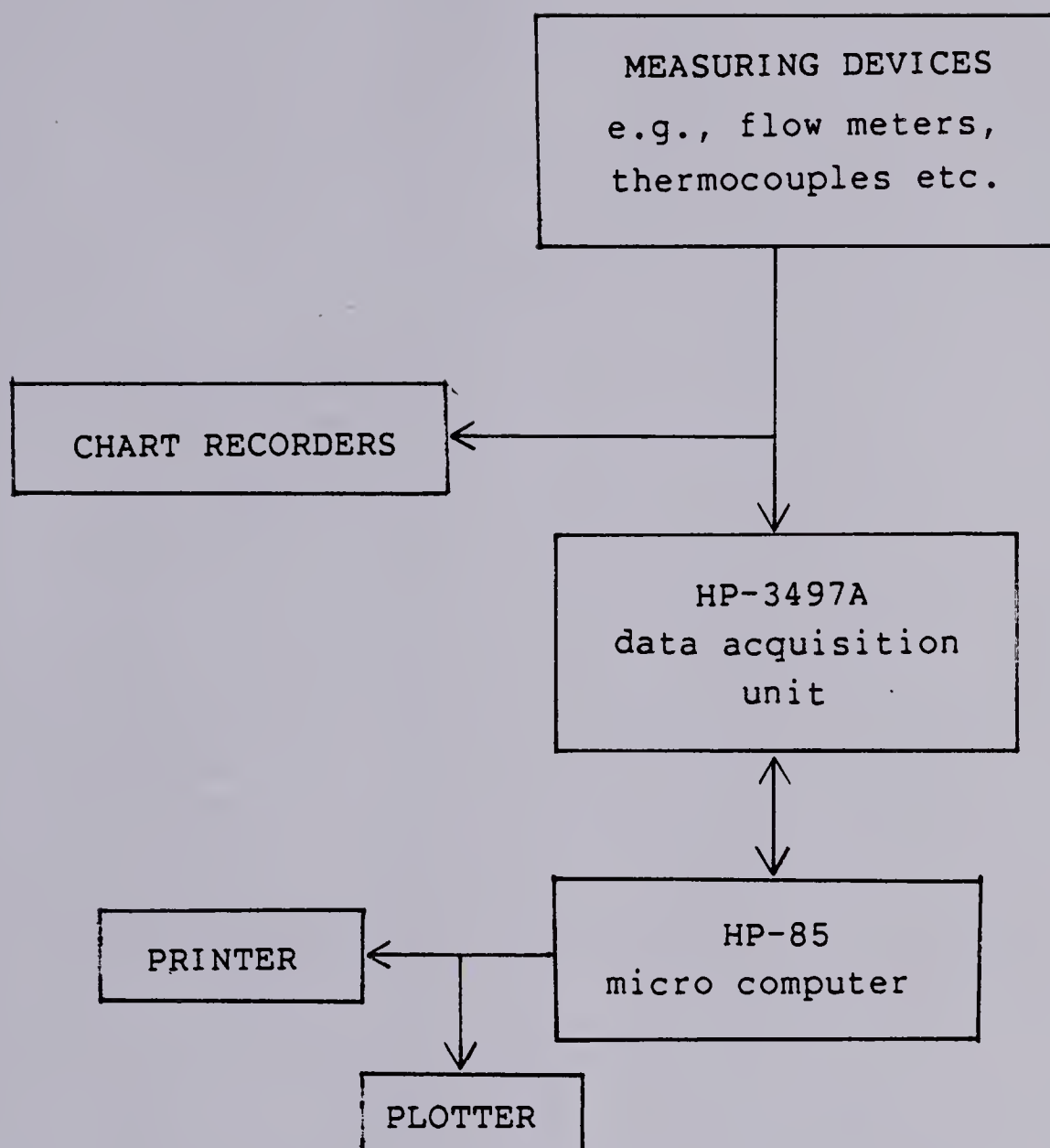


Fig. A.1 Flow chart of the data acquisition system used in experiments.

B30384